NORTHWESTERN UNIVERSITY

Fundamental Electron Transfer and Spin Dynamics in Organic Donor-Acceptor Systems for Quantum Information Science Applications

A DISSERTATION

SUMBITTED TO THE GRADUATE SCHOOL IN PARTIAL FULFILLMENT OF THE REQUIREMENTS

for the degree

DOCTOR OF PHILOSOPHY

Field of Chemistry

By

Laura Bancroft

EVANSTON, ILLINIOS

September 2022

Abstract

Fundamental Electron Transfer and Spin Dynamics in Organic Donor-Acceptor Systems for Quantum Information Science Applications

Laura Bancroft

This thesis contains two research projects. The first research project examined the coherent nature of electron transfer in two donor-acceptor dyads – one single acceptor control compound and one dual acceptor molecule of interest. Using transient absorption spectroscopy in the ultraviolet/visible/near-infrared and mid-infrared regions, magnetic field effect experiments, and theoretical calculations, we determined that charge recombination in the molecule of interest is electronically incoherent and spin coherent at 295 K in toluene. The second research project explored the effect of laser positioning in electron spin teleportation in a donor-acceptor-radical triad. We used pulse electron paramagnetic resonance spectroscopy and density matrix model simulations to observe the spin echo as a function of laser delay. The resulting data show damped oscillations as a function of delay, and simulations of this system agree with experimental results and provide fundamental insight into the spin dynamics of this system. Teleportation fidelity as a function of laser delay was also calculated to show oscillations also due to the phase factor between the quadrature detection channels.

Acknowledgements

There are lots of individuals to thank for all their help, guidance, and support over the years. I will do my best to remember and acknowledge everyone here, and I apologize for anyone I may have missed.

Thank you to Prof. Michael R. Wasielewski for providing financial support over the course of my time here. Also thank you to Prof. Joseph T. Hupp and Prof. Eric Weitz for serving on my committee and giving good advice about my work and ideas. Thank you to my chair, Prof. Emily A. Weiss, for her no-nonsense attitude during my qualifying exam.

Thank you to all the program coordinators that have served us all in countless ways. Some of the people who have impacted me directly include Melanie Sandberg, Gregory Mandell, Tory Helgeson, Nick Huryk, and Amanda Mahoney. All your help with scheduling, organizing, ordering, and expediting has been much appreciated. I would like to extend a special thank you to Amanda for all her genuine kindness through some trying times.

I would like to thank all the coauthors and collaborators on all the projects I've worked on over the years here at Northwestern and also at Wellesley. Even the projects that did not make it to publication taught me many things, and I am grateful for everyone who helped me along with each project I was part of. In particular, I would like to thank Emma Roesner for being the absolute best collaborator. Her patience and willingness to venture into unfamiliar or unknown territory made working with her so wonderful.

To start naming some specific coauthors, coworkers, and collaborators that have made an especially potent impact, thank you Dr. Nikolai Tcyrulnikov, one of our fabulous research

professors in the Waz group. He has helped me and the whole group in so many more ways than his job description could ever describe, including being a second copy of my grandmother in many ways (it's a huge compliment, trust me). Thank you for serving as a reference for the many many jobs I applied to. Thank you also to Dr. Ryan M. Young, another research professor who goes above and beyond for everyone. I am thankful for his guidance in navigating grad school and the world beyond, and for his rigorous approach to kinetic analyses and just about anything else he does. I forgive him for making me cry the night before my qualifying exam.

There are many phenomenal Waz group members who have graduated before me. Thank you to Dr. Noah Horwitz, who paved the way for my first project in grad school. Even though the project didn't quite get off the ground, I learned so much about lasers, optics, emission, LabVIEW, and zero quantum coherence. Thank you to Dr. Joseph Christensen for passing the torch of safety designate to me. That position opened a lot of doors for me to participate in the safety realm of NU and beyond which I have really enjoyed. Thank you to Dr. Natalia Powers-Riggs for your sage wisdom and genuine kindness. Hearing her honesty about the suckiness of various stages of grad school life, as well as stories about the light that actually exists at the end of the grad school tunnel was so helpful. Thank you to Dr. Joaquin Alzola for being so kind between the extended moments of sarcasm and wit. Not sure if I should thank him for knighting me with the Waz group grumpy person title, but yeah. Thank you to Dr. Jenna Logsdon for bringing so much life and silliness to the group. I can't even begin to name all the times you made me laugh and how much we still talk about your legacy. Thank you to Dr. Su Chen for being an incredible friend and supporter. It took so long for me to win him over as a friend in the old days of our office, but I'm so glad I kept

pushing. Thank you to both Jenna and Su for helping me pull myself together the night before my qualifying exam. And of course, thank you so so so much to Dr. Brandon Rugg, the OG Rugg Doctor, for being so friendly from the day I stepped into the office. I learned so much from him about EPR, organic synthesis and sample preparation, TV references, and all sorts of other useful discussions about anything and everything we had in the office. Also, I am thankful for all the times he included me in some of his shenanigans with Joe.

I am so grateful for the little lunch crew that formed during my last year or so in grad school. These people included Oscar Huang, Elisabeth Latawiec, Emmaline Lorenzo, Malik Williams, and Hannah Eckvahl as well as the occasional drifter, like Colin Tichvon and Paige Brown. To Oscar, all the chocolates and other treats were so great, as well as the support of a wonderful friend. My apologies for taking Elisabeth's backpack's chair so often, and I want to thank Elisabeth for being a calm and warm east coast compatriot in this midwestern meh. Emmaline's thank-you is in the next paragraph. To Malik, thank you for being a great support and for always knowing and sharing what's going on, always. To Hannah, thank you for being a great biking buddy and for introducing me to so many internet things. I wouldn't have entrusted Jade to just anyone, so thank you to Colin for keeping my baby safe while I was away and also thank you for joining our lunches and adding the wildest vibes. Paige's thank-you is in the next paragraph. To everyone, having something to look forward to in the middle of the day made the mornings more manageable, and socializing fueled me for the rest of the day. So thank you all for the laughs and discussions and good times.

I am so incredibly, deeply thankful for the Spinsters, Dr. Samantha Harvey (aka Lisa), Leanna Kantt (aka Lehannah), Paige Brown (aka Paigej), and Emmaline Lorenzo (no nickname yet). Sam was probably my first true friend in the Waz group, and I remember giving her a high-five in the hallway and feeling so relieved that I had found an equally silly soul to match mine. Sam has helped me through scientific conundrums and personal crises, and I will forever be thankful to her and her fiancé, Karl, for inviting me over for the coziest Christmas dinner possible in the throes of 2020. Leanna and I came together in the strangest of ways, from almost meeting twice during her visit weekend/s to sitting next to each other a meeting for worship at the Evanston Friends Meetinghouse to being officemates and friends. The universe was trying very hard to bring us together! I am so proud of her for using her determined and stubborn spirit to look out for herself. Paige and I met over her visit weekend, and I thought she was way too cool to be my friend. But thankfully that was not the case, and we have had adventures in and out of the lab, and her lawless loyalty warms my heart. Emmaline has given such great advice and hugs over the years, and also makes a mean banana bread. Her level-headed approach to life has given me so much perspective about what balance can actually look like in grad school. These phenomenal women were so incredibly supportive in their individual ways, and so inspiring as a collective badass group. I hope I can give them even a fraction of the love they have shown me.

Thank you to the whole Waz group during the time that I've been here. We have had so many fun times and have grown so much, so thank you for being part of this journey.

There are lots of people to thank for all the teaching-related activities I've done at NU. I want to extend a huge thank-you to Brendan Kerwin for making my second time around with

Chem 110 such a dream (go dream team!) and for being an ever-supportive friend even when things were bad for both of us. Thank you to Prof. Stephanie Knezz for both the guidance and freedom during new grad student TA training. Thank you to Prof. Frederick Northrup for trusting me with Chem 110 things and letting me discover my love for teaching. Thank you to Prof. Katie Gesmundo for serving as a mentor and helping me with the job search process. And finally, thank you so much to Prof. Veronica Berns for mentoring me through preparing for and teaching my first-year seminar. The seminar times were incredibly difficult, and I'm so glad I had your wisdom and faith to help me through. I also want to extend a general thank-you to everyone in the various teaching programs I participated in for all the times of good discussion and learning.

In the realm of safety, there are so many people at the Office of Research Safety (ORS) and in Research Safety Student Initiative (RSSI) at NU to thank. Thank you to Dr. Glen Svenningsen for supporting RSSI and being an entertaining partner at the CPR/AED training course way back. Thank you to Anna Stasek for all the work you did for RSSI to make our materials so much more appealing than any other safety-related content I have seen. Thank you to Gwen Sullivan for all the help she has given me and RSSI over the years, including things that she definitely didn't have to do for us. Thank you to Dr. Michael Blayney for somehow, magically, knowing exactly what kind words of encouragement I needed to hear and popping up out of nowhere exactly when I needed to hear them. Thank you to Dr. Benjamin Williams for helping me out with safety designate things in the Waz group and assisting RSSI with the many events that benefitted from your input. It has been so comforting to know he will always be on the side of supporting researchers to conduct their work safely and efficiently. And thank you to everyone

else at ORS that help the whole of NU and the events for RSSI run smoothly and... safely. Thank you to Dr. Megan Wasson for inviting me to join the RSSI board and to Dr. Rachel Dicken for helping us with all the details. And thank you to everyone else on the past and present board that helped the group run through a pandemic into today and beyond.

On a less technical and less academic note, thank you to the light guy at NU. I never got his name, but he replaced the lights in our lab and office spaces. Whenever I see him in the hallway, he still asks if everything is okay and if we need him to replace any lights. What an incredible human being he is. Thank you also to Harry, who I often see sweeping and cleaning in Tech. He has such a kind soul that brightens my day even if we just say hi in passing, but often we have slightly longer conversations that give me just a little more oomph to continue through my day. And thank you to Salomon Rodriguez, the student machine shop manager, for teaching me loads about machining, helping with many projects, and making the machine shop a friendly place to work.

Moving back to my Wellesley days, there are so many professors I am thankful for. These professors include Prof. Christopher Arumainayagam (for all his faith in me and his incredibly flexible office hours), Prof. Paul Reisberg (for showing us the human side of chemistry and coming to my talk at Wellesley after he had retired), Prof. James Moyer (for encouraging me in a discipline of chemistry I was very hesitant to take and taking a genuine interest in his students' well-being), Geraldine Echebiri (for the laughs in physical chemistry lab and her very kind speech during the chemistry majors dinner), Prof. Nolan Flynn (for teaching analytical chemistry in such a way that it was not only my favorite class, but also a huge inspiration for my teaching), Prof. Rachel Stanley

(for all the tea in her office and later inviting me to speak at Wellesley), Dr. Carla Verschoor (for the organized inorganic chemistry labs, tasty treats, and honest career advice), Prof. Alexander Diesl (for giving me such a fun and solid base in linear algebra and serving as the non-chemistry person on my senior thesis committee), and Dr. Jonathan Tannenhauser (for all the fun and all the challenges, and for being so accessible and approachable). And thank you to Prof. David Haines. I don't know of many professors who are as dedicated to their students as he is. Even before retirement, he made time to keep in contact with his students. His wisdom is so deep that I'm usually surprised at the fantastic advice he gives. That combination of knowing his students and seemingly unending wisdom leads to his facilitating connections between his students (such as me and the esteemed Prof. Tamara Hendrickson, who also knew exactly how to build me up when there wasn't a whole lot of me still up – how did David know to connect me with someone so good for that moment? Magic.). I cannot thank him enough for all the support during and after Wellesley.

There are many classmates from Wellesley that I would also like to thank. These people include Anita Wo (for all the yummy food we've made and the Cape Cod and Chicago adventures we've had), Sara Eslami (for teaching me to make tea the Persian way, aka the right way), Bridget Schreiner (for being the best roomie ever, for our many adventures way below and way above ground, and for understanding what I needed when I was lost), Ciaran Gallagher (for all the amusing meal times in Pom and the silly times everywhere), Elle Friedberg (for our fun times in biochem and inorganic and for sharing her artwork), Edie Sharon (for each and every postcard, and for your refreshingly formally informal vibes), Kathleen Chen (for the dog pictures and

honesty about grad school struggles, especially at the start of our post-Wellesley journeys), Alice Zhou (for perfectly pairing humility and humor, and for humoring me), Jane Vaughan (for being so authentic, open, and unapologetic, and for hanging out with me during the Chicago times), and Helen Cumberbatch (for being absolutely hilarious and such a great study partner and friend, and for all the fantastic wolf shirts).

Moving way back to my Falmouth High School days, there are a few people whose impact lasted through my chemistry journeys. First, I would like to thank Michael Feeney for always having faith in me and letting me know that he believed in me. Hearing that as a high schooler from a teacher I thought highly of meant so much. And I could not go one sentence further without thanking Dr. Miguel Zamora. I have heard so many horror stories of people who had terrible high school chemistry experiences, and my experience was so far removed from those horrendous stories because of this phenomenal educator. After sophomore chemistry, I was about to take AP biology because AP chemistry was widely known as basically the hardest class at FHS. But I learned so much and loved the puzzle-like nature of chemistry, so decided to pursue another year of chemistry with Dr. Zamora. The course was challenging, as promised, but I learned how to problem-solve and how to connect areas of chemistry in a non-linear way, which prepared me so well for all the chemistry to come. Dr. Zamora spent countless hours answering my questions, letting me do homework in his classroom after school, giving incredible life advice. I would not have pursued this path through chemistry without his support and guidance and I cannot thank him enough.

There are some very previous friends and extended family members who have supported me throughout the years. Thank you to Zach Erdody for hearing my gripes and giving some much-needed perspective. I am also so thankful for the two-way street we have formed in our friendship that allows us to be honest and help each other. Thank you to the Gentilhommes: Scott, Patty, Alex, and Britt. They are a second family to me, and I thank them for all the exploration, laughs, and learning of the past and future. A special thank-you to Britt for helping me so much through the drudgery of grad school with her trips out here, our little and big adventures, and her thoughtful notes and gifts.

There are so many family members to thank for guiding me into my position here at the end of grad school. Thank you to my soon-to-be neighbors, Uncle Mike (for all his trouble-making and devious ideas, and for taking the time to teach me things like scuba diving basics) and Casey (for all the games we played as kids and for teaching us all what a moohog is). Thank you to the California Bancrofts: Uncle A (for teaching me how to relax and have fun, especially with toys that have engines), Jess (for letting me live my dream as the adult flower girl in her wedding), Dylan (for inspiring me with his energy and creativity), and Lucy (for supporting me in my bookend duties by holding the middle Bancroft cousins in their places). Thank you to Roman for being a grounding point for me to rediscover my sanity when it vacates the continent, and for supporting me in everything from making a fun workout plan to navigating the job search process. I hope I can give him the same thoughtfulness and love he gives me. Thank you to Mimi for showing me what a true-hearted caretaker looks like. She is my mental image of someone who cares so deeply for others and also listens to herself for what she needs. Thank you to Papa for

being such an incredibly warm presence throughout my life. Whether we talk about light-hearted or serious topics, I come away from our conversation feeling a little lighter and more at peace. Thank you to Vovo for taking unbelievably large leaps of faith for the sake of her family. Her bravery is something unmatched, and in making my own difficult decisions, reflecting on her decisions gives me much-needed perspective. Thank you to Adam for helping bring out my inner fighter through all our confrontations – both real and over-dramatized. He put up with my bossiness so well, so thanks for being such a champ. I'm also so glad we can lean on each other now that we are adults with fairly different life experiences and areas of expertise. Thank you to my parents for giving me the space and freedom to do my own thing. For better or worse, they have given me so much choice – even to make an unwise decision (such as touching an electrical outlet or the woodstove). To Mom, thank you for having so much patience with me (yes, you do indeed have patience) as I've figured out life, and thank you for your careful eye at all the essays and dilemmas over the years. I hope to acquire even half the wisdom you have in my lifetime. To Dad, thank you for teaching me to problem-solve and think critically about mechanical things. That specific knowledge has served me so well in grad school, and the bigger-picture skills have served me throughout life. And finally, to Mimi, Vovo, and Mom, thank you so much for showing me how much strength Portuguese women have and how resourceful we are. You three have done so much work to ensure that my path to my current position and the road ahead is as smooth as it can be, and I hope I can help to pave your future paths as well.

Last, but most certainly not least, there are some non-human creatures I would like to thank that have brought me joy throughout grad school. Thank you to the Waz group pets Bowie (our

night after Joe's on Weed Street will never be forgotten), Tungsten (for all the biscuits he made on my lap), Moly (her sassiness was an inspiration to all), Copper (I will forever cherish Christmas Day 2020 as the first day of our friendship), Rosy (for snuggling with me for approximately ten whole seconds inside the blanket I was using – magical times), Rosie (for keeping Roman and I entertained with her adorable antics and impressing us with her fetch skills), Dennis (for always keeping me on my toes – whose food will he try to eat next?), Nikki (for warming my heart with her snuggles), and Kirby (for inspiring the most elaborate funeral service ever). I also want to thank the pack of Bancroft dogs that gave me a much-needed cheerful reprieve from the throes of grad school: Lilly (for lightening my spirit with her games – and hopefully I spelled her name right), Dash (for having an affinity to bubbles and for putting up with Bo), and Mr. Bojangles (for his entertainment, snuggles, kisses, and precious little face). Thank you also to two beloved souls who didn't make it to see the end of my journey in grad school but brought me joy at some point along the way. Thank you to Marlee for sticking it out just a little longer than everyone expected so I could say goodbye before moving away. And thank you to Jade for being my companion for nearly seventeen years, and gracing us all with her sass, charm, and persistence.

Table of Contents

List of Figures

List of Tables

List of Equations

Chapter 1: Charge Transfer and Spin Dynamics in a Zinc Porphyrin Donor Covalently Linked to One or Two Naphthalenediimide Acceptors

This chapter is from the published work titled as above with the authors listed below.[1]

Laura Bancroft,[1] Jinyuan Zhang,[1] Samantha M. Harvey,[1] Matthew D. Krzyaniak,[1] Peng Zhang,[2] Richard D. Schaller,[1,4] David N. Beratan,[2,3*] Ryan M. Young,[1,*] and Michael R. Wasielewski[1,*]

[1]Department of Chemistry and Institute for Sustainability and Energy at Northwestern, Northwestern University, Evanston, IL 60208-3113, USA

[2]Department of Chemistry, Duke University, Durham, NC 27708

[3]Departments of Biochemistry and Physics, Duke University, Durham, NC 27708

[4]Center for Nanoscale Materials, Argonne National Laboratory, Lemont, IL 60439, USA

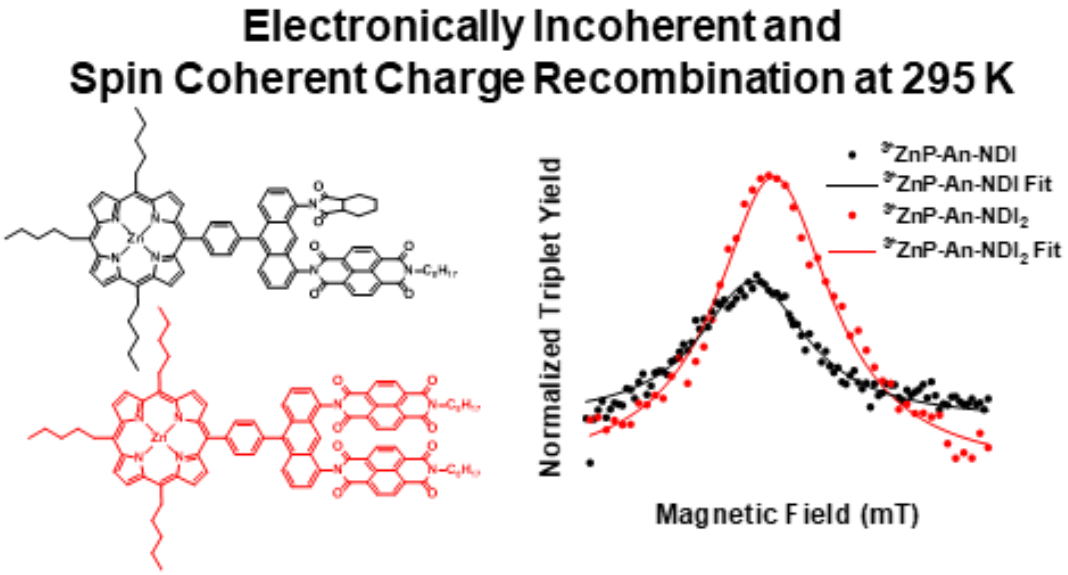

1.1 Abstract

Quantum coherence effects on charge transfer and spin dynamics in a system having two degenerate electron acceptors are studied using a zinc 5,10,15-tri(n-pentyl)-20-phenylporphyrin (ZnP) electron donor covalently linked to either one or two naphthalene-1,8:4,5-bis(dicarboximide) (NDI) electron acceptors using an anthracene (An) spacer, ZnP-An-NDI (**1**) and ZnP-An-NDI_2 (**2**), respectively. Following photoexcitation of **1** and **2** in toluene at 295 K, femtosecond transient absorption spectroscopy shows that the electron transfer (ET) rate constant for **2** is about three times larger than that of **1**, which can be accounted for by the statistical nature of incoherent ET as well as the electron couplings for the charge separation reactions. In contrast, the rate constant for charge recombination (CR) of **1** is about 25% faster than that of **2**. Using femtosecond transient infrared spectroscopy and theoretical analysis, we find that the electron on $NDI_2^{\bullet-}$ in **2** localizes onto one of the two NDIs prior to CR, thus precluding electronically coherent CR from $NDI_2^{\bullet-}$. Conversely, CR in both **1** and **2** is spin coherent as indicated by the observation of a resonance in the ^{3*}ZnP yield following CR as a function of applied magnetic field, giving spin-spin exchange interaction energies of $2J$ = 210 and 236 mT, respectively, where the linewidth of the resonance for **2** is greater than **1**. These data show that while CR is a spin-coherent process, incoherent hopping of the electron between the two NDIs in **2,** consistent with the lack of delocalization noted above, results in greater spin decoherence in **2** relative to **1**.

1.2 Introduction

Expanding simple electron donor-acceptor (D-A) systems to larger structures with multiple donors and/or acceptors raises the possibility that site-to-site charge (spin) hopping or complete delocalization, where the wavefunction simultaneously involves two or more sites, can influence both charge transfer and spin dynamics. Previously, systems with either two identical donors or acceptors have been studied using non-covalent D/A mixtures[2-4] and assemblies,[5] as well as covalent D-A dyads[6] and triads,[7, 8] all of which have the potential for electron/hole hopping or delocalization between the two A or D species, respectively.[9, 10]

In the specific case of two degenerate electron acceptors, D-A_2, we have shown that electron transfer can proceed coherently to a delocalized state of the dimeric acceptor. The charge transfer is a consequence of renormalization of the electronic coupling for electron transfer as well as the system bath interactions.[11] Under cryogenic conditions, delocalization is maintained throughout the charge separation process, resulting in a non-statistical rate enhancement for charge transfer to two acceptors relative to one acceptor. We demonstrated this fully-coherent charge transfer in a triptycene-bridged anthracene-benzoquinone system, where electron transfer from the anthracene lowest excited singlet state to two equivalent benzoquinones occurs five times faster than to a single benzoquinone acceptor. Similarly, using a *p*-(9-anthryl)-*N*,*N*-dimethylaniline (DMA-An) donor and a dimeric naphthalene-1,8:4,5-bis(dicarboximide) (NDI) acceptor, we observed a smaller non-statistical rate enhancement factor of 2.6 ± 0.2 for charge separation, and also a factor of 2.0 ± 0.2 for charge recombination.[12]

Coherent electron spin dynamics also play an important role in D-A systems intrinsic to natural[13, 14] and artificial[15, 16] photosynthesis, avian navigation,[17, 18] and quantum information science (QIS).[19-23] In the context of natural and artificial photosynthesis, the polarization and delocalization of spin among multiple cofactors plays a crucial role in dictating the reaction mechanism and kinetics.[24, 25] With regard to QIS, photogenerated radical pairs in organic D-A molecules have many desirable qualities that make them promising spin qubit pairs (SQPs) and that fulfill the well-known DiVincenzo criteria for viable qubits.[26] For example, sub-nanosecond electron transfer from D to A following laser photoexcitation produces an entangled SQP having a well-defined spin state, which allows for reliable execution of quantum gate operations without the use of ultralow temperatures or high magnetic fields.[22, 23]

Spin hopping or delocalization can have a significant impact on SQP spin coherence.[8, 27-35] For example, we recently compared the spin dynamics of a covalent $D^{\bullet+}$-C-$A_2^{\bullet-}$ triad system to the corresponding $D^{\bullet+}$-C-$A^{\bullet-}$ system, where C is a light-absorbing chromophoric acceptor.[8] Photogeneration of the SQP in a magnetic field, B_0, results in Zeeman splitting of the SQP triplet

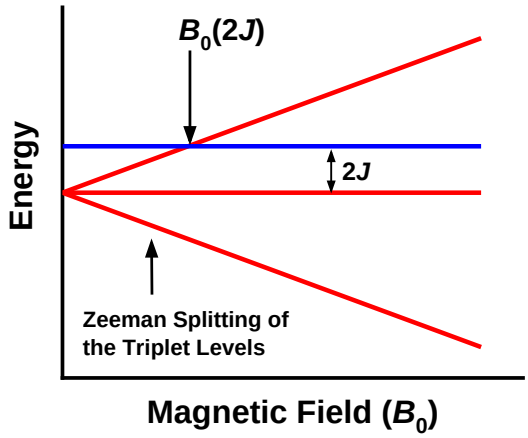

Figure 1.1. Zeeman splitting of RP energy levels (2J > 0).

sublevels (Figure 1.1), where the spin-spin exchange coupling, 2*J*, is the energy gap between the singlet and triplet SQP states. This coupling is primarily a through-bond interaction, while the corresponding spin-spin dipolar interaction, *D*, is a through-space interaction. When $B_0 >> 2J$ and *D*, the $|T_{+1}\rangle$, $|T_0\rangle$, and $|T_{-1}\rangle$ eigenstates are quantized along B_0 and the $|S\rangle$ and $|T_0\rangle$ state energies remain field invariant.[36-39] Under these conditions, mixing between the initially-populated $|S\rangle$ and unpopulated $|T_0\rangle$ states of the SQP results in zero quantum coherence between $|S\rangle$ and $|T_0\rangle$. The value of 2*J* is < 5 mT in $D^{\bullet+}$-C-$A^{\bullet-}$ and $D^{\bullet+}$-C-$A_2^{\bullet-}$ because there are a large number of bonds separating the two radicals in these triads. In addition, the value of *D* is also less than 0.2 mT because of the long distance between the two spins. Our earlier work showed that rapid electron hopping within the dimeric acceptor of $D^{\bullet+}$-C-$A_2^{\bullet-}$ results in faster decoherence of the mixed $|S\rangle$ and $|T_0\rangle$ states than in the single acceptor $D^{\bullet+}$-C-$A^{\bullet-}$ reference system.[8] This work also showed magnetic field dependent changes in the SQP population since 2*J* is comparable to both the differential hyperfine interactions and the relaxation effects between $D^{\bullet+}$-C-$A^{\bullet-}$ and $D^{\bullet+}$-C-$A_2^{\bullet-}$. In contrast, if 2*J* is large, coherent spin evolution is generally inhibited when $B_0 = 0$ and the system can remain locked in the initially populated $|S\rangle$ state for long times.[40] However, applying a

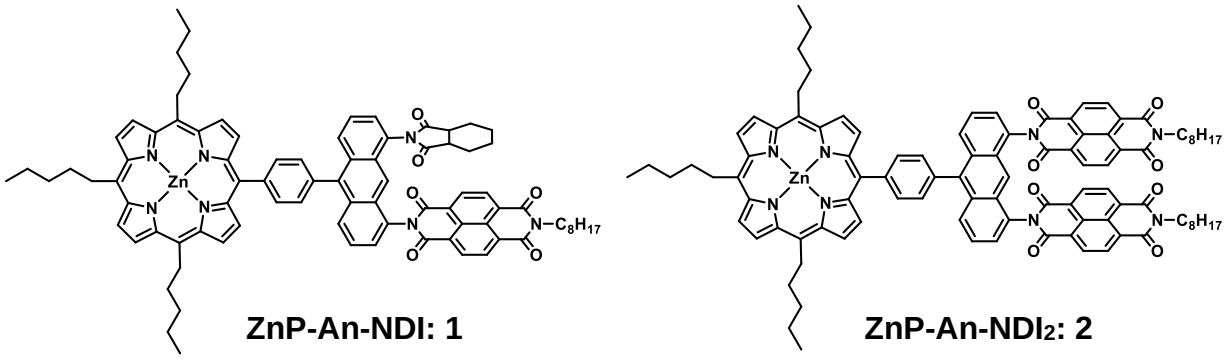

Figure 1.2. Chemical structures of molecules studied.

magnetic field $B_0 = 2J$ turns on $|S\rangle \leftrightarrow |T_{+1}\rangle$ ($2J > 0$) or $|S\rangle \leftrightarrow |T_{-1}\rangle$ ($2J < 0$) spin mixing, which allows one to probe the spin dynamics of the system.

To explore charge transfer and spin coherence in a system where $2J$ is much larger than the hyperfine interactions, recombination is slow, and a local triplet state is energetically favorable, we designed a covalent D-A_2 molecule comprising a zinc 5,10,15-tri(*n*-pentyl)-20-phenylporphyrin (ZnP) chromophoric electron donor and one or two NDI electron acceptors linked by an anthracene (An) spacer, ZnP-An-NDI (**1**) and ZnP-An-NDI_2 (**2),** respectively (Figure 1.2). Compound **2** has two π-stacked NDI acceptors, while **1** has a photo- and electro-chemically innocent 1,2-cyclohexanedicarboximide in place of the second NDI acceptor. The An spacer places the two NDI acceptors of **2** in a π-stacked geometry,[41] which has been shown previously to result in significant electronic coupling between them.[42] The combination of the ZnP donor and NDI acceptor(s) yields a large free energy of reaction for charge separation and the An spacer places the SQP sufficiently close to ensure large $2J$ values.[43, 44] The energy of the ZnP triplet state is 1.6 eV,[45] which opens a triplet charge recombination pathway and enables the direct measurement of $2J$ using magnetic field-resolved transient absorption spectroscopy. The measured $2J$ values, in combination with transient infrared absorption measurements and theoretical analysis, allow us to assess the influence of quantum coherence on the charge recombination and spin dynamics of the SQP in **2.**

1.3 Methods

1.3.1 Steady-State Spectroscopy. UV-visible absorption spectra were obtained using a Shimadzu UV-1800 spectrometer in a quartz cuvette with a 1 mm path length.

1.3.2 Transient Absorption Spectroscopy. Femtosecond transient absorption experiments were performed using the instruments described in previous accounts.[46] The 560 nm ~100 fs pump pulse was generated using a commercial collinear optical parametric amplifier (TOPAS-Prime, Light-Conversion, LLC) while the 414 nm pump was the second harmonic of the fundamental. The pump pulse was depolarized to suppress polarization-dependent dynamics in the signal. The pump pulses had energies of 1 μJ/pulse. Spectra were collected using a customized Helios/EOS spectrometer (Ultrafast Systems, LLC). All transient absorption data sets were collected on samples with a path length of 1 mm and an optical density of ~0.5 at 414 nm for the toluene data and ~0.25 at 560 nm for the 1,4-dioxane-d_8 data. All samples were put through three freeze-pump-thaw cycles to remove oxygen. Solution samples were stirred during run time to avoid degradation from localized heating. All datasets were background-subtracted to remove scatter from the pump pulse and corrected for time zero offsets and group delay dispersion using Surface Xplorer (Ultrafast Systems, LLC). The datasets were then each subjected to a global wavelength fitting analysis using a sequential 2-step model: A → B → C for the femtosecond transient absorption data and B → C → G for the nanosecond transient absorption data. For fitting the femtosecond transient absorption data, the rate constant k_{BC} was fixed at the value obtained from the nanosecond transient absorption data fit. The kinetic traces were fit at 5-6 wavelengths across the relevant spectral features of the species formed in each of the experiments.

1.3.3 Transient Femtosecond Infrared Spectroscopy. The femtosecond time-resolved infrared (fs IR) absorption apparatus has also been described previously, and was equipped with a Helios-FIRE IR spectrometer (Ultrafast Systems, LLC).[47] The 560 nm excitation pulses were attenuated

to 2 μJ/pulse and depolarized. The time resolution was ~500 fs. Difference spectra were obtained by modulating the pump at 500 Hz using the optical chopper in the Helios-IR spectrometer. Spectra were acquired in 1000 nm windows spanning 5600-8200 nm (1219-1785 cm^{-1}) and combined without scaling prior to kinetic analysis. The fs IR spectra were calibrated using the ground state FTIR spectra. The samples were prepared in 1,4-dioxane-d_8 with an optical density of ~0.125 at 560 nm in a demountable cell (Harrick Scientific) with a 500 μm Teflon spacer with 2 mm CaF_2 windows. The sample holder was rastered during experiments to reduce the effects of local heating. Both datasets were background-subtracted to remove pump pulse scatter and corrected for time zero offsets and group delay dispersion using Surface Xplorer (Ultrafast Systems, LLC). The datasets were then each subjected to a global wavelength fitting analysis using a sequential 2-step model: A → B → C. The kinetic traces were fit at 5 wavelengths across the relevant spectral features of the species observed in each of the experiments.

1.3.4 Magnetic Field Effects. NsTA experiments were performed to monitor the charge recombination triplet yield of ^{3*}ZnP as a function of applied magnetic field using an instrument described previously.[48] A 414 nm excitation pump pulse was used to excite the Soret band of the ZnP subunit. The optical density of the samples was ~0.5 with a 1 mm path length at 414 nm. The nsTA spectra were integrated over 450-500 nm and 0.5-10 μs at each magnetic field value to ensure that only ^{3*}ZnP was monitored. Periodically, the magnetic field was brought back to 0 mT to monitor the baseline and the ^{3*}ZnP yields were then normalized to the yield at zero magnetic field.

1.3.5 Computational Details. Molecular structures of the ground and excited state species were optimized using density functional theory (DFT) and time-dependent density functional theory

(TDDFT) with the phe0 functional and the ma-def2-SVP basis set.[49, 50] The solvent effects were included using the PCM model (for toluene). The empirical dispersion correction with the Becke-Johnson damping[51] was used in the DFT calculations. All of the computations were performed using the Gaussian 16 program.[52] The donor-acceptor electron transfer coupling was computed using the generalized Mulliken-Hush approach[53] with TDDFT computed dipole moments and transition dipole moments. The transition dipole moments between excited states were approximated using the response functions derived from linear response TDDFT calculations, and this approximation was validated by quadratic response TDDFT computations implemented in the DALTON2018 program.[54] We benchmarked a wide range of DFT functionals and found that the donor-acceptor system of interest is best described using the pbe0 functional.

1.4 Results

1.4.1 Synthesis. Details of the synthetic procedures and characterization of **1** and **2** are given in the Supporting Information (SI).

1.4.2 Steady-State Spectroscopy. The normalized steady-state absorption spectra of **1** and **2** in toluene are shown in Figure 1.3. Both **1** and **2** have similar absorption features with the NDI vibronic progression seen at 338, 360, and 381 nm. The intensity of these features is stronger in **2** owing to the second NDI unit. The normalized absorption intensity of **2** is not exactly twice that of **1** likely because of electronic coupling due to *H*-aggregation between the two NDI units.[55, 56] The Soret band of ZnP occurs at 425 nm along with a shoulder at 404 nm. The Q(1,0) band of ZnP appears at 555 nm and the Q(0,0) band at 595 nm in both compounds. The An absorption is

observed in the UV with small contributions to the spectrum between 300-350 nm that overlaps with the 338 and 360 nm NDI absorptions.[57]

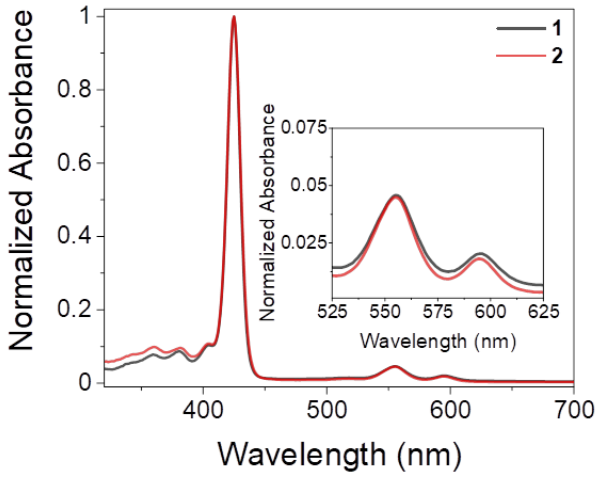

Figure 1.3. Normalized steady-state UV-visible absorption of 1 and 2 in toluene at 295 K. Inset expands the ZnP Q-band region of the spectra.

1.4.3 Transient Absorption Spectroscopy. Femtosecond and nanosecond transient absorption spectroscopies, fsTA and nsTA, respectively, were used to elucidate the excited-state dynamics of **1** and **2**. The excited singlet state of ZnP (^{1*}ZnP) was populated by exciting the Soret band using 414 nm laser pulses. Experiments were carried out in toluene at 295 K under a nitrogen atmosphere. The fsTA spectra for **1** and **2** (Figure 1.4) have many of the same spectral features; however, the excited-state dynamics are different. Immediately after photoexcitation, the spectra show features of ^{1*}ZnP; namely, excited-state absorptions at 380, 459, and 1281 nm; ground-state bleaching of the Soret band at 425 nm; ground-state bleaching of the Q(1,0) band at 554 nm, overlapping ground-state bleaching and stimulated emission of the Q(0,0) band at 595 nm; and stimulated emission of the Q(1,0) band at 652 nm. As the features of ^{1*}ZnP decay, the absorption

features of $ZnP^{\bullet+}$ at 411 nm and $NDI^{\bullet-}$ at 473 and 608 nm, as well as the ground-state bleaches of NDI at 357 and 399 nm appear, which together are indicative of charge separation. This charge-separated species is present throughout the ~8 ns pump-probe time delay range of the fsTA experiment and is the first species observed at the start of the nsTA experiment. At these longer times, the features of ^{3*}ZnP appear as positive absorptions at 391 and 458 nm as the SQP features decay.

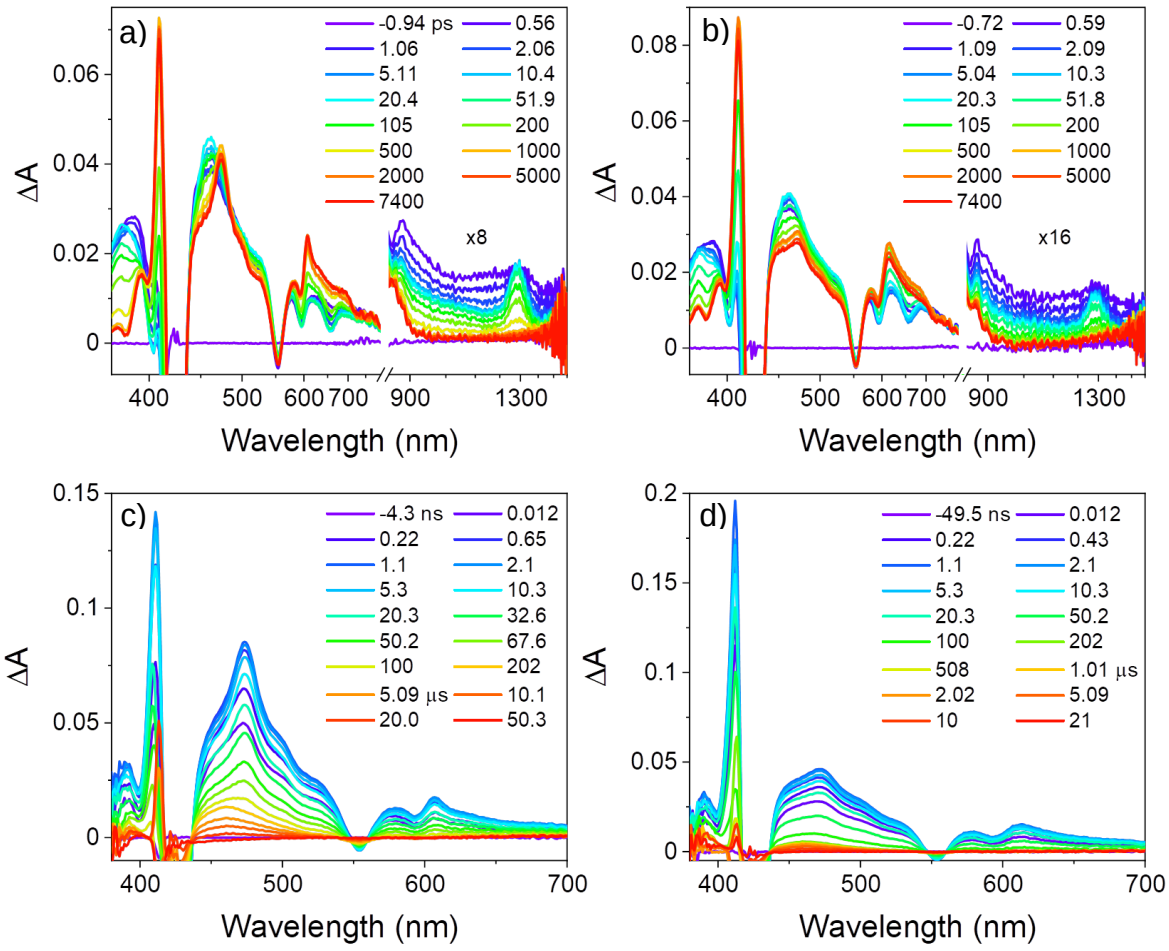

Figure 1.4. Transient absorption spectra at 295 K in toluene. FsTA spectra for (a) **1** and (b) **2**. NsTA spectra for (c) **1** and (d) **2**.

The fsTA and nsTA data were subjected to global analysis with states A, B, C, and G representing the ^{1*}ZnP, ZnP$^{\bullet+}$-An-NDI$^{\bullet-}$ or ZnP$^{\bullet+}$-An-NDI$_2^{\bullet-}$, ^{3*}ZnP and the ground states, respectively. The evolution-associated spectra (EAS) along with kinetic fits and model populations are shown in Figures S1.1-S1.2. The effective ^{1*}ZnP decay rate constant k_{AB} is the sum of the rate constants for the processes indicated in Figure 1.5. The rate constant k_{BC} is a composite of several processes involving the SQP including charge recombination from the singlet and triplet SQP states to the ground state (k_{CRS}) and ^{3*}ZnP (k_{CRT}), respectively, and spin mixing of the singlet and

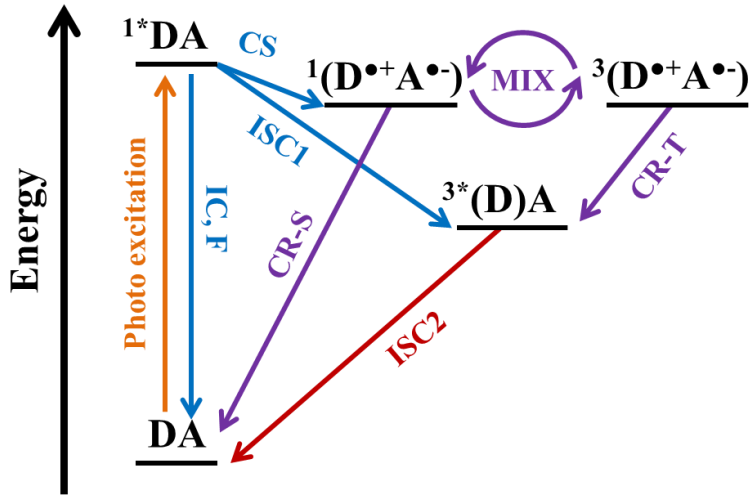

Figure 1.5. Jablonski diagram for 1 and 2. IC = Internal Conversion, F = Fluorescence, CS = Charge Separation, ISC = Intersystem Crossing, MIX = Singlet-Triplet SQP Spin Mixing, CRS = Charge Recombination to Singlet, CRT = Charge Recombination to Triplet.

Table 1.1. Rate constants in toluene at 295 K obtained from the transient absorption spectroscopy data. k_{AB} values are from the fsTA data, while k_{BC} and k_{CG} values are from the nsTA data.

Rate Constant	**1 (s^{-1})**	**2 (s^{-1})**
k_{AB}	$(3.20 \pm 0.01) \times 10^9$	$(8.90 \pm 0.05) \times 10^9$
k_{BC}	$(2.71 \pm 0.05) \times 10^7$	$(2.16 \pm 0.05) \times 10^7$
k_{CG}	$(8.26 \pm 0.03) \times 10^4$	$(7.70 \pm 0.01) \times 10^4$

triplet SQP states which can be kinetically modeled using an equilibrium constant (K_{MIX}).[58, 59] The rate constant k_{CG} captures the decay of ^{3*}ZnP to the singlet ground state (k_{ISC2}). A summary of the rate constants obtained from global fitting are given in Table 1.1.

1.4.4 Magnetic Field Effects. NsTA measurements show that the ^{3*}ZnP yield resulting from charge recombination within the ^{3}(ZnP$^{\bullet+}$-An-NDI$^{\bullet-}$) and ^{3}(ZnP$^{\bullet+}$-An-NDI$_2^{\bullet-}$) SQPs is magnetic field dependent (Figure 1.6). The Zeeman interaction changes the energies of the $|T_{+1}\rangle$ and $|T_{-1}\rangle$ states of these SQPs,[37] which results in an observed resonance in the ^{3*}ZnP yield at the magnetic field where $|T_{+1}\rangle$ crosses $|S\rangle$ ($2J > 0$) that directly yields $2J$ (Figure 1.1).[37, 60] Fitting the data to Lorentzian functions gives maxima at $2J_1$ = 210 mT for ^{3*}ZnP-An-NDI and $2J_2$ = 236 mT for ^{3*}ZnP-An-NDI$_2$ (Figure 1.6).

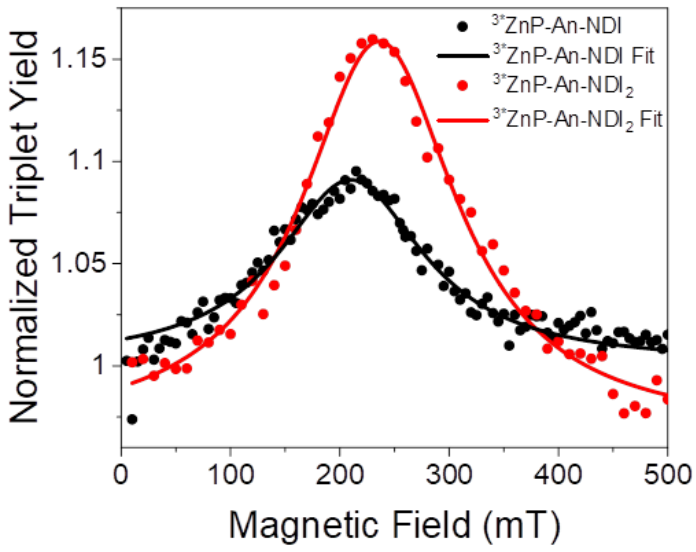

Figure 1.6. Magnetic field dependence of the normalized yield of ^{3*}ZnP-An-NDI and ^{3*}ZnP-An-NDI$_2$ in toluene at 295 K with associated fits.

1.5 Discussion

1.5.1 Charge Transfer Dynamics. The charge separation rate constants (k_{CS}) of **1** and **2** are obtained by subtracting the rate constant for the decay of ^{1*}ZnP with no acceptors ($4.2 \pm 0.1 \times 10^8$ s^{-1})[61] from k_{AB}, which gives $(2.78 \pm 0.01) \times 10^9$ s^{-1} and $(8.48 \pm 0.05) \times 10^9$ s^{-1} for **1** and **2**, respectively, with charge separation quantum yields of 0.87 and 0.95, respectively. Given that **2** has two NDI acceptors and **1** has one NDI acceptor, using a purely statistical basis one would expect k_{CS} for **2** to be twice that of **1**, whereas it is about three times as large. The free energy changes for the charge separation reactions ^{1*}ZnP-An-NDI $\rightarrow$ ZnP$^{\bullet+}$-An-NDI$^{\bullet-}$ and ^{1*}ZnP-An-NDI$_2$ $\rightarrow$ ZnP$^{\bullet+}$-An-NDI$_2^{\bullet-}$ are ΔG_{CS} = -0.27 eV and -0.36 eV, respectively, while the total nuclear reorganization energies for these same processes are λ = 0.29 eV for **1** and λ = 0.32 eV for **2** (see SI). Comparing ΔG_{CS} to λ shows that charge separation for both molecules occurs near the maximum of the Marcus rate vs. free energy dependence.[62, 63] which suggests that a small increase in the electronic coupling matrix element, V_{CS}, for charge separation in **2** relative to **1** may be responsible for the observed k_{CS}(**2**)/k_{CS}(**1**) rate ratio. Using Equation 1.1:[64]

Equation 1.1

$$k_{CS} = \frac{2\pi}{\hbar} |V_{CS}|^2 (4\pi\lambda_S k_B T)^{-1/2} \sum_{m=0}^{\infty} (s^m e^{-s}/m!)\, e^{-(\Delta G_{CS}+\lambda_S+m\omega)^2/(4\lambda_S k_B T)}$$

where k_{CS} and ΔG_{CS} are given above, the internal and solvent reorganization energies λ_i and λ_S are obtained as described in the SI, $S = \lambda_i/\hbar\omega$, and ω is assumed to be approximately 1500 cm^{-1} as is typical for aromatic donors and acceptors, the values of V_{CS} for **1** and **2** are 2.9 cm^{-1} and 7.4 cm^{-1}, respectively.

The free energies of reaction for charge recombination to the singlet ground state are ΔG_{CRS} = -1.79 eV for $ZnP^{\bullet+}$-An-$NDI^{\bullet-}$ and -1.70 eV for $ZnP^{\bullet+}$-An-$NDI_2^{\bullet-}$, while those for charge recombination to ^{3*}ZnP (E_T = 1.6 eV) are ΔG_{CRT} = -0.19 eV and -0.10 eV, respectively (see SI). Charge recombination to the singlet ground state for both compounds falls well into the Marcus inverted region,[65, 66] while charge recombination to ^{3*}ZnP is in the Marcus normal region for both compounds, as is common for these reactions. Given the relative values of ΔG_{CRS} for ^{1}($ZnP^{\bullet+}$-An-$NDI^{\bullet-}$) and ^{1}($ZnP^{\bullet+}$-An-$NDI_2^{\bullet-}$), electron transfer theory predicts that k_{CRS} for ^{1}($ZnP^{\bullet+}$-An-$NDI_2^{\bullet-}$) should be larger than ^{1}($ZnP^{\bullet+}$-An-$NDI^{\bullet-}$), while the relative values of ΔG_{CRT} for ^{3}($ZnP^{\bullet+}$-An-$NDI^{\bullet-}$) and ^{3}($ZnP^{\bullet+}$-An-$NDI_2^{\bullet-}$) predict that k_{CRT} for ^{3}($ZnP^{\bullet+}$-An-$NDI^{\bullet-}$) should be larger than ^{3}($ZnP^{\bullet+}$-An-$NDI_2^{\bullet-}$). Thus, the fact that the overall experimental charge recombination rate constant k_{CR} for **1** is larger than that of **2** (k_{BC} in Table 1.1) suggests that $k_{CRT} > k_{CRS}$. However, one needs to be cautious because the kinetic competition between the singlet and triplet recombination pathways is also modulated by K_{MIX} between the $|S\rangle$ and $|T_0\rangle$ states.

The charge recombination dynamics are well-described by a single exponential decay process in the nsTA data. This implies either that the electron hopping rate constant, k_{hop}, between the two NDI units in **2** is either much larger than k_{CRS} and k_{CRT} or that the electron is delocalized between the two NDI units. If hopping occurs, the rate is estimated to be $k_{hop} \gtrsim 10^{10}$ s^{-1} at 295 K based on the observation of hopping in a similar covalent NDI dimer using continuous-wave electron paramagnetic resonance (CW-EPR) spectroscopy.[42] Such a rapid hopping time is well below the instrument resolution of the nanosecond transient absorption measurement (~0.6 ns) and is indeed on the same timescale or faster than the initial charge separation event, ensuring that

electron hopping is not directly observable in this experiment. Fast hopping processes have been shown to be a source of spin decoherence in SQPs.[8]

Electron delocalization between the acceptors can be probed directly using time-resolved femtosecond infrared (fsIR) spectroscopy. Charge delocalization is expected to result in a change in the vibrational frequencies associated with the dimeric acceptor compared to those of the single localized anion due to mode softening from differences in bond orders. The fsIR spectra for **1** and **2** in 1,4-dioxane-d_8 following 560 nm excitation are shown in Figures S1.7 and S1.8, respectively, and were subjected to the same kinetic analysis as the fsTA data discussed above. 1,4-Dioxane-d_8 was used instead of toluene for the fsIR and FTIR measurements to avoid the vibrational modes of toluene overlapping with our desired signals. Mode assignments and fitting information are given in the SI. The IR spectrum of ^{1*}ZnP is weak and featureless and is replaced by strong absorptions in both compounds at 1270, 1518, 1600, and 1635 cm^{-1}, along with bleaches of the NDI C=O stretches at frequencies above 1650 cm^{-1}. These features appear with k_{AB} = (3.79 ± 0.06) × 10^9 s^{-1} and (1.19 ± 0.01) × 10^{10} s^{-1}, respectively, which are very somewhat faster than the rate constants observed in toluene (Table 1.1) and then decay to a combination of ground and triplet states (Figure 1.7). The CR rate constants are also faster in 1,4-dioxane-d_8 relative to those in toluene with k_{BC} = (1.36 ± 0.01) × 10^8 s^{-1} and (1.05 ± 0.01) × 10^8 s^{-1}, respectively. The difference in rate constants between 1,4-dioxane-d_8 and toluene is likely a consequence of coordination of the Zn in the ZnP donor to an oxygen atom of 1,4-dioxane-d_8 resulting in ZnP being slightly easier to oxidize and thus ΔG_{CS} becoming more negative for both **1** and **2**, which is a well-known phenomenon for zinc porphyrins.[67] The corresponding fsTA spectra for **1** and **2** in 1,4-dioxane-d_8

are given in Figures S1.3-S1.6. A comparison of the SQP EAS (state B) of each compound shows that the spectra are nearly identical (Figure 1.7); this finding is consistent with our previous work on π-stacked acceptors.[68-70] The spectral similarity indicates that at room temperature the electron is localized on a single NDI unit and that any hopping must be occurring on a timescale slower than the vibrational periods probed and thus the electron is not delocalized between the two NDI units.

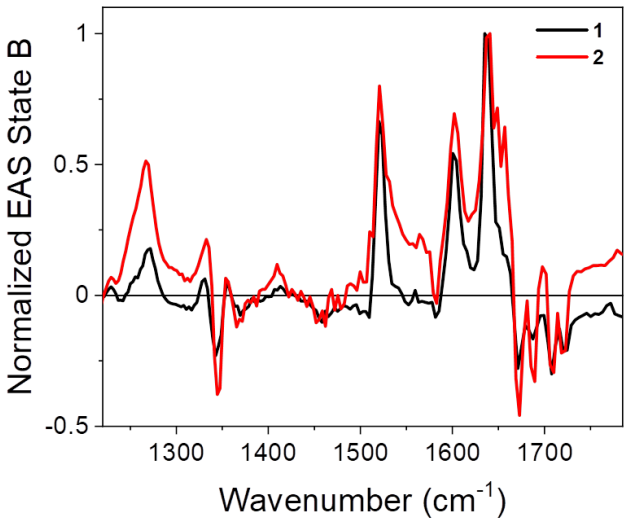

Figure 1.7. Normalized state B from the fsIR EAS for 1 and 2. Samples were prepared in 1,4-dioxane-d_8 and excited at 560 nm.

Theoretical analysis supports the extent of charge localization indicated by the IR spectra. For the equilibrium geometry of the singlet charge separated state, the singly occupied molecular orbital is only partially delocalized (Figure S1.10) between the two NDI acceptors in **2**. The computed negative charges, i.e. the Hirshfeld charge populations, are -0.77 and -0.12 for the two NDI acceptors. Stretching the structure slightly along the two NDI bending modes at an energy cost of about 300 cm^{-1} leads to essentially full charge localization. The computed singlet charge

separation couplings (Tables S1.1-S1.4) agree within factors of 3-4 with the values derived from experiment using Equation 1.1, in addition to predicting that V_{CS} (**2**) > V_{CS} (**1**). Furthermore, the computed donor-acceptor charge recombination electronic couplings, V_{CR}, (Tables S1.5-S1.8) are comparable in magnitude irrespective of whether there are one or two NDI acceptors.

Delocalization of the charge must be supported by an appropriate acceptor-acceptor coupling interaction, V_{AA}. Since thermal fluctuations tend to localize charges through modulations of the local electronic and environmental symmetries, for coherence to be maintained V_{AA} must be larger than k_BT. At the same time, the coupling cannot be so strong that the reaction free energy is dramatically changed, and the symmetric combination of acceptor orbitals is overly stabilized. Here, the splitting between the reduction potentials, $2V_{AA}$ = 90 meV,[41] shows that V_{AA} is less than two times k_BT at room temperature. While this coupling strength satisfies the first criterion, it may not be is sufficiently large to overcome the influence of thermal fluctuations that will tend to produce charge localization on a single acceptor species.

As we have discussed earlier,[11, 12] coherent charge recombination from a delocalized acceptor would result in a factor of $\sqrt{2}$ higher DA coupling compared to the case of localization on a single acceptor, and thus a factor of 2 enhancement in the recombination rate, according to Equation 1.1. However, the observed total recombination rate to the singlet ground and lowest triplet states in **2** is actually slower than in **1**. The free energies for recombination discussed above are different enough that Equation 1.1 adequately predicts the behavior of the rates in the absence of coherent delocalization on the two acceptors. Moreover, the similarity of the fsIR spectra strongly suggests that the charge has localized prior to recombination; since charge hopping

between the two NDIs is incoherent, the electron density is always restricted to one NDI unit on the vibrational time scale.

1.5.2 Spin Dynamics. Focusing on the triplet state, the ^{3*}ZnP quantum yield in the absence of the NDI acceptors that results from spin-orbit-induced intersystem crossing is 0.9.[71] Assuming internal conversion is negligible, $\phi_{ISC1} = \phi_T(1 - \phi_{CS})$, thus $\phi_{ISC1} = 0.07 \pm 0.02$ for **1** and 0.03 ± 0.02 for **2**. In contrast, the observed ^{3*}ZnP yields for **1** and **2** determined from the nsTA data and the extinction coefficients of closely related Zn porphyrins,[71, 72] are 0.95 ± 0.02 and 0.60 ± 0.02, respectively (see SI). This shows that the majority of the observed ^{3*}ZnP is derived from SQP recombination (k_{CRT}, Figure 1.5) and only a small portion of ^{3*}ZnP comes from the intersystem crossing mechanism.

The spin-spin exchange coupling 2*J* of an SQP is related to the electronic coupling matrix elements between the SQP and nearby electronic states.[73-76] Given that the principal states coupled to the SQP are the ^{1*}ZnP-An-NDI (or NDI_2) excited states that precede charge separation and the ZnP-An-NDI (or NDI_2) ground and ^{3*}ZnP-An-NDI (or NDI_2) states that result from charge recombination, then

Equation 1.2

$$2J = \frac{V_{CRT}^2}{\Delta G_{CRT} + \lambda} - \frac{V_{CRS}^2}{\Delta G_{CRS} + \lambda} - \frac{V_{CS}^2}{\Delta G_{CS} + \lambda}$$

where the indicated matrix elements V_{CS}, V_{CRS}, and V_{CRT} couple the singlet and triplet SQP states to ^{1*}ZnP, the singlet ground state, and ^{3*}ZnP, respectively, ΔG_{CS}, ΔG_{CRS}, ΔG_{CRT}, and λ were defined and given earlier, and it is assumed that λ is the same for each charge transfer process. Given that

the donor and acceptor both involve relatively large π systems, we also assume that $V_{CRS}^2 = V_{CRT}^2$ for each SQP, so that Equation 1.2 can be simplified to

Equation 1.3

$$2J = V_{CR}^2\left[\frac{1}{\Delta G_{CRT}+\lambda} - \frac{1}{\Delta G_{CRS}+\lambda}\right] - \frac{V_{CS}^2}{\Delta G_{CS}+\lambda}$$

Using V_{CS} for **1** and **2** obtained from our data and Equation 1.1, the corresponding experimental values of $2J_1$ and $2J_2$, as well as ΔG_{CS}, ΔG_{CRS}, ΔG_{CRT}, and λ for **1** and **2** given above, Equation 1.3 yields $V_{CR}(\mathbf{1})$ = 15 cm^{-1} and $V_{CR}(\mathbf{2})$ = 10 cm^{-1}, which is consistent with the observation that $k_{CR}(\mathbf{1}) > k_{CR}(\mathbf{2})$ (Table 1.1) and the computed values of V_{CR} (Tables S1.5-S1.8). As noted above, theory predicts that CR proceeding by a coherent superexchange mechanism comprising two equivalent pathways from a delocalized acceptor would give $V_{CR}(\mathbf{2}) = \sqrt{2}\,V_{CR}(\mathbf{1})$.[41, 77-79] Based on free energy, reorganization energy, and V_{CS} estimates described above, we found $V_{CR}(\mathbf{2})$ = 0.67 $V_{CR}(\mathbf{1})$, meaning CR for **2** is not an electronically coherent process. Nevertheless, our studies of related multi-acceptor systems show that incoherent electron hopping between nearly equivalent sites occurs with $k_{hop} \gtrsim 10^{10}$ s^{-1} at 295 K.[42]

Although CR is electronically incoherent, the observed magnetic field effects are consistent with CR for both **1** and **2** being spin coherent. The resonance line shapes in the magnetic field effect data (Figure 1.6) for **1** and **2** provide information on hyperfine interactions, and spin decoherence and relaxation effects.[80] Given the relatively small *g*-factor difference between the radicals that comprise each SQP, the hyperfine interaction primarily determines $|S\rangle \leftrightarrow |T_{+1}\rangle$ mixing. However, the mean hyperfine fields of **1** and **2** are only 1.46 mT and 1.38 mT, respectively,

using models[81] that employ previously-reported values for the radicals.[42, 82] Using these mean hyperfine fields and a previously reported model (see SI),[83] the resulting rate constants for hyperfine mixing of $^{1,3}(ZnP^{\bullet+}\text{-}An\text{-}NDI^{\bullet-})$ and $^{1,3}(ZnP^{\bullet+}\text{-}An\text{-}NDI_2^{\bullet-})$ are 4.1×10^6 s^{-1} and 3.9×10^6 s^{-1}, respectively. Given the similarities of the two estimated hyperfine contributions, these interactions do not adequately account for the differences in line shape and width of the field dependent ^{3*}ZnP yield data for **1** and **2** (Figure 1.6). The large full-width at half-maximum values of 163 mT for **1** and 173 mT for **2** indicate that spin decoherence contributes to line broadening to a larger degree in **2** relative to **1**.[80] Additionally, the asymmetric baseline in **2**, specifically the normalized triplet yield dropping below 1 at high magnetic fields, also supports the important role of decoherence effects.[80] Interestingly, since the D-C-A and D-C-A_2 systems studied in our previous investigation had 2*J* values that were relatively small,[8] both hyperfine interactions and relaxation effects gave rise to differences in both the shape and peak position of the 2*J* resonance. Compounds **1** and **2** provide an advantage over that earlier study in that they illustrate the fact that rapid electron hopping between the two NDI sites in **2** affects spin decoherence in a regime where the relative hyperfine interactions are not a factor.

1.6 Conclusions

Following photoexcitation of **1** and **2** in toluene at 295 K, femtosecond transient absorption spectroscopy shows that the ET rate constant for **2** is about three times larger than that of **1**, which can be accounted for by the statistical nature of incoherent ET as well as a small change in free energy of reaction. In contrast, the rate constant for CR of **1** is about 25% faster than that of **2**. Using femtosecond transient infrared spectroscopy and theoretical analysis, we find that the

electron on $NDI_2^{\bullet-}$ in **2** localizes onto one of the two NDIs prior to CR, thus precluding electronically coherent CR from $NDI_2^{\bullet-}$. Conversely, CR in both **1** and **2** is spin coherent as indicated by the observation of a resonance in the ^{3*}ZnP yield following CR as a function of applied magnetic field, giving spin-spin exchange interaction energies of $2J$ = 210 and 236 mT, respectively, where the linewidth of the resonance for **2** is greater than **1**. These data show that while CR is a spin-coherent process, incoherent hopping of the electron between the two NDIs in **2,** consistent with the lack of delocalization noted above, results in greater spin decoherence in **2** relative to **1**.

Designing D-A_2 systems that achieve coherent electron transfer at room temperature poses a particular challenge due to the localizing nature of thermal fluctuations. The requirements of $k_BT << 2V_{AA}$ and small V_{AA} necessarily restrict the operable temperature range. While lowering the temperature has been shown to enable delocalization, increasing V_{AA} will only reduce the probability for coherent electron transfer, because of the free energy effects discussed above. A balance of these factors may exist, where a carefully tuned V_{AA} would enable this process. The acceptor-acceptor coupling must be modulated in such a way that the V_{DA} between the donor and each acceptor remains approximately equal. This constraint rules out the use of asymmetric spacers and typical slip-stacking strategies, which would bias one acceptor in favor of another. Alternatively, modification of the solubilizing tails or side groups could splay the acceptors slightly, lessening their electronic coupling. The use of a different linker group, where the acceptors are non-cofacially oriented could also be used to greater effect, although this would also

impart greater flexibility and disorder, which could also disrupt the required degeneracy. Overall, much work needs to be done to identify molecules that meet all of these requirements.

1.7 Supporting Information

1.7.1 Synthesis and Characterization

Reagents and solvents were purchased from commercial sources and used as received unless otherwise noted. Compounds **A, B,** and **C** were synthesized according to existing literature procedures.[12, 84] ^{1}H and ^{13}C NMR spectra were recorded on a Varian 500 MHz spectrometer at room temperature. ^{1}H and ^{13}C chemical shifts are listed in parts per million (ppm) and are referenced to residual protons or carbons of the deuterated solvents. High Resolution Mass Spectra (HRMS) were obtained with an Agilent LCTOF 6200 series mass spectrometer using electrospray ionization (ESI) and APPI.

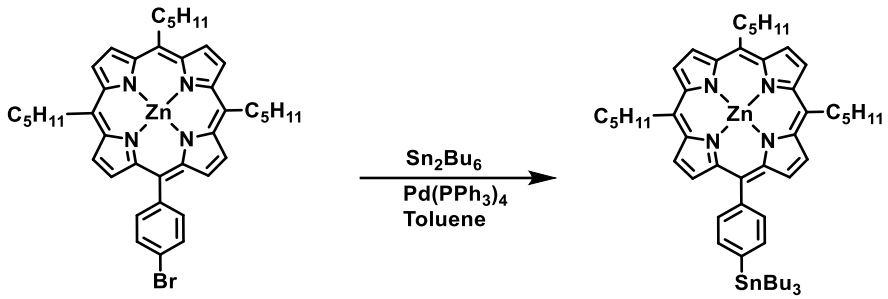

Compound A **ZnP-SnBu$_3$ 25%**

ZnP-SnBu$_3$. 158 mg of **Compound A** (0.21 mmol), 600 mg of hexabutylditin (1.05 mmol) were combined in 10 mL anhydrous toluene and this solution was purged with nitrogen for 15 min. After adding 10 mg of tetrakis(triphenylphosphine)palladium(0) (0.01 mmol) to the solution, the solution was purged with nitrogen for another 15 min. The solution was then heated at 110°C for 12 h. The reaction mixture was cooled and then the solvent was then removed by rotary

evaporation. The crude product was quickly run through a 5 cm neutral alumina plug with hexanes/DCM (90/10) as the mobile phase, yielding **ZnP-SnBu$_3$** (50 mg, 25%). The product was directly used for next step without further purification due to lack of stability.

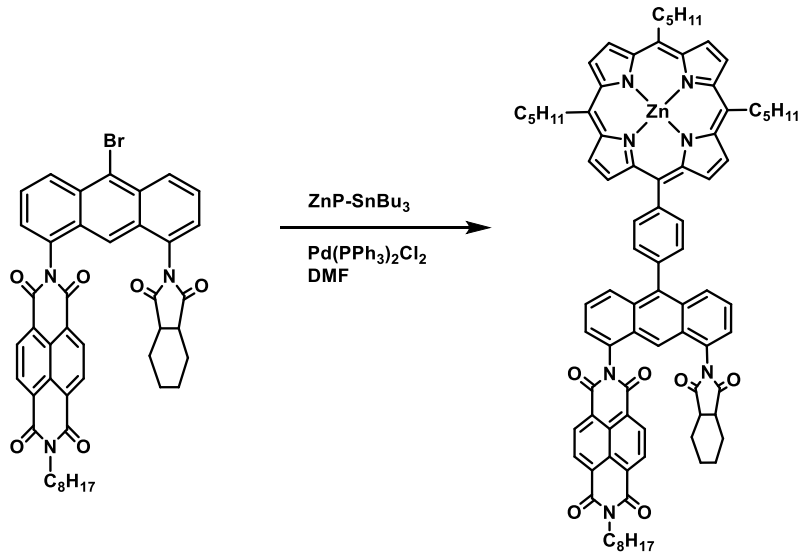

Compound B **ZnP-An-NDI (1) 25%**

ZnP-An-NDI (1). 36 mg of **ZnP-SnBu$_3$** (0.038 mmol), 20 mg of **Compound B** (0.025 mmol) were combined in 10 mL anhydrous DMF and this solution was purged with nitrogen for 15 min. After adding 3 mg of Bis(triphenylphosphine)palladium(II) dichloride (0.004 mmol) to the solution, the solution was purged with nitrogen for another 15 min. The solution was then heated at 80°C for 16 h. The reaction mixture was cooled and then the solvent was then removed by rotary evaporation. The crude product was first purified by silica gel column chromatography with hexanes/ethyl acetate (70/30) as the mobile phase. The resulting product was again purified by neutral alumina column chromatography with DCM/ethyl acetate (90/10) as the mobile phase yielding **1** (13 mg, 25%). ^{1}H NMR (500 MHz, $CDCl_3$): δ 9.64 (s, 6H), 9.20-9.16 (m, 4H), 8.91 (d, *J* = 7.5 Hz, 2H), 8.86 (d, *J* = 7.5 Hz, 2H), 8.46 (d, *J* = 7.5 Hz, 2H), 8.37 (d, *J* = 8.5 Hz, 1H), 8.29

(d, *J* = 8.5 Hz, 1H), 8.13 (s, 1H), 7.88 (d, *J* = 7.5 Hz, 2H), 7.81-7.75 (m, 2H), 7.68-7.62 (m, 2H), 7.39 (d, *J* = 7.5 Hz, 2H), 5.07-5.02 (m, 5H), 4.31-4.27 (m, 3H), 3.71-3.68 (m, 2H), 2.92-2.88 (m, 1H), 2.63-2.58 (m, 5H), 1.91-1.78 (m, 9H), 1.65-1.55 (m, 7H), 1.45-1.25 (m, 13 H)1.05-1.01 (m, 8H), 0.93-0.88 (m, 4H). ^{13}C NMR was not obtained due to aggregation in highly concentrated solution. HRMS (m/z) for $C_{85}H_{83}N_7O_6Zn$ calculated: 1361.56963, found: 1361.57197.

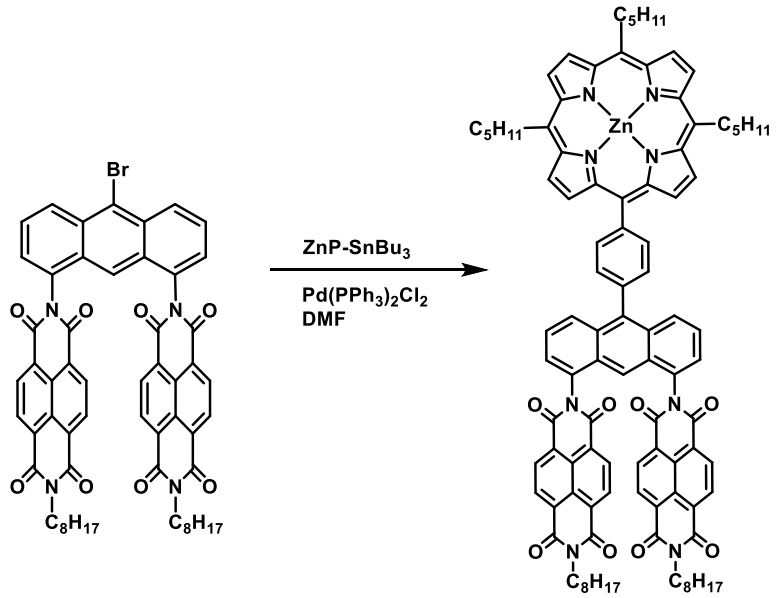

ZnP-An-NDI$_2$ (2). 36 mg of **ZnP-SnBu$_3$** (0.038 mmol), 25 mg of **Compound C** (0.025 mmol) were combined in 10 mL anhydrous DMF and this solution was purged with nitrogen for 15 min. After adding 3 mg of Bis(triphenylphosphine)palladium(II) dichloride (0.004 mmol) to the solution, the solution was purged with nitrogen for another 15 min. The solution was then heated at 80°C for 16 h. The reaction mixture was cooled and then the solvent was then removed by rotary evaporation. The crude product was first purified by silica gel column chromatography with hexanes/ethyl acetate (70/30) as the mobile phase. The resulting product was again purified by

neutral alumina column chromatography with DCM/ethyl acetate (90/10) as the mobile phase yielding **2** (17 mg, 30%). ^{1}H NMR (500 MHz, $CDCl_3$): δ 9.67 (s, 4H), 9.65 (d, *J* = 5.0 Hz, 2H), 9.20 (d, *J* = 5.0 Hz, 2H), 8.45-8.40 (m, 10H),, 8.37 (d, *J* = 9.0 Hz, 1H), 7.93 (d, *J* = 8.0 Hz, 2H), 7.86 (s, 1H), 7.77 (dd, *J* = 7.0 Hz, *J* = 8.0 Hz, 2H), 7.81-7.75 (m, 2H), 7.63 (d, *J* = 9.0 Hz, 1H), 5.06-5.02 (m, 5H), 4.29-4.24 (m, 3H), 2.68-2.60 (m, 4H), 1.91-1.84 (m, 4H), 1.82-1.75 (m, 3H), 1.65-1.58 (m, 5H), 1.54-1.20 (m, 20H), 1.06-1.01 (m, 8H), 0.93-0.88 (m, 6H). ^{13}C NMR was not obtained due to aggregation in highly concentrated solution. HRMS (m/z) for $C_{99}H_{94}N_8O_8Zn$ calculated: 1586.64861, found: 1586.64549.

1.7.2 Visible and NIR Transient Absorption Spectroscopy

Toluene Data

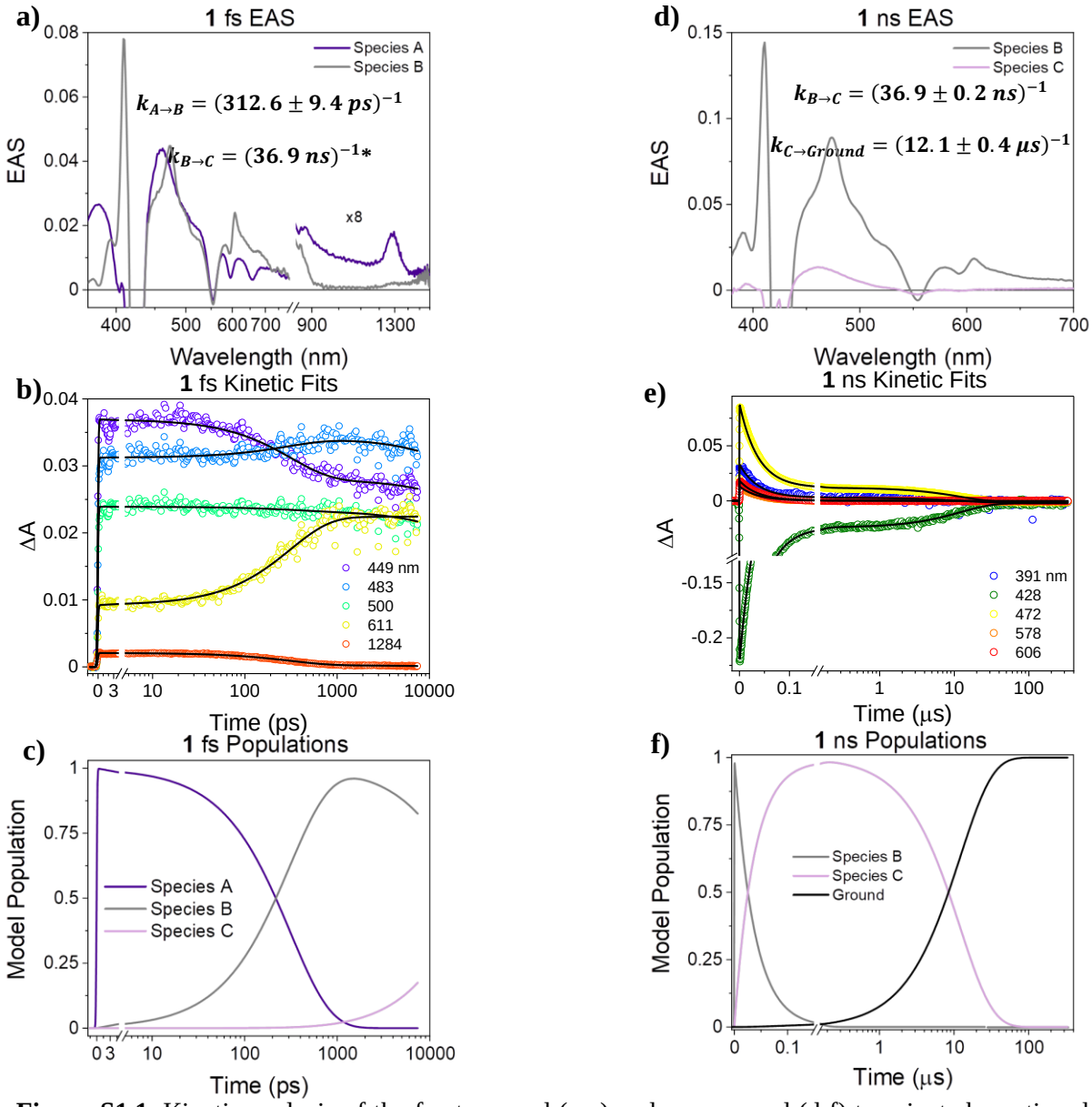

Figure S1.1. Kinetic analysis of the femtosecond (a-c) and nanosecond (d-f) transient absorption data for **1** photo excited at 414 nm in room temperature toluene. Femtosecond data were fit to an A → B → C kinetic model with the B → C rate constant held fixed from the corresponding nanosecond data fit. Nanosecond data were fit to a B → C → Ground kinetic model. (a and d) Evolution-associated spectra (EAS) with rates. Uncertainties are errors of the fits. (b and e) Kinetic time traces and their associated fits. (c and f) Population models for the species in the EAS.

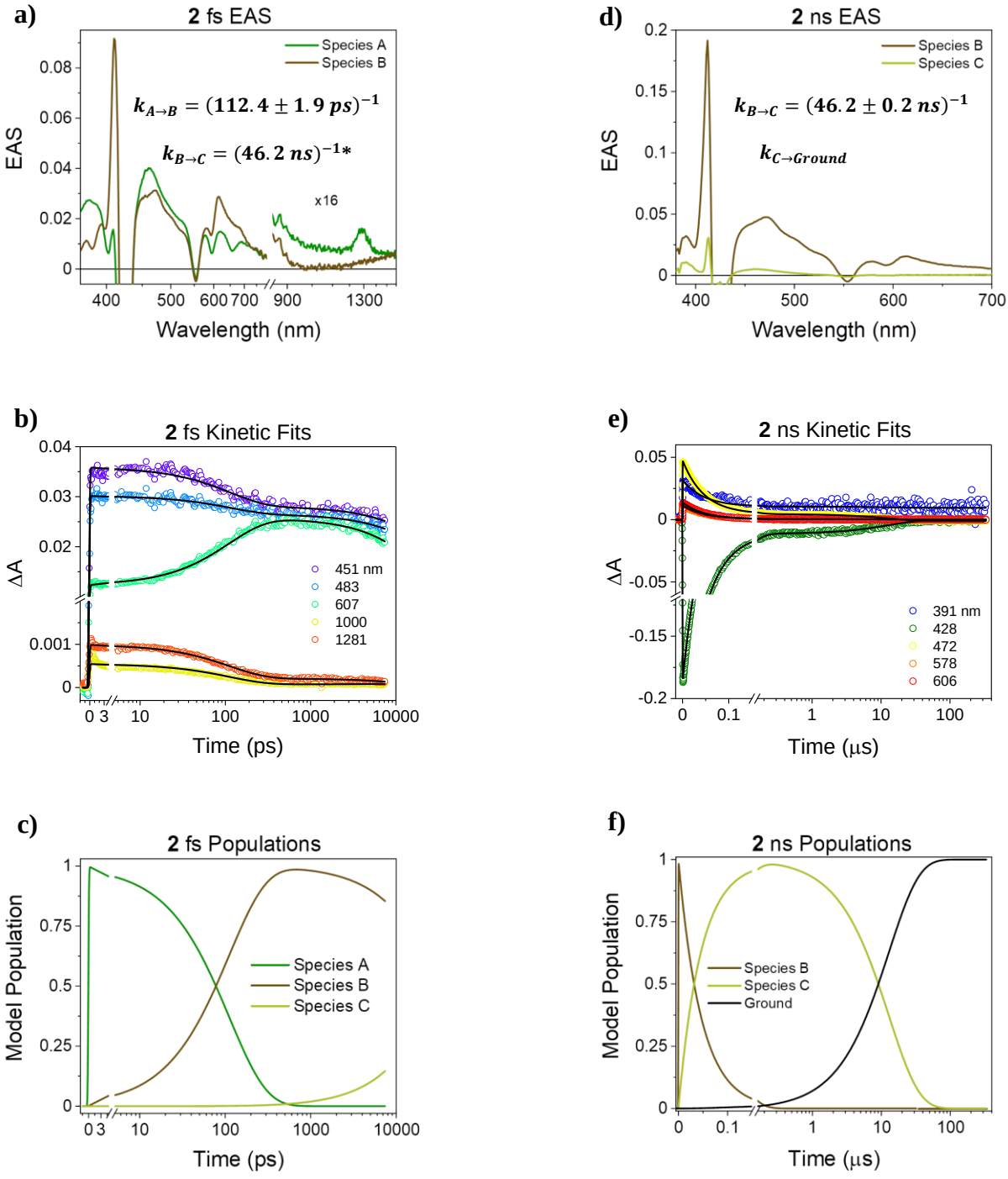

Figure S1.2. Kinetic analysis of the femtosecond (a-c) and nanosecond (d-f) transient absorption data for **2** photo excited at 414 nm in room temperature toluene. Femtosecond data were fit to an A → B → C kinetic model with the B → C rate constant held fixed from the corresponding nanosecond data fit. Nanosecond data were fit to a B → C → Ground kinetic model. (a and d) Evolution-associated spectra (EAS) with rates. Uncertainties are errors of the fits. (b and e) Kinetic time traces and their associated fits. (c and f) Population models for the species in the EAS.

1,4-Dioxane-d_8 Data

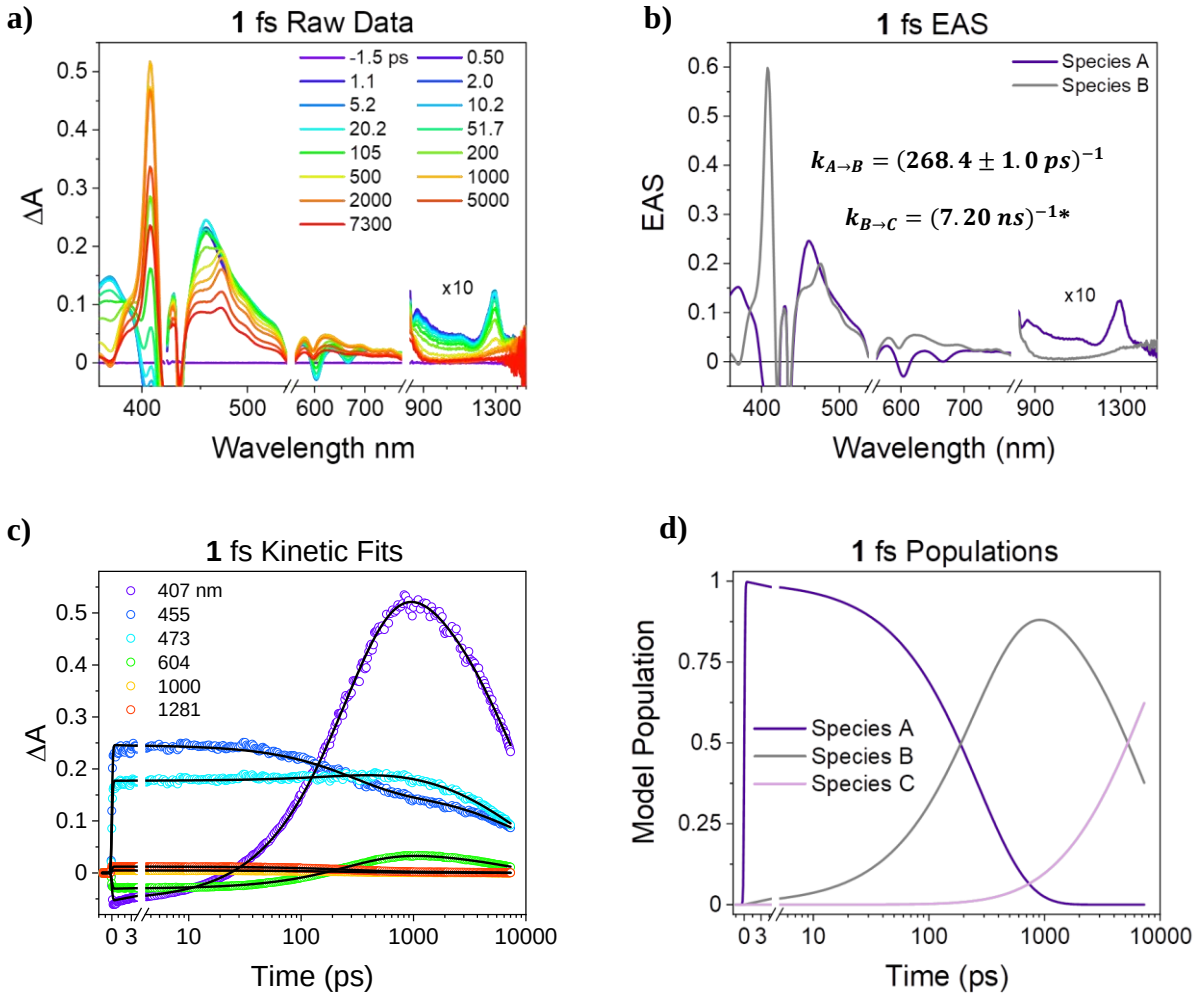

Figure S1.3. Kinetic analysis of the femtosecond transient absorption data for **1** photo excited at 560 nm in room temperature 1,4-dioxane-d_8. Femtosecond data were fit to an A → B → C kinetic model with the B → C rate constant held fixed from the corresponding nanosecond data fit (Figure S1.4). (a) Raw data with select spectral traces. Spectral features appear at approximately the same wavelengths as described in the toluene data in the main text. (b) Evolution-associated spectra (EAS) with rates. Uncertainties are errors of the fits. Particular species and associated rates are described by the same physical phenomena as outlined in the toluene data in the main text. (c) Kinetic time traces and their associated fits. (d) Population models for the species in the EAS.

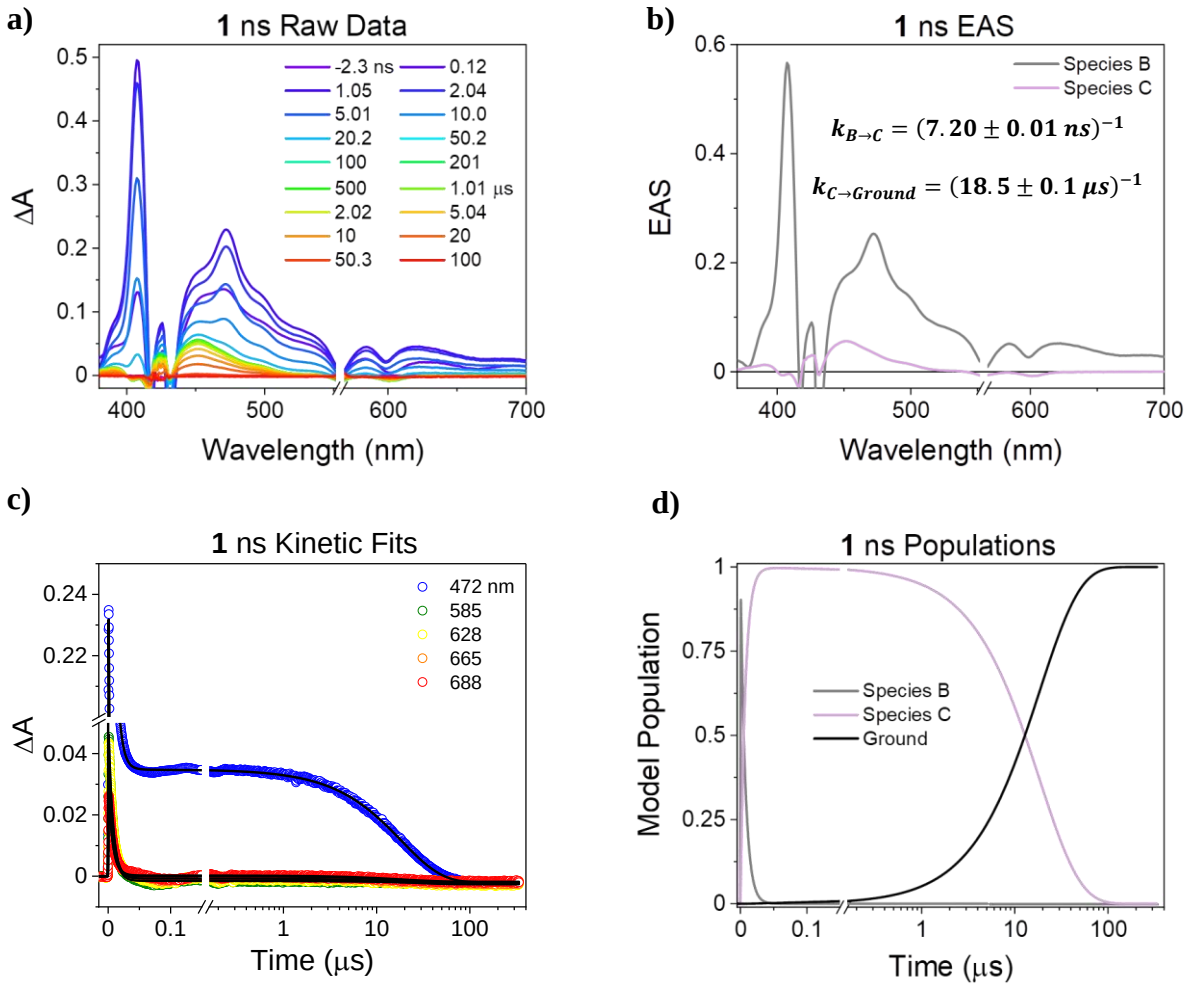

Figure S1.4. Kinetic analysis of the nanosecond transient absorption data for **1** photo excited at 560 nm in room temperature 1,4-dioxane-d_8. Nanosecond data were fit to a B → C → Ground kinetic model. (a) Raw data with select spectral traces. Spectral features appear at approximately the same wavelengths as described in the toluene data in the main text. (b) Evolution-associated spectra (EAS) with rates. Uncertainties are errors of the fits. Particular species and associated rates are described by the same physical phenomena as outlined in the toluene data in the main text. (c) Kinetic time traces and their associated fits. (d) Population models for the species in the EAS.

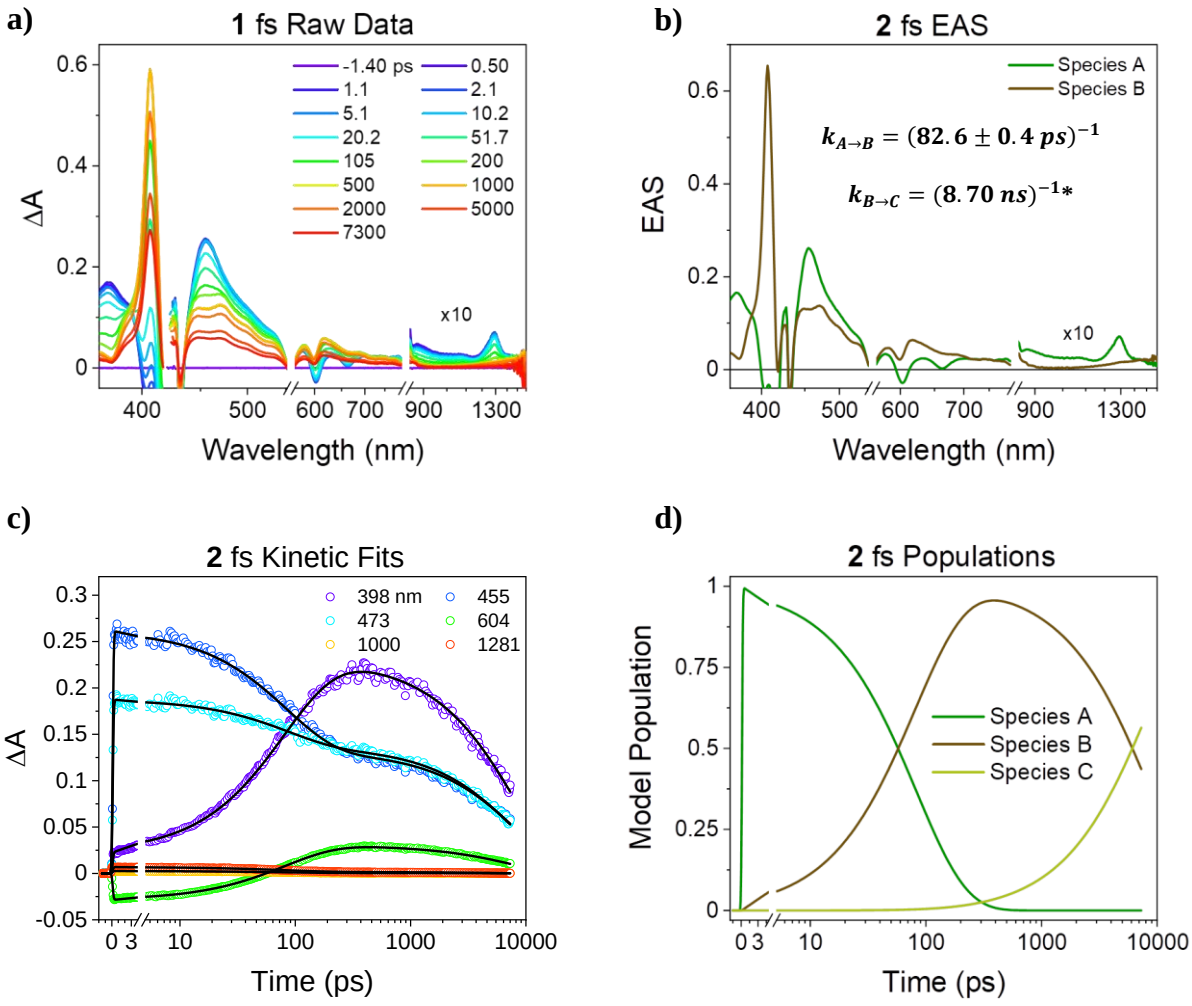

Figure S1.5. Kinetic analysis of the femtosecond transient absorption data for **2** photo excited at 560 nm in room temperature 1,4-dioxane-d_8. Femtosecond data were fit to an A → B → C kinetic model with the B → C rate constant held fixed from the corresponding nanosecond data fit (Figure S1.6). (a) Raw data with select spectral traces. Spectral features appear at approximately the same wavelengths as described in the toluene data in the main text. (b) Evolution-associated spectra (EAS) with rates. Uncertainties are errors of the fits. Particular species and associated rates are described by the same physical phenomena as outlined in the toluene data in the main text. (c) Kinetic time traces and their associated fits. (d) Population models for the species in the EAS.

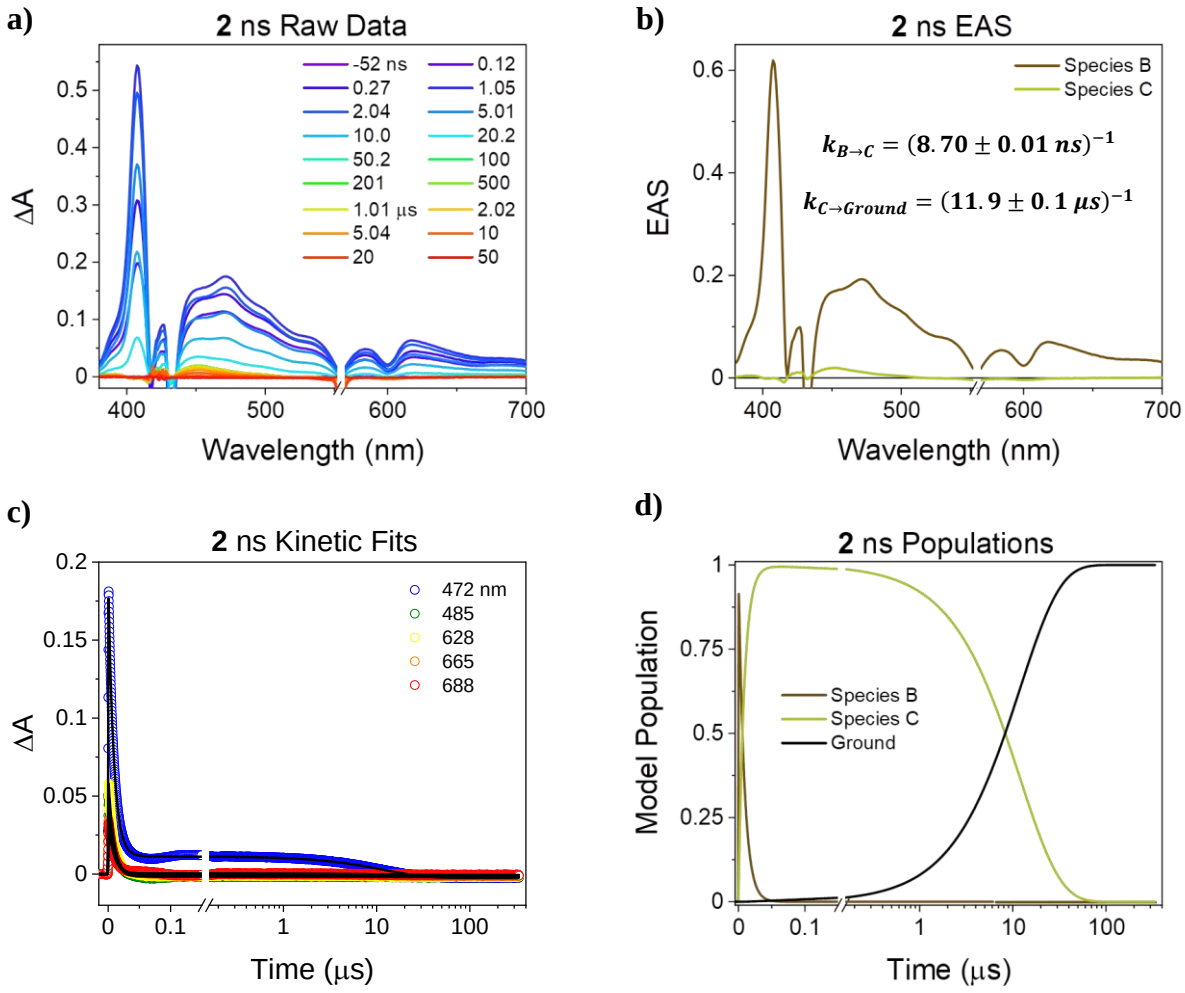

Figure S1.6. Kinetic analysis of the nanosecond transient absorption data for **2** photoexcited at 560 nm in room temperature 1,4-dioxane-d_8. Nanosecond data were fit to a B → C → Ground kinetic model. (a) Raw data with select spectral traces. Spectral features appear at approximately the same wavelengths as described in the toluene data in the main text. (b) Evolution-associated spectra (EAS) with rates. Uncertainties are errors of the fits. Particular species and associated rates are described by the same physical phenomena as outlined in the toluene data in the main text. (c) Kinetic time traces and their associated fits. (d) Population models for the species in the EAS.

1.7.3 Transient Femtosecond IR Spectroscopy

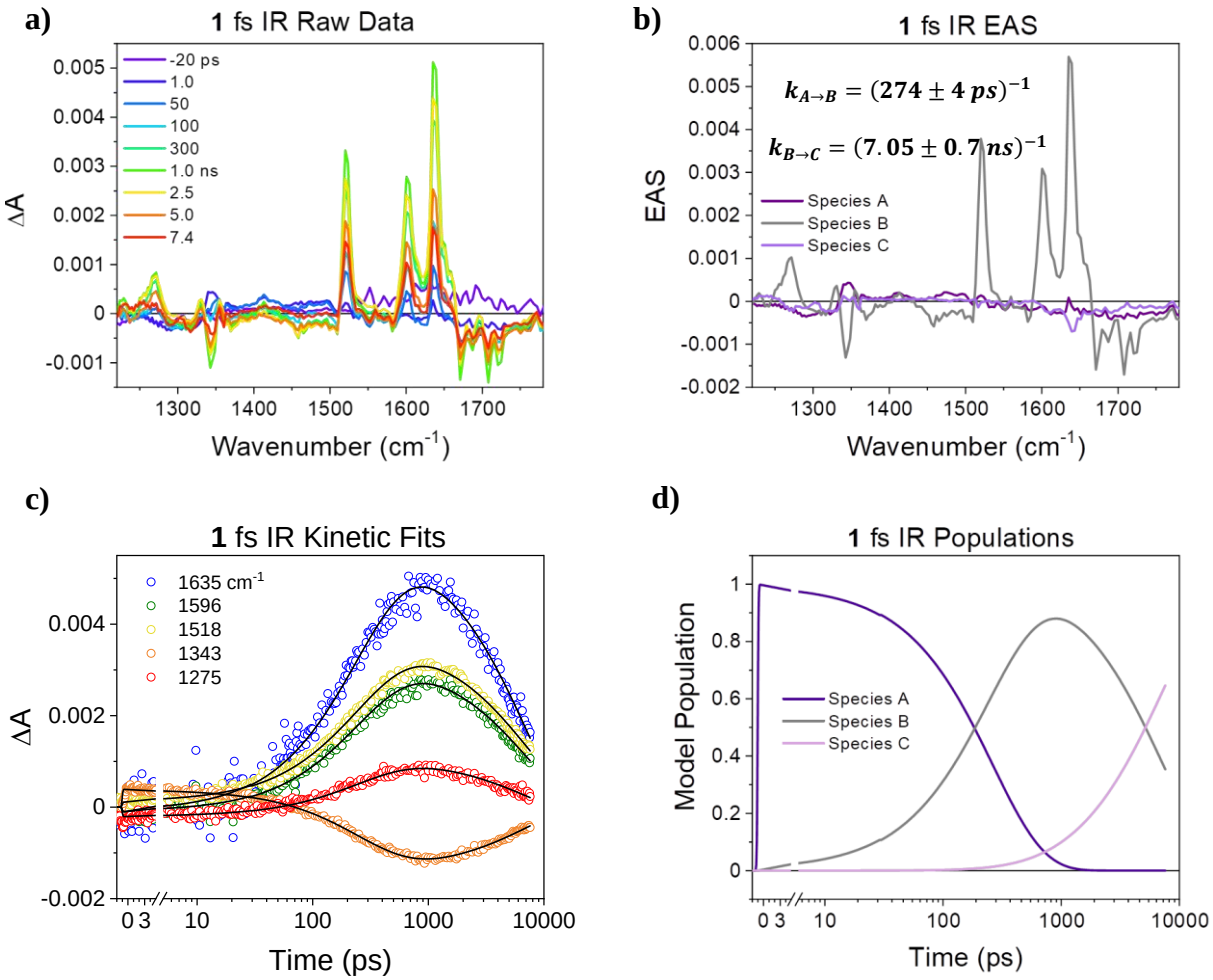

Figure S1.7. Kinetic analysis of the corrected (see Figure S1.9) femtosecond infrared transient absorption data for **1** photo excited at 560 nm in room temperature 1,4-dioxane-d_8. Femtosecond data were fit to an A → B → C kinetic model. (a) Raw data with select spectral traces. (b) Evolution-associated spectra (EAS) with rates. Uncertainties are errors of the fits. Particular species and associated rates are described by the same physical phenomena as outlined in the toluene data in the main text. (c) Kinetic time traces and their associated fits. (d) Population models for the species in the EAS. See section 1.7.8 for mode assignments.

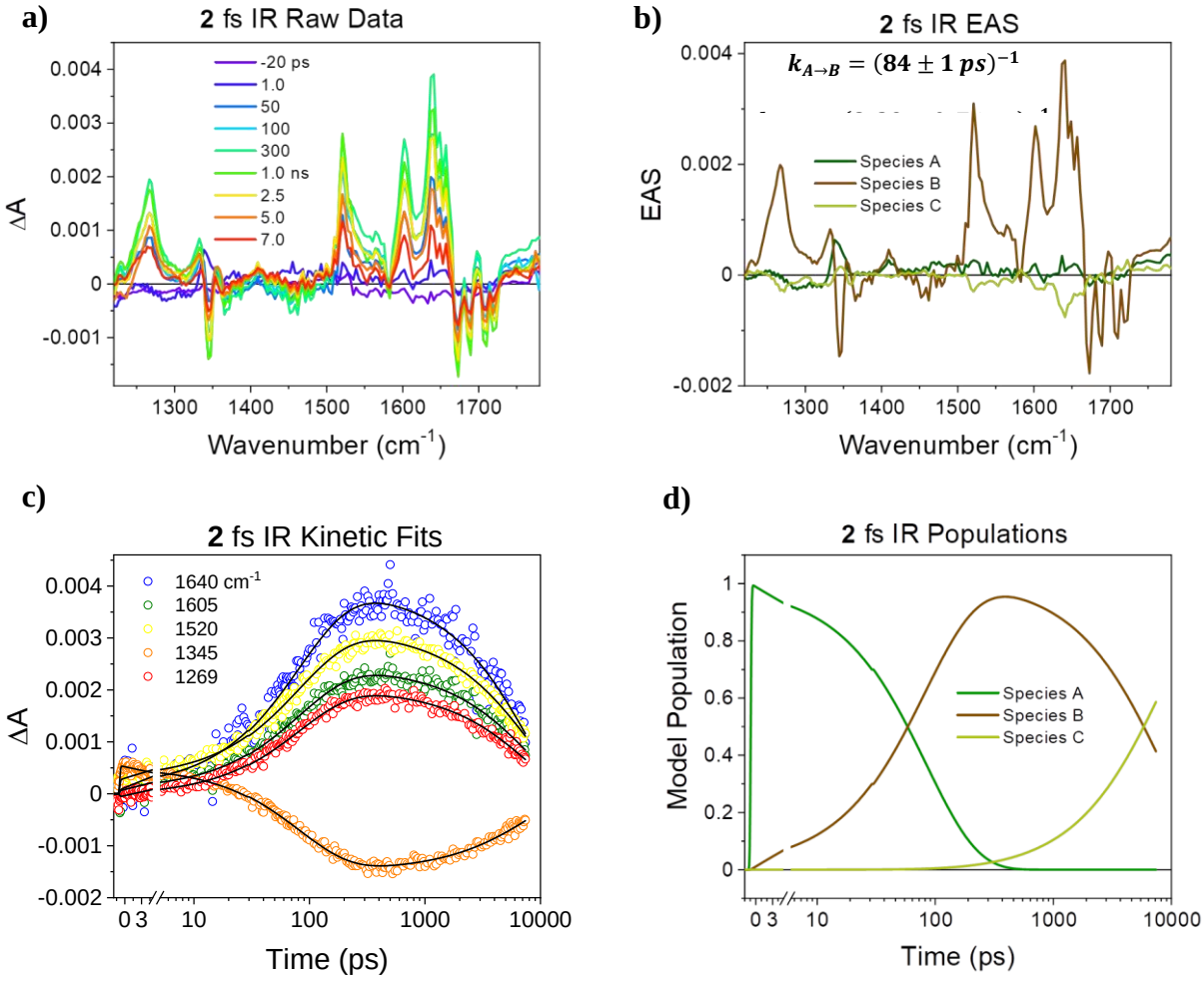

Figure S1.8. Kinetic analysis of the corrected (see Figure S1.9) femtosecond infrared transient absorption data for **2** photo excited at 560 nm in room temperature 1,4-dioxane-d_8. Femtosecond data were fit to an A → B → C kinetic model. (a) Raw data with select spectral traces. (b) Evolution-associated spectra (EAS) with rates. Uncertainties are errors of the fits. Particular species and associated rates are described by the same physical phenomena as outlined in the toluene data in the main text. (c) Kinetic time traces and their associated fits. (d) Population models for the species in the EAS. See section 1.7.8 for mode assignments.

1.7.4 Fourier-Transform IR (FT-IR) Spectroscopy

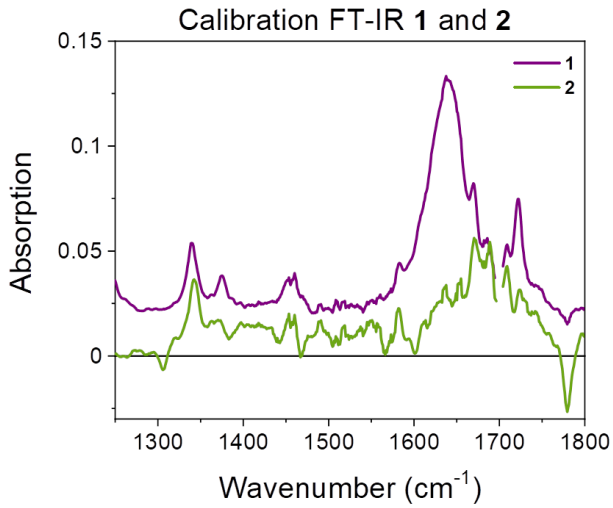

Figure S1.9. FT-IR steady-state spectroscopy data for **1** and **2**. These data were collected in 1,4-dioxane-d_8 with an optical density of ~0.125 at 560 nm with a 500 μm path length. The fs IR data was calibrated by correlating the wavenumber of certain features in these data with those in the fs IR data. Then a quadratic relationship was established between the two data sets to correct the frequency-axes of the fs IR data. See section 1.7.8 for mode assignments.

1.7.5 Calculation of Free Energies of Reaction and Reorganization Energies

The free energy of charge separation ΔG_{CS} was computed using the formulation of Weller:[85]

Equation S1.1

$$\Delta G_{CS} = \Delta G_{IP} - E_{00} = e(E_D - E_A) - \frac{e^2}{r_{DA}\varepsilon_s} + e^2\left(\frac{1}{2r_D} + \frac{1}{2r_A}\right)\left(\frac{1}{\varepsilon_s} - \frac{1}{\varepsilon_{sp}}\right) - E_{00}$$

where ΔG_{IP} is the free energy of the radical ion pair, E_{00} is the energy of the donor singlet excited state, and ε_{sp} is the dielectric constant of the polar solvent used in the electrochemistry experiments for the donor and acceptor e is the charge of the electron; r_D and r_A are the radii of the donor and acceptor radical ions, respectively, and r_{DA} is the center-to-center distance between the radical ions. The one-electron oxidation potential of ZnP is E_D = 0.65 V vs. SCE in butyronitrile,[86] while the one-electron reduction potentials E_A = -0.54 V for NDI and -0.45 V for NDI_2 **(**both vs. SCE) in dichloromethane.[12] For **1** and **2**, r_D = 5.0 Å r_A = 4.3 Å and r_{DA} = 17.2 Å, were determined using DFT geometry-optimized structures. Using E_{00} = 2.06 eV,[61] we calculated $\Delta G_{CS} = -0.27$ and -0.36 eV for **1** and **2**, respectively.

The total reorganization energy for charge separation (and recombination) is the sum of the internal (λ_i) and solvent (λ_s) reorganization energies: $\lambda = \lambda_i + \lambda_s$. The internal reorganization energies λ_i were determined via density functional theory (DFT) computations (see section 1.7.8 below), giving λ_i = 0.24 eV for **1** and 0.27 eV for **2**. The solvent reorganization energy is calculated based on the dielectric continuum model:[66]

Equation S1.2

$$\lambda_s = e^2\left(\frac{1}{2r_D}+\frac{1}{2r_A}-\frac{1}{r_{DA}}\right)\left(\frac{1}{\varepsilon_{op}}-\frac{1}{\varepsilon_s}\right)$$

where ε_{op} is the high-frequency dielectric constant of the solvent, which is approximately equal to the square of the refractive index (ε_{op} = 2.25 for toluene) and ε_s is the dielectric constant of the solvent (ε_{op} = 2.38 for toluene). Using the values of r_D, r_A, and r_{DA} given above, λ_s= 0.05 eV for both **1** and **2**. Thus, the total reorganization energies are 0.29 eV and 0.32 eV for **1** and **2**, respectively.

1.7.6 Estimation of Observed ^{3*}ZnP Yield in 295 K Toluene

Using the EAS of both **1** and **2** on the nanosecond to microsecond time scale shown in Figures S4b and S6b, respectively, the initial bleach of the Q band at 555 nm (ΔA_{555}) was used to determine the initial amount of ZnP excited and the absorption band at 458 nm was used to determine the amount of ^{3*}ZnP formed. The ZnP Q-band at 555 nm has an extinction coefficient ϵ_{555} = 2.0 x 10^4 M^{-1} cm^{-1},[87] while the extinction coefficient of ^{3*}ZnP at 458 nm is 8 x 10^3 M^{-1} cm^{-1}.[71, 72] The yield of ^{3*}ZnP produced by charge recombination was calculated using the following expression:

Equation S1.3

$$\phi_T = \frac{\Delta A_{458} \cdot \epsilon_{555}}{\Delta A_{555} \cdot \epsilon_{458}}$$

1.7.7 Magnetic Field Effect Transient Absorption Experiments

Estimation of mean hyperfine fields was performed using the previously-described model[81] which includes the following equations:

Equation S1.4

$$B_{hfi} = \sqrt{3(B_1^2 + B_2^2)}$$

Each B_i is the hyperfine field of a particular radical species given by

Equation S1.5

$$B_i = \sqrt{\sum_k a_{ik}^2 I_{ik}(I_{ik} + 1)}$$

with a_{ik} being the isotropic hyperfine coupling constant of a certain nucleus *k* as part of a certain radical *i* and I_{ik} being the nuclear spin quantum number of the nucleus *k* interacting with radical *i*. Using previously-reported values,[42, 82] the hyperfine fields for the ZnP, NDI, and NDI_2 moieties were estimated as B_{ZnTAP} = 0.75 mT, B_{NDI_1} = 0.38 mT, and B_{NDI_2} = 0.27 mT. These values were then used to estimate the mean hyperfine fields as 1.46 mT for NDI1 and 1.38 mT for NDI_2.

The rate constants of hyperfine mixing were estimated using a model described previously:[83]

Equation S1.6

$$k_{hfi} \approx \frac{1}{2\pi} g \mu_B B_{hfi}$$

where *g* is the mean *g*-value of the radical, μ_B is the Bohr magneton, and B_{hfi} is the mean hyperfine field as described and estimated above. This gives estimated hyperfine mixing rate constants of 4.1 x 10^6 s^{-1} and 3.9 x 10^6 s^{-1} for ZnP-An-NDI and ZnP-An-NDI_2, respectively.

1.7.8 Results of DFT and TDDFT Computations

Internal Reorganization Energy Computations

The internal reorganization energy λ_i can be decomposed into contributions from the cation and anion moieties, $\lambda_i = \lambda_{i+} + \lambda_{i-}$, which were determined via density functional theory (DFT) computations. The calculations were performed on the molecular fragments in neutral, singly oxidized (for ZnP-Ph), and/or singly reduced (for An-NDI and An-NDI_2) states to calculate the internal reorganization energy (λ_i) of each unit. This quantity can be calculated using the single-point energies of the ionic species at their respective optimized geometries and the energies of the ionic species at the optimized neutral geometries, as shown in Equation S1.7.

Equation S1.7

$$\lambda_i^{+/-} = E_{neutral}^{+/-} - E_{opt}^{+/-}$$

where $\lambda_i^{+/-}$ is the internal reorganization energy for oxidation of the donor and reduction of the acceptor, $E_{neutral}^{+/-}$ is the energy of the oxidized donor or reduced acceptor at the neutral geometry, and $E_{opt}^{+/-}$ is the energy of the oxidized donor or reduced acceptor at the optimized ionic geometry. The ZnP cation contribution is λ_{i+}= 0.05 eV and the two NDI anion contributions are λ_{i-} = 0.19 eV for **1** and 0.22 eV for **2**. When combined, λ_i = 0.24 eV for **1** and 0.27 eV for **2**.

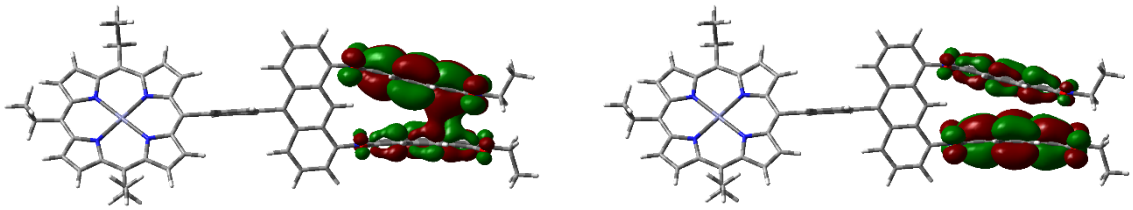

Figure S1.10. Singly occupied molecular orbitals of the lowest charge separated triplet $^{3}D^{+}A_{2}^{-}$ state computed using the pbe0 functional. The wave functions are partially delocalized between the two NDI fragments.

Computed Electronic Couplings

Table S1.1. DA_2 singlet charge separation coupling ($^{1}D^{*}A_{2} \rightarrow {}^{1}D^{+}A_{2}^{-}$) evaluated at the Franck-Condon geometry.

	LE1 (meV)	**LE2 (meV)**
CS1	1.76	0.14
CS2	0.76	0.16
CS3	0.05	0.86
CS4	0.10	0.41

Table S1.2. DA_2 singlet charge separation coupling ($^1D^*A_2 \rightarrow {}^1D^+A_2^-$) evaluated at the optimized minimum geometry of the initial locally excited state (D^*A_2, LE1).

	LE1 (meV)	**LE2 (meV)**
CS1	1.50	0.16
CS2	0.69	0.14
CS3	0.06	0.68
CS4	0.09	0.38

Table S1.3. DA charge separation coupling ($^1D^*A \rightarrow {}^1D^+A^-$) evaluated at the Franck-Condon geometry.

	LE1 (meV)	**LE2 (meV)**
CS1	2.12	0.15
CS2	0.06	1.21

Table S1.4. DA charge separation coupling ($^1D^*A \rightarrow {}^1D^+A^-$) evaluated at the optimized minimum geometry of the initial locally excited state (D^*A, LE1).

	LE1 (meV)	**LE2 (meV)**
CS1	2.08	0.93
CS2	0.41	0.98

Table S1.5. DA_2 charge recombination coupling ($^3D^+A_2^- \rightarrow {}^3D^*A_2$) evaluated at the optimized geometry of the lowest local triplet excited state ($^3D^*A_2$, LE1). LE and CS refer to the locally excited state and charge separated state respectively.

	LE1 (meV)	**LE2 (meV)**
CS1	0.62	0.76
CS2	0.28	0.49
CS3	0.14	0.29
CS4	0.12	0.15

Table S1.6. DA_2 charge recombination coupling ($^3D^+A_2^- \rightarrow {}^3D^*A_2$) evaluated at the optimized geometry of the lowest charge separated excited state ($^3D^+A_2^-$, CS1). LE and CS refer to the locally excited state and charge separated state respectively.

	LE1 (meV)	**LE2 (meV)**
CS1	2.65	1.22
CS2	0.10	0.11
CS3	0.11	0.27
CS4	0.10	0.15

Table S1.7. DA charge recombination coupling ($^3D^+A^- \rightarrow {}^3D^*A$) evaluated at the optimized geometry of the lowest locally excited state ($^3D^*A$, LE1). LE and CS refer to the locally excited state and charge separated state respectively.

	LE1 (meV)	**LE2 (meV)**
CS1	0.80	0.95
CS2	0.19	0.40

Table S1.8. DA charge recombination coupling ($^3D^+A^- \rightarrow {}^3D^*A$) evaluated at the optimized geometry of the lowest charge separated excited state ($^3D^+A^-$, CS1). LE and CS refer to the locally excited state and charge separated state respectively.

	LE1 (meV)	**LE2 (meV)**
CS1	2.90	22.38
CS2	0.40	1.47

Selected IR Peak Assignments and Intensities

Table S1.9. 1 (Ground State)

Exp. (cm^{-1})	Calc. (cm^{-1})	Strength	Intensity (km mol^{-1})	Assignment
1345	1432	strong	272.9	ZnP ω(C-H_2), An ρ(C-H)
1369	1436.9	weak	128.7	Cy. hex. dicarb. ω(C-H_2)
1455	1505	weak	319.3	NDI ν(C=C)
1584	1655	weak	196	NDI ν(C=C)
1671	1772	strong	669.8	NDI ν(C=O)
1689	1791.5	strong	374.5	NDI ν(C=O)
1709	1814.2	strong	532.2	NDI ν(C=O)
1722	1832.1	strong	218.3	NDI ν(C=O)

Table S1.10. 1 (Charge-Separated State)

Exp. (cm^{-1})	Calc. (cm^{-1})	Strength	Intensity (km mol^{-1})	Assignment
1265	1347	strong	1305.7	ZnP ω(C-H_2)
1331	1419	weak	259.3	ZnP ω(C-H_2)
1410	1478.6	weak	233.3	ZnP ω(C-H_2)
1519	1583	strong	1076.9	NDI ν(C=C)
1602	1653.2	strong	280.3	NDI ν(C=C)
1637	1701	strong	459	NDI ν(C=O)
1698	1737	strong	2408.3	NDI ν(C=O)

Table S1.11. 2 (Ground State)

Exp. (cm^{-1})	Calc. (cm^{-1})	Strength	Intensity (km mol^{-1})	Assignment
1345	1406	strong	157.6	ZnP ω(C-H_2), An ρ(C-H)
1369	1423	weak	173.2	Cy. hex. dicarb. ω(C-H_2)
1455	1507	weak	561.3	NDI ν(C=C)
1584	1657.2	weak	404.8	NDI ν(C=C)
1671	1778.3	strong	1210	NDI ν(C=O)
1689	1792.1	strong	798.2	NDI ν(C=O)
1709	1817.2	strong	1017.4	NDI ν(C=O)
1722	1831.2	strong	249.2	NDI ν(C=O)

Table S1.12. 2 (Charge-Separated State)

Exp. (cm^{-1})	Calc. (cm^{-1})	Strength	Intensity (km mol^{-1})	Assignment
1265	1321	strong	3634	ZnP ω(C-H_2)
1331	1389	weak	788.4	ZnP ω(C-H_2)
1410	1481	weak	1001.7	ZnP ω(C-H_2)
1519	1596.5	strong	892	NDI ν(C=C)
1602	1652.4	strong	1479.7	NDI ν(C=C)
1637	1743	strong	301.7	NDI ν(C=O)
1698	1775	strong	747.4	NDI ν(C=O)

Cartesian Coordinates

Optimized single NDI acceptor (DA) structure on the ground state.

C	-4.82275098	2.46200411	-0.43248448
C	-5.76573052	3.43515565	-0.57272945
C	-7.05576538	2.78476313	-0.53255464
N	-6.87715969	1.43565202	-0.37734446
C	-5.53113576	1.20928634	-0.32227114
C	-5.88651565	-3.48730143	0.18417435
C	-4.90950354	-2.54374645	0.07851540
C	-5.57421360	-1.26687977	-0.02596118
N	-6.92744053	-1.44832608	0.01230864
C	-7.15335317	-2.79283610	0.14357768
C	-4.90552842	-0.03926406	-0.16806179
C	-11.86848376	-2.39966792	0.28217358
C	-10.92329556	-3.37692597	0.36566721
C	-9.63856454	-2.73643644	0.21339696
N	-9.82232203	-1.39080127	0.04539244
C	-11.17017093	-1.15324247	0.07471022
C	-8.40752966	-3.41985613	0.23799446
C	-10.80408865	3.52738914	-0.54972685
C	-11.78288346	2.59324151	-0.39263497
C	-11.12789596	1.31375404	-0.25747134
N	-9.77245839	1.49105616	-0.32981089
C	-9.54194116	2.82787921	-0.50872576
C	-8.28689032	3.45637398	-0.62183554
C	-11.80476505	0.09357127	-0.07623552
Zn	-8.34938673	0.02116298	-0.16818537
H	-3.74243661	2.58210878	-0.40100115
H	-5.58617761	4.50245213	-0.67648826
H	-5.74362668	-4.56082477	0.28006599
H	-3.83338392	-2.69935434	0.06181260
H	-12.94481488	-2.53158741	0.35992519
H	-11.10036980	-4.43793018	0.52346918
H	-10.94423807	4.59811047	-0.67582750
H	-12.85435272	2.77566855	-0.36906773
C	-13.31270070	0.13460120	0.03470092
H	-13.73930239	-0.79302213	-0.36980056
H	-13.70980293	0.93187866	-0.60787641
C	-13.80260342	0.34081511	1.46686552
H	-14.90280764	0.36485099	1.50772572
H	-13.45475014	-0.46979651	2.12516383
H	-13.42532423	1.28777794	1.88203217
C	-8.26170693	4.96169393	-0.76651237
H	-7.38419929	5.26097260	-1.35555279
H	-9.12602769	5.29011105	-1.35975556
C	-8.25224233	5.69537862	0.57344560
H	-7.37042824	5.41762894	1.17067432

H	-8.23387893	6.78645136	0.42552024
H	-9.14443454	5.44700272	1.16813295
C	-8.43385496	-4.91629963	0.45504813
H	-9.33203703	-5.34255715	-0.01177055
H	-7.59166254	-5.38081196	-0.07558655
C	-8.38701753	-5.31029216	1.93028266
H	-9.24452185	-4.89278779	2.47969309
H	-8.40765592	-6.40510639	2.04697253
H	-7.47176659	-4.93352000	2.41170108
C	-3.41639304	-0.06446761	-0.15773755
C	-2.68771870	0.21520247	-1.32063273
C	-2.71287884	-0.37007819	1.01406345
C	-1.29514102	0.18905885	-1.31322801
H	-3.22334185	0.44919607	-2.24370994
C	-1.32023271	-0.39520146	1.02368360
H	-3.26801963	-0.58498204	1.93022698
C	-0.59535318	-0.11645018	-0.14049855
H	-0.73941779	0.40435972	-2.22905574
H	-0.78386839	-0.63169116	1.94581130
C	0.89155110	-0.14683720	-0.13177466
C	1.61379900	1.00706351	0.23932998
C	1.56820110	-1.33051455	-0.49292188
C	3.05095218	0.96921264	0.24204667
C	0.96738524	2.22760258	0.60517617
C	3.00463860	-1.35070636	-0.48157455
C	0.87867809	-2.52482707	-0.86840605
C	3.77054737	2.14871338	0.62130220
C	3.70832929	-0.20288485	-0.12267758
C	1.69435048	3.33430221	0.95564153
H	-0.12304399	2.26540804	0.60033858
C	3.67548097	-2.56571389	-0.83449984
C	1.56437384	-3.66105130	-1.20762117
H	-0.21233161	-2.51825478	-0.88009806
C	3.11466929	3.29756538	0.96733084
H	4.79590769	-0.21669098	-0.11984575
H	1.18366361	4.25918132	1.23091650
C	2.98570482	-3.68766600	-1.18808607
H	1.01924363	-4.56325084	-1.49182174
H	3.68836761	4.18248218	1.24776763
H	3.52790477	-4.59800319	-1.44834483
C	5.96373727	1.46022826	1.57227621
C	5.96199527	2.57911107	-0.46642217
N	5.19113159	2.09957339	0.59935928
O	5.52017010	0.90702935	2.54674352
O	5.54038599	3.25108748	-1.37180097
C	5.68438343	-2.76390867	0.48411030
C	5.77857598	-2.05825031	-1.90799988
C	7.08992234	-2.32225725	0.65508451
C	7.19355419	-1.65413599	-1.71562054

C	7.79052042	-1.76354310	-0.43841633
C	7.68540169	-2.39411510	1.90198581
C	7.89555713	-1.08935885	-2.76687447
C	9.10211819	-1.26275098	-0.23978575
C	8.98699462	-1.89830694	2.09763120
H	7.11684143	-2.81718539	2.73158508
C	9.19939854	-0.60080880	-2.57033248
H	7.40828421	-1.00818425	-3.73994882
C	9.68513531	-1.33077610	1.04595580
C	9.79255866	-0.67297977	-1.32172777
H	9.45580862	-1.93282212	3.08241903
H	9.75219784	-0.13721370	-3.38901054
C	11.02932569	-0.74810868	1.27752869
C	11.14034068	-0.09115959	-1.10712757
N	11.64627302	-0.13105548	0.19019620
O	11.56979902	-0.78214541	2.36444468
O	11.77228939	0.42109356	-2.00919972
C	12.96276383	0.46805980	0.41669620
H	13.04797026	1.31502357	-0.27482407
H	12.96497484	0.84641466	1.44614034
C	14.09486527	-0.51998207	0.20229472
H	14.09701457	-0.89958889	-0.82959580
H	15.06031217	-0.02560659	0.38442848
H	14.01275569	-1.37012831	0.89465911
N	5.10830449	-2.53606627	-0.77543590
O	5.03770125	-3.24884465	1.38356928
O	5.20467111	-1.93728972	-2.96699346
C	8.49614711	2.85599394	-0.85857711
H	9.33403335	2.18278986	-1.09953476
H	8.16604359	3.29196210	-1.81391023
C	8.99201683	3.93183005	0.09832670
H	8.23425967	4.72933429	0.19783330
H	9.89072184	4.40893778	-0.32225438
C	9.28315089	3.34501932	1.47373927
H	9.69267625	4.11465079	2.14630840
H	10.05629595	2.55881063	1.39016036
C	8.01415633	2.76320660	2.07894275
H	7.27606620	3.57703116	2.19300273
H	8.18886299	2.35901749	3.08693036
C	7.41716147	1.65268864	1.19768093
H	7.96129089	0.71599192	1.37866466
C	7.35966076	2.01650899	-0.29090482
H	7.30816975	1.07662007	-0.87096856

Optimized single NDI acceptor (DA) structure of the triplet local excited state.

C	-4.87738470	2.50846907	-0.69955081
C	-5.84817813	3.43920239	-0.89869064

C	-7.12015667	2.74994606	-0.81801743
N	-6.90139977	1.41738044	-0.58768956
C	-5.54740701	1.23810652	-0.52086189
C	-5.83315161	-3.45958615	0.19662326
C	-4.86195598	-2.48588975	-0.01550004
C	-5.54313973	-1.24897959	-0.08313846
N	-6.89130328	-1.44153724	0.07184805
C	-7.07649743	-2.78800418	0.25035750
C	-4.89835375	0.01699270	-0.30091136
C	-11.80272496	-2.47053456	0.78955806
C	-10.83710666	-3.42186328	0.87910184
C	-9.58177043	-2.78515037	0.53742716
N	-9.80650518	-1.46335735	0.25346775
C	-11.15082802	-1.24143051	0.38456875
C	-8.34307709	-3.43460216	0.50046224
C	-10.89227207	3.36062735	-0.81778735
C	-11.85788312	2.41030147	-0.50420077
C	-11.16877766	1.20601362	-0.23199652
N	-9.81827387	1.39966276	-0.36815743
C	-9.63922786	2.71248376	-0.72468257
C	-8.37160080	3.36582354	-0.93458299
C	-11.81069940	-0.02917996	0.14602476
Zn	-8.35407577	-0.02135571	-0.16006750
H	-3.80211728	2.66629170	-0.66739013
H	-5.70323278	4.50461104	-1.06022571
H	-5.66286957	-4.52786151	0.30325640
H	-3.79039621	-2.63437450	-0.12279451
H	-12.86346499	-2.60278874	0.98731741
H	-10.97497517	-4.46218422	1.16326846
H	-11.07215540	4.40089236	-1.07675602
H	-12.93261073	2.56996708	-0.47471045
C	-13.30025932	0.02299871	0.36377747
H	-13.74509683	-0.95997944	0.16138041
H	-13.75200725	0.70476819	-0.36986441
C	-13.67370405	0.47157547	1.77753110
H	-14.76719311	0.52006651	1.89469512
H	-13.28064013	-0.22865178	2.53020076
H	-13.26153572	1.46692014	1.99989546
C	-8.40897283	4.84707517	-1.20644919
H	-7.53241284	5.14009697	-1.79943191
H	-9.27934161	5.07819727	-1.83628511
C	-8.46506816	5.68492092	0.07208232
H	-7.57393177	5.51459802	0.69503486
H	-8.51355757	6.75817826	-0.16775193
H	-9.34788007	5.42904281	0.67619022
C	-8.29825281	-4.90495254	0.82294045
H	-9.24483111	-5.38143612	0.53615454
H	-7.52841364	-5.38749690	0.20455320
C	-8.01367420	-5.17954332	2.30045624

H	-8.80287391	-4.75534953	2.93959356
H	-7.96411802	-6.26230447	2.49241715
H	-7.05718034	-4.73342347	2.61023075
C	-3.41473619	0.01188393	-0.29250777
C	-2.68310310	0.33980602	-1.44134936
C	-2.71452061	-0.33654722	0.87100297
C	-1.29036489	0.31634195	-1.42893763
H	-3.21472468	0.60133484	-2.35920178
C	-1.32345413	-0.34855430	0.88666615
H	-3.27229299	-0.59705814	1.77316873
C	-0.59394657	-0.02766172	-0.26504927
H	-0.73249674	0.56337350	-2.33539013
H	-0.78997218	-0.61633093	1.80185783
C	0.89188923	-0.06807702	-0.24895247
C	1.61794930	0.99746063	0.32576183
C	1.56496777	-1.17986860	-0.79892138
C	3.05453289	0.94073318	0.34914123
C	0.97750923	2.15094401	0.87426671
C	3.00066766	-1.21646845	-0.76923995
C	0.87444277	-2.29062675	-1.37593862
C	3.77855722	2.02770601	0.93814487
C	3.70751564	-0.15877551	-0.20119503
C	1.70849777	3.17217129	1.42102223
H	-0.11163876	2.20908068	0.84870517
C	3.66970199	-2.35694221	-1.31917695
C	1.55847213	-3.35697795	-1.89692618
H	-0.21627583	-2.27916877	-1.39429850
C	3.12723087	3.11130705	1.45950288
H	4.79430404	-0.18888965	-0.17832351
H	1.20192030	4.04713994	1.83303215
C	2.97928888	-3.39575416	-1.86993810
H	1.01141674	-4.19507955	-2.33298706
H	3.70377455	3.92755577	1.89793571
H	3.51995261	-4.25113966	-2.27778360
C	5.93908517	1.16287342	1.81669964
C	6.00600736	2.62261372	0.00778013
N	5.19904440	1.96392068	0.94305758
O	5.46265070	0.44621452	2.66031973
O	5.61399217	3.44094640	-0.78322220
C	5.66197854	-2.80091621	-0.03483435
C	5.78358062	-1.66257233	-2.25282915
C	7.06536296	-2.40107922	0.23106381
C	7.19306793	-1.29620093	-1.96923151
C	7.77618088	-1.64482938	-0.72902832
C	7.64879987	-2.71010075	1.44698829
C	7.90537114	-0.54299532	-2.88696242
C	9.08629325	-1.19458870	-0.42665577
C	8.94924201	-2.26498930	1.74495728
H	7.07210282	-3.28239483	2.17514255

C	9.20703134	-0.10266707	-2.58824254
H	7.42872606	-0.27887264	-3.83244487
C	9.65808811	-1.51002144	0.82680637
C	9.78835636	-0.41298537	-1.37095660
H	9.40938740	-2.48950074	2.70860717
H	9.76819889	0.50627500	-3.29883890
C	11.00392005	-0.99240087	1.17451080
C	11.13690775	0.10892852	-1.03923119
N	11.63317107	-0.18364710	0.22925830
O	11.53570578	-1.23846203	2.23814833
O	11.77844478	0.78095709	-1.82167689
C	12.95293336	0.34864342	0.57302889
H	13.04826210	1.31339147	0.06023654
H	12.95289722	0.51887442	1.65648418
C	14.07852951	-0.58825664	0.17412060
H	14.08242082	-0.76044983	-0.91177894
H	15.04677994	-0.14650753	0.45155224
H	13.98726205	-1.55589831	0.68805924
N	5.10158784	-2.34565731	-1.23848698
O	5.00475151	-3.44131874	0.75281551
O	5.22208228	-1.34879703	-3.27833496
C	8.54907606	2.98029021	-0.21968432
H	9.40730678	2.36722285	-0.53822258
H	8.25317263	3.57549161	-1.09713868
C	8.98674046	3.87356728	0.93317326
H	8.21179710	4.63304754	1.13998024
H	9.89329110	4.42688465	0.64313734
C	9.23226870	3.05376573	2.19343807
H	9.60073265	3.69498214	3.00920788
H	10.02172697	2.30310753	2.00457145
C	7.95039630	2.36084356	2.63090193
H	7.19628247	3.13476220	2.86001742
H	8.09214838	1.78295847	3.55602385
C	7.40429098	1.42193218	1.54091414
H	7.95117191	0.46980172	1.57578283
C	7.40259555	2.04447702	0.13955431
H	7.39174250	1.22370946	-0.60071889

Optimized single NDI acceptor (DA) structure of the triplet charge separated excited state.

C	-4.87171529	2.46478800	-0.70619529
C	-5.84022978	3.39989270	-0.92623937
C	-7.10536717	2.71602259	-0.84435603
N	-6.89876542	1.39077619	-0.59783305
C	-5.54916573	1.20837078	-0.52051253
C	-5.81163887	-3.46109387	0.29989431
C	-4.85418080	-2.51333782	0.08612815
C	-5.54244867	-1.25516960	-0.03387733

N	-6.88481699	-1.44286899	0.09262308
C	-7.07979881	-2.77872086	0.30761372
C	-4.89564868	-0.01923388	-0.27611615
C	-11.79333201	-2.42253495	0.73528343
C	-10.82677871	-3.37706956	0.85582228
C	-9.57381520	-2.74147915	0.54234996
N	-9.78580017	-1.42815654	0.24650094
C	-11.12979978	-1.20573221	0.34475644
C	-8.32323554	-3.40687850	0.53514908
C	-10.88093529	3.38421374	-0.84757231
C	-11.83528529	2.45935343	-0.54139931
C	-11.14647765	1.22464851	-0.27102887
N	-9.80209512	1.40953645	-0.40698718
C	-9.60973549	2.71550555	-0.75857007
C	-8.36412252	3.34788582	-0.97481771
C	-11.79054955	0.01565676	0.08742945
Zn	-8.34094461	-0.01849084	-0.17354466
H	-3.79709252	2.61975356	-0.66272022
H	-5.68798835	4.46166856	-1.10061507
H	-5.64835403	-4.52699453	0.43229152
H	-3.78140400	-2.66176063	-0.00211870
H	-12.85830223	-2.55598904	0.90450618
H	-10.97383617	-4.41578144	1.13912447
H	-11.04825325	4.42665927	-1.10449229
H	-12.90853931	2.62494343	-0.50772800
C	-13.28406745	0.05316407	0.27188960
H	-13.71443609	-0.92291738	0.01641409
H	-13.72720964	0.76271523	-0.43809927
C	-13.68376821	0.43599742	1.69887607
H	-14.77916315	0.45596725	1.79454058
H	-13.28950951	-0.28520177	2.42985374
H	-13.29876747	1.43067045	1.96766122
C	-8.37299799	4.82184483	-1.28006373
H	-7.50704112	5.07317678	-1.90536128
H	-9.25404667	5.06674458	-1.88704963
C	-8.36393826	5.68359533	-0.01504380
H	-7.46998114	5.48773751	0.59501187
H	-8.36780051	6.75026304	-0.28237094
H	-9.24634503	5.48400232	0.61043344
C	-8.31262939	-4.87323299	0.87304713
H	-9.23933359	-5.34246751	0.51979869
H	-7.50332725	-5.37273153	0.32569602
C	-8.14542272	-5.12218003	2.37423581
H	-8.96319959	-4.66312249	2.94912384
H	-8.14500626	-6.20196011	2.58222513
H	-7.19836388	-4.70255329	2.74388870
C	-3.41561232	-0.02109193	-0.26513061
C	-2.68635489	0.32985532	-1.40992429
C	-2.72120699	-0.38494480	0.89773508

C	-1.29543857	0.30233588	-1.39347970
H	-3.21453046	0.60177905	-2.32670091
C	-1.33086666	-0.38746862	0.91567194
H	-3.27756891	-0.65171500	1.79921451
C	-0.59972165	-0.05207259	-0.23084290
H	-0.73420978	0.55780852	-2.29496120
H	-0.79707791	-0.66053799	1.82860218
C	0.88555714	-0.08323446	-0.21145421
C	1.59704527	0.96263756	0.41407921
C	1.56541887	-1.16495435	-0.81016467
C	3.03363433	0.91514208	0.43763509
C	0.95062349	2.08937503	1.01007723
C	3.00112036	-1.18808156	-0.78216747
C	0.88920181	-2.25899347	-1.43429394
C	3.75204345	1.97633470	1.08047276
C	3.69644205	-0.14992322	-0.16609357
C	1.67609858	3.08867090	1.60345247
H	-0.13850309	2.14997190	0.98440031
C	3.69560955	-2.28987334	-1.38039766
C	1.59244773	-3.29038354	-1.99826541
H	-0.20151302	-2.26758126	-1.45529388
C	3.09510012	3.03282409	1.64772369
H	4.78388517	-0.17693217	-0.15376402
H	1.16352770	3.94277172	2.05105900
C	3.01387460	-3.31085682	-1.97395430
H	1.05792068	-4.11751532	-2.47060903
H	3.66697740	3.82871723	2.12718725
H	3.56616104	-4.13886190	-2.42012702
C	5.89029858	1.03816672	1.92093133
C	5.98920344	2.58967138	0.18607875
N	5.16860323	1.90377155	1.09099608
O	5.39040605	0.32796155	2.75672096
O	5.61209152	3.47432009	-0.54048557
C	5.69121104	-2.73718635	-0.11221401
C	5.77913606	-1.52496787	-2.31370966
C	7.07034294	-2.34567497	0.13519834
C	7.16381549	-1.17341157	-2.04124193
C	7.76311957	-1.56146834	-0.81785602
C	7.68733678	-2.69287182	1.35339110
C	7.87989391	-0.38097166	-2.96186107
C	9.08930242	-1.11342198	-0.51863305
C	8.96670782	-2.25658646	1.64240020
H	7.11703034	-3.29020525	2.06521982
C	9.16398081	0.04195818	-2.67495425
H	7.38573475	-0.09778544	-3.89195323
C	9.67443519	-1.45725724	0.72250515
C	9.77629355	-0.30597504	-1.45478461
H	9.44776545	-2.50119027	2.59008482
H	9.72392485	0.66767135	-3.37091605

C	10.99410932	-0.94564362	1.06778556
C	11.10280979	0.20455560	-1.13635294
N	11.61272472	-0.11974316	0.12421198
O	11.55683778	-1.19173575	2.13266336
O	11.75687176	0.90940871	-1.90272971
C	12.92684603	0.41098828	0.46613372
H	13.01815340	1.38392321	-0.03230902
H	12.94004075	0.55650024	1.55341171
C	14.05498314	-0.51257273	0.04025578
H	14.04836048	-0.65946386	-1.04954760
H	15.02710217	-0.07963795	0.32102447
H	13.96293736	-1.49255914	0.53056675
N	5.12138440	-2.25789151	-1.30849050
O	5.00995086	-3.39822646	0.66045747
O	5.16366119	-1.18699036	-3.31804452
C	8.54338253	2.84489348	-0.06789179
H	9.35140280	2.20812897	-0.45746675
H	8.25772493	3.51847305	-0.89029099
C	9.06730378	3.62249832	1.13184538
H	8.34719552	4.40868421	1.42332028
H	9.99753187	4.14093154	0.85121944
C	9.30243813	2.69575265	2.31794222
H	9.73826862	3.24884139	3.16489906
H	10.03318143	1.91378088	2.04394566
C	7.99374888	2.05162840	2.75018244
H	7.29742491	2.85060469	3.06342731
H	8.13082817	1.39631548	3.62297167
C	7.35731227	1.23055706	1.61523097
H	7.84460509	0.24786098	1.56396881
C	7.35730518	1.94658087	0.25755632
H	7.29467382	1.17436851	-0.53186034

Optimized single NDI acceptor (DA) structure of the singlet local excited state.

C	-4.87608401	2.47722294	-0.70176049
C	-5.85075533	3.41802296	-0.91058488
C	-7.11370886	2.73882210	-0.82112052
N	-6.90142972	1.40526267	-0.57854128
C	-5.54922082	1.22026690	-0.51063564
C	-5.82295283	-3.45512105	0.31744628
C	-4.86405934	-2.50653077	0.10968719
C	-5.54817818	-1.24137387	-0.01952753
N	-6.89652832	-1.43466398	0.10002113
C	-7.09589257	-2.77883635	0.31406601
C	-4.89822708	-0.01501373	-0.26733379
C	-11.81117243	-2.42947964	0.73397139
C	-10.84067967	-3.38985650	0.84648520

C	-9.58900518	-2.75651243	0.53832155
N	-9.80388972	-1.43291074	0.25033141
C	-11.14958715	-1.20919348	0.35007433
C	-8.33396630	-3.41499224	0.52782594
C	-10.89105898	3.39615326	-0.79438847
C	-11.84529098	2.46895487	-0.49385418
C	-11.16043841	1.22171667	-0.24265310
N	-9.81013285	1.41132047	-0.38415587
C	-9.61543256	2.72892301	-0.72340581
C	-8.37815032	3.36665093	-0.94136149
C	-11.80965348	0.01901509	0.09795206
Zn	-8.35371562	-0.01288221	-0.16058426
H	-3.80085971	2.63327286	-0.66971450
H	-5.70013370	4.48094915	-1.08203535
H	-5.65944934	-4.52101343	0.45491363
H	-3.79034452	-2.65699078	0.03079721
H	-12.87646471	-2.56055329	0.90590752
H	-10.98701056	-4.43027532	1.12568346
H	-11.05884415	4.44309308	-1.03443744
H	-12.91845540	2.63596728	-0.44875937
C	-13.30677826	0.04789590	0.27174383
H	-13.73075788	-0.92229618	-0.02346858
H	-13.74907307	0.77711079	-0.42072028
C	-13.73759141	0.37896560	1.70160804
H	-14.83526578	0.38086532	1.79089762
H	-13.33796400	-0.35655361	2.41614405
H	-13.36799936	1.37032500	2.00480598
C	-8.38893564	4.84581099	-1.23273945
H	-7.53228901	5.09921788	-1.87272899
H	-9.27828093	5.10074012	-1.82519718
C	-8.35528314	5.70704270	0.03116729
H	-7.45582375	5.49827132	0.62962017
H	-8.35412615	6.77776523	-0.22551423
H	-9.23058015	5.50858842	0.66778919
C	-8.32286395	-4.88785989	0.84837187
H	-9.24449132	-5.35315996	0.47241262
H	-7.50632609	-5.38039402	0.30313331
C	-8.17910215	-5.17259682	2.34445354
H	-9.00295339	-4.71894939	2.91568190
H	-8.18481880	-6.25644161	2.53810731
H	-7.23690942	-4.76024796	2.73569283
C	-3.41687435	-0.01804300	-0.26550937
C	-2.68753379	0.32910015	-1.41292078
C	-2.70528870	-0.37569911	0.89005398
C	-1.29584458	0.30594040	-1.40880950
H	-3.22369086	0.60186997	-2.32485509
C	-1.31388340	-0.38799252	0.89790863
H	-3.25635367	-0.63704032	1.79638885
C	-0.59063261	-0.05224371	-0.25296282

H	-0.74355555	0.56450142	-2.31560621
H	-0.77559922	-0.66343998	1.80814089
C	0.89484997	-0.08687142	-0.24422124
C	1.61874898	0.96651587	0.35603779
C	1.57137460	-1.18095230	-0.82543142
C	3.05564564	0.91582727	0.37241462
C	0.97563229	2.10321794	0.93541657
C	3.00719321	-1.21329630	-0.79885343
C	0.88414554	-2.27959176	-1.42865549
C	3.77736587	1.99165403	0.98417458
C	3.71142288	-0.16715440	-0.20661484
C	1.70435865	3.11354506	1.50525042
H	-0.11377993	2.15799573	0.91432733
C	3.67936194	-2.33854059	-1.37559604
C	1.57105369	-3.33068356	-1.97650651
H	-0.20664627	-2.27132230	-1.44504466
C	3.12342899	3.05858528	1.53584559
H	4.79827365	-0.19361281	-0.18664833
H	1.19545589	3.97578878	1.94055152
C	2.99189543	-3.36606086	-1.95084571
H	1.02626649	-4.15970212	-2.43235773
H	3.69818811	3.86688262	1.99106830
H	3.53493576	-4.21019320	-2.37851675
C	5.95046889	1.12438574	1.83059994
C	5.99360001	2.61741757	0.04843964
N	5.19834805	1.93653319	0.97790596
O	5.48560625	0.38784759	2.66353850
O	5.58982332	3.44677793	-0.72496413
C	5.66932834	-2.80140281	-0.09558279
C	5.79448992	-1.62351632	-2.29256802
C	7.07082280	-2.40301203	0.18172656
C	7.20262386	-1.25962613	-1.99857055
C	7.78284428	-1.62865764	-0.76290756
C	7.65132235	-2.73238471	1.39368669
C	7.91631718	-0.48935233	-2.90095093
C	9.09136346	-1.18169140	-0.44893257
C	8.95033428	-2.29084746	1.70293904
H	7.07351679	-3.31827289	2.11003793
C	9.21616081	-0.05169221	-2.59057026
H	7.44204630	-0.20977718	-3.84318685
C	9.66048867	-1.51884921	0.80011285
C	9.79452434	-0.38204202	-1.37711991
H	9.40829359	-2.53179806	2.66365538
H	9.77816435	0.57071219	-3.28873128
C	11.00484193	-1.00599724	1.16033519
C	11.14081503	0.13708096	-1.03198557
N	11.63473606	-0.17844011	0.23191877
O	11.53486343	-1.27137841	2.22020752
O	11.78255812	0.82547267	-1.79992135

C	12.95250520	0.35001511	0.58898462
H	13.04728154	1.32413913	0.09415173
H	12.94923663	0.50045827	1.67536282
C	14.08100537	-0.57726394	0.17608571
H	14.08813106	-0.72948265	-0.91278101
H	15.04764758	-0.13887575	0.46424097
H	13.99015538	-1.55437029	0.67187479
N	5.11114888	-2.32591379	-1.29244733
O	5.01139062	-3.45750609	0.67845534
O	5.23535297	-1.29270314	-3.31399086
C	8.53229770	2.99782826	-0.19089885
H	9.39283833	2.39701855	-0.52625851
H	8.22566811	3.60629551	-1.05548609
C	8.97116900	3.87396824	0.97459157
H	8.19198275	4.62377446	1.19996649
H	9.87151328	4.43922227	0.68825877
C	9.23161803	3.03411995	2.21856537
H	9.60043345	3.66391358	3.04303726
H	10.02588355	2.29345079	2.01126293
C	7.95830088	2.32323889	2.65237738
H	7.19986865	3.08687275	2.90080883
H	8.11121712	1.72996219	3.56591933
C	7.41163454	1.39977309	1.54950005
H	7.96595390	0.45151800	1.56349974
C	7.39532286	2.04724039	0.15961733
H	7.38553377	1.23977007	-0.59514916

Optimized single NDI acceptor (DA) structure of the singlet charge separated excited state.

C	-4.87191890	2.46512715	-0.70592145
C	-5.84055375	3.40010020	-0.92602393
C	-7.10559715	2.71606377	-0.84419697
N	-6.89890475	1.39094181	-0.59760609
C	-5.54921796	1.20863496	-0.52022053
C	-5.81135247	-3.46104464	0.29894954
C	-4.85400845	-2.51310503	0.08549049
C	-5.54244973	-1.25500167	-0.03409689
N	-6.88473439	-1.44283585	0.09235923
C	-7.07959915	-2.77883150	0.30695021
C	-4.89569699	-0.01887429	-0.27600369
C	-11.79296900	-2.42278667	0.73619808
C	-10.82633118	-3.37727213	0.85637904
C	-9.57354088	-2.74165139	0.54225164
N	-9.78563697	-1.42845872	0.24636442
C	-11.12966490	-1.20599387	0.34519429
C	-8.32286485	-3.40707803	0.53453736
C	-10.88130947	3.38371330	-0.84819346
C	-11.83552422	2.45874753	-0.54189573
C	-11.14650390	1.22428357	-0.27102180

N	-9.80221615	1.40933916	-0.40679579
C	-9.60998627	2.71532110	-0.75875230
C	-8.36452332	3.34780428	-0.97484543
C	-11.79047668	0.01522286	0.08786694
Zn	-8.34091222	-0.01845238	-0.17353808
H	-3.79731701	2.62023229	-0.66238125
H	-5.68844143	4.46187800	-1.10049649
H	-5.64794931	-4.52697906	0.43092709
H	-3.78121225	-2.66135207	-0.00282517
H	-12.85785254	-2.55623813	0.90597263
H	-10.97318740	-4.41596469	1.13986052
H	-11.04881127	4.42602861	-1.10551572
H	-12.90882342	2.62410294	-0.50858210
C	-13.28395103	0.05282298	0.27264365
H	-13.71439005	-0.92346018	0.01808703
H	-13.72726589	0.76178973	-0.43783105
C	-13.68329544	0.43681412	1.69942520
H	-14.77866700	0.45693064	1.79534515
H	-13.28891763	-0.28387941	2.43083722
H	-13.29816548	1.43165541	1.96739491
C	-8.37342890	4.82172994	-1.28021210
H	-7.50753754	5.07301044	-1.90563203
H	-9.25455140	5.06665473	-1.88706939
C	-8.36422269	5.68349203	-0.01517716
H	-7.47027801	5.48756961	0.59487206
H	-8.36801150	6.75016652	-0.28248402
H	-9.24664597	5.48394495	0.61029014
C	-8.31226675	-4.87354498	0.87192679
H	-9.23895904	-5.34263119	0.51841453
H	-7.50292079	-5.37284551	0.32446549
C	-8.14513739	-5.12306621	2.37303310
H	-8.96290261	-4.66422047	2.94810455
H	-8.14474421	-6.20292760	2.58060148
H	-7.19807611	-4.70359833	2.74285843
C	-3.41565509	-0.02071602	-0.26496996
C	-2.68634656	0.33037909	-1.40967904
C	-2.72127384	-0.38477369	0.89784557
C	-1.29542170	0.30290138	-1.39317883
H	-3.21449920	0.60237791	-2.32645031
C	-1.33093278	-0.38737767	0.91581073
H	-3.27767117	-0.65172498	1.79925376
C	-0.59974809	-0.05175744	-0.23059931
H	-0.73417243	0.55850275	-2.29460493
H	-0.79718462	-0.66070787	1.82868238
C	0.88554399	-0.08296407	-0.21126991
C	1.59709613	0.96301173	0.41397397
C	1.56533118	-1.16485734	-0.80973935
C	3.03369088	0.91544661	0.43751263
C	0.95074434	2.08992185	1.00974357

C	3.00103308	-1.18801683	-0.78185139
C	0.88903231	-2.25900231	-1.43358624
C	3.75217035	1.97672497	1.08015671
C	3.69641308	-0.14974894	-0.16603668
C	1.67628798	3.08932617	1.60283439
H	-0.13838313	2.15053640	0.98410643
C	3.69545706	-2.28995589	-1.37988858
C	1.59220580	-3.29053435	-1.99737217
H	-0.20168622	-2.26754663	-1.45451083
C	3.09529155	3.03338424	1.64713213
H	4.78385775	-0.17677948	-0.15380978
H	1.16379304	3.94358327	2.05022943
C	3.01363389	-3.31103654	-1.97315432
H	1.05763363	-4.11777968	-2.46946578
H	3.66720775	3.82934933	2.12643077
H	3.56584154	-4.13917349	-2.41918152
C	5.89029392	1.03837641	1.92078268
C	5.98943157	2.58977862	0.18585124
N	5.16871118	1.90403113	1.09076080
O	5.39030275	0.32831313	2.75662802
O	5.61247438	3.47441576	-0.54082790
C	5.69103916	-2.73706286	-0.11166600
C	5.77892994	-1.52513973	-2.31333870
C	7.07022652	-2.34558469	0.13560527
C	7.16364641	-1.17368979	-2.04102118
C	7.76298457	-1.56157209	-0.81759424
C	7.68724539	-2.69260479	1.35383783
C	7.87974759	-0.38147806	-2.96183643
C	9.08919568	-1.11349551	-0.51849165
C	8.96662686	-2.25628630	1.64274382
H	7.11693710	-3.28979332	2.06578528
C	9.16387297	0.04141435	-2.67508057
H	7.38554800	-0.09841147	-3.89194134
C	9.67433824	-1.45709669	0.72269944
C	9.77619237	-0.30628103	-1.45483139
H	9.44769639	-2.50070711	2.59046939
H	9.72385394	0.66692272	-3.37119564
C	10.99407138	-0.94552535	1.06782393
C	11.10280153	0.20411774	-1.13660964
N	11.61269292	-0.11985735	0.12405137
O	11.55688705	-1.19157999	2.13266371
O	11.75698029	0.90861202	-1.90322076
C	12.92695446	0.41067824	0.46566987
H	13.01825188	1.38367754	-0.03265459
H	12.94043435	0.55603726	1.55296113
C	14.05488328	-0.51294827	0.03940031
H	14.04800720	-0.65967091	-1.05041948
H	15.02709952	-0.08014391	0.32004542
H	13.96283650	-1.49299613	0.52959350

N	5.12122113	-2.25806865	-1.30803616
O	5.00980419	-3.39791341	0.66118249
O	5.16335902	-1.18725246	-3.31763260
C	8.54368136	2.84464428	-0.06800833
H	9.35162325	2.20762470	-0.45735181
H	8.25821902	3.51805261	-0.89061876
C	9.06757313	3.62243920	1.13160227
H	8.34754197	4.40879433	1.42281152
H	9.99791039	4.14066877	0.85096501
C	9.30246724	2.69589543	2.31791281
H	9.73817305	3.24911449	3.16484883
H	10.03323721	1.91386604	2.04416301
C	7.99369866	2.05187941	2.75006580
H	7.29732410	2.85091568	3.06305485
H	8.13062846	1.39673797	3.62300375
C	7.35733984	1.23065615	1.61516904
H	7.84457138	0.24791076	1.56409621
C	7.35746144	1.94652981	0.25743991
H	7.29477892	1.17430419	-0.53196484

Optimized double NDI acceptor (DA_2) structure on the ground state.

C	-6.24743649	2.39749223	-0.88758264
C	-7.25338027	3.25283152	-1.22299335
C	-8.49341407	2.52256022	-1.08946585
N	-8.22221951	1.24191243	-0.68700966
C	-6.86601982	1.13366870	-0.56510148
C	-6.90065871	-3.40863470	0.78417935
C	-5.99075780	-2.43060549	0.51677656
C	-6.74138318	-1.24538100	0.17715082
N	-8.07876263	-1.51691200	0.23415668
C	-8.21219901	-2.82814251	0.60755054
C	-6.15773835	-0.01573401	-0.17449139
C	-12.94571813	-2.76692787	0.62542054
C	-11.93590464	-3.63841162	0.90169159
C	-10.69642140	-2.94380638	0.64597942
N	-10.97121436	-1.67041465	0.22775548
C	-12.33260718	-1.53239613	0.19593311
C	-9.42054716	-3.51752804	0.80769635
C	-12.28369956	2.96299419	-1.29641537
C	-13.19726217	2.00435579	-0.97732201
C	-12.45664977	0.82556911	-0.59469654
N	-11.11584893	1.08746660	-0.68251148
C	-10.97637230	2.38038872	-1.10823832
C	-9.76692870	3.06988471	-1.32060783
C	-13.04955975	-0.38625134	-0.19466290
Zn	-9.59632090	-0.21633437	-0.23295590
H	-5.18076186	2.60634118	-0.85545930

H	-7.14805251	4.29457827	-1.51605064
H	-6.68360624	-4.43380133	1.07390514
H	-4.90636575	-2.50865695	0.53674541
H	-14.01156615	-2.96207191	0.71386329
H	-12.04133310	-4.66169438	1.25342506
H	-12.49649533	3.97734937	-1.62463338
H	-14.27925316	2.10755524	-1.00163385
C	-14.55893493	-0.43798283	-0.11245029
H	-14.90789436	-1.45352569	-0.34262099
H	-14.99427291	0.19492717	-0.89729920
C	-15.09993352	-0.00788468	1.24988573
H	-16.19975096	-0.05830283	1.27125278
H	-14.71340473	-0.65502866	2.05187598
H	-14.80138812	1.02471670	1.48651327
C	-9.84624491	4.51948724	-1.74487225
H	-8.97507829	4.77019226	-2.36508118
H	-10.71344064	4.66442670	-2.40353696
C	-9.93094052	5.48838840	-0.56686107
H	-9.05026565	5.39496777	0.08659120
H	-9.98647942	6.53090992	-0.91704231
H	-10.82086193	5.28769938	0.04881875
C	-9.34536393	-4.94489067	1.30165753
H	-10.20010648	-5.51638241	0.91546790
H	-8.46040426	-5.43696836	0.87602990
C	-9.30434820	-5.05082941	2.82506957
H	-10.20193727	-4.60297059	3.27802161
H	-9.24913496	-6.10275319	3.14596104
H	-8.42968610	-4.52316889	3.23480023
C	-4.67239724	0.07391399	-0.12703995
C	-3.92336933	0.23039938	-1.30035397
C	-3.99003942	-0.00166453	1.09409763
C	-2.53360806	0.30436308	-1.25515204
H	-4.44035620	0.28652410	-2.26121758
C	-2.60070523	0.07462788	1.14125261
H	-4.56035870	-0.11863306	2.01860511
C	-1.85351684	0.22631866	-0.03345376
H	-1.96351721	0.42274275	-2.17986176
H	-2.08342394	0.01364021	2.10187742
C	-0.37091781	0.29700704	0.01693495
C	0.26126303	1.44342360	0.54764379
C	0.40018794	-0.78629014	-0.46200420
C	1.69485748	1.48490390	0.61718352
C	-0.46268889	2.58458300	1.01439683
C	1.83408579	-0.70009554	-0.42392284
C	-0.18511729	-1.98540837	-0.97351934
C	2.32737451	2.63178904	1.19144131
C	2.44413803	0.42150500	0.12405506
C	0.18719639	3.67125491	1.53826968
H	-1.55129468	2.58178602	0.94534226

C	2.60762112	-1.78103718	-0.94596039
C	0.59510420	-3.00949644	-1.44213162
H	-1.27178305	-2.07878951	-0.98405965
C	1.60522489	3.69666206	1.64166762
H	3.53056824	0.45949350	0.16438058
H	-0.38643183	4.53258576	1.88614036
C	2.01209232	-2.90521846	-1.44170242
H	0.12867109	-3.91887940	-1.82599310
H	2.11611848	4.55666599	2.07732671
H	2.62668112	-3.71625282	-1.83631334
C	4.74127739	-2.02838089	0.18620523
C	4.59812547	-1.04859287	-2.10261186
C	6.22048078	-1.92993616	0.11831637
C	6.07776322	-0.96165381	-2.14245528
C	6.84098027	-1.43543246	-1.05192750
C	6.99148844	-2.36653558	1.18144291
C	6.70915671	-0.46094749	-3.26799785
C	8.25589244	-1.43736780	-1.14364287
C	8.39530831	-2.37555505	1.08722954
H	6.49016179	-2.73041083	2.07984350
C	8.11253573	-0.46078621	-3.35614017
H	6.09689456	-0.09171284	-4.09251198
C	9.02161186	-1.93972747	-0.06737067
C	8.87868829	-0.96136106	-2.31847475
H	9.00912476	-2.74612485	1.91007517
H	8.61754434	-0.08926256	-4.24939666
C	10.49694131	-2.04252017	-0.19665816
C	10.35412156	-1.03724613	-2.45498206
N	11.06277250	-1.56786705	-1.37637442
O	11.18472034	-2.52936619	0.67895137
O	10.92764608	-0.68432822	-3.46398556
C	12.50978948	-1.71141228	-1.54213441
H	12.85215351	-0.83880189	-2.11210641
H	12.94846070	-1.67824587	-0.53863619
C	12.88408687	-3.00384552	-2.24509591
H	12.44582143	-3.04851087	-3.25216195
H	13.97721292	-3.06883296	-2.34706328
H	12.54451992	-3.87715934	-1.66940525
N	4.03821537	-1.64847083	-0.96450194
O	4.15700050	-2.43353869	1.16640537
O	3.89542137	-0.65236202	-3.00490603
C	4.47901173	2.87729846	0.12571624
C	4.27065159	1.94254072	2.43129274
C	5.90570705	2.47304642	0.10868849
C	5.70440872	1.57014562	2.39369829
C	6.47229867	1.83905002	1.23833931
C	6.67354091	2.70262020	-1.01979720
C	6.28084218	0.94167290	3.48389175
C	7.84167032	1.47420317	1.21570130

C	8.03153975	2.33936461	-1.04137204
H	6.20736507	3.17905903	-1.88383051
C	7.64087232	0.58774984	3.46295856
H	5.66131183	0.73501360	4.35813578
C	8.61449401	1.74812571	0.06581185
C	8.41615520	0.85717631	2.34879204
H	8.64879845	2.53060864	-1.92049147
H	8.10724030	0.10608742	4.32400591
C	10.06189581	1.42819516	0.05725576
C	9.86130778	0.52737318	2.35471576
N	3.75703899	2.57246229	1.28762721
N	10.58984282	0.84920092	1.20917876
O	3.55885053	1.70266875	3.38023692
O	3.94080007	3.41388675	-0.81654571
O	10.76475924	1.66231454	-0.90625736
O	10.40317232	0.01388055	3.31177193
C	12.03645245	0.62930973	1.26083954
H	12.37073689	0.51012475	0.22516349
H	12.19973834	-0.31199236	1.79854206
C	12.76484752	1.78251367	1.92702111
H	13.84546228	1.57923452	1.94264576
H	12.60391985	2.72155392	1.37743565
H	12.43026134	1.91625502	2.96555084

Optimized double NDI acceptor (DA_2) structure of the triplet local excited state.

C	-6.256238	2.394220	-0.806962
C	-7.283483	3.266701	-1.152917
C	-8.487496	2.528942	-1.070265
N	-8.223780	1.238701	-0.693175
C	-6.864179	1.145638	-0.540137
C	-6.878041	-3.449603	0.735157
C	-5.969129	-2.471221	0.480450
C	-6.720371	-1.271579	0.178748
N	-8.059522	-1.536723	0.247136
C	-8.192114	-2.857161	0.589802
C	-6.147414	-0.038479	-0.158170
C	-12.949369	-2.724098	0.678486
C	-11.919247	-3.617428	0.950872
C	-10.710378	-2.944075	0.658891
N	-10.977780	-1.670924	0.225613
C	-12.341627	-1.529917	0.225354
C	-9.401214	-3.533146	0.790127
C	-12.316716	2.973885	-1.349101
C	-13.228368	2.021839	-1.020547
C	-12.485950	0.848141	-0.607620
N	-11.144551	1.110023	-0.684786
C	-11.005595	2.397288	-1.135064

C	-9.797772	3.074687	-1.335978
C	-13.067610	-0.356141	-0.189922
Zn	-9.600225	-0.218003	-0.235298
H	-5.194059	2.616902	-0.743995
H	-7.177731	4.315527	-1.418700
H	-6.663086	-4.482875	0.996100
H	-4.885046	-2.554456	0.481843
H	-14.013532	-2.913230	0.794325
H	-12.028097	-4.634207	1.319698
H	-12.527384	3.981607	-1.698399
H	-14.310396	2.120805	-1.056341
C	-14.569719	-0.420302	-0.094877
H	-14.906631	-1.438892	-0.330672
H	-15.021654	0.222383	-0.861816
C	-15.092178	-0.012483	1.283683
H	-16.189514	-0.090814	1.322946
H	-14.675205	-0.655442	2.072845
H	-14.815599	1.026403	1.519118
C	-9.855372	4.514647	-1.774649
H	-8.976660	4.739600	-2.394721
H	-10.724037	4.671346	-2.428378
C	-9.919388	5.492307	-0.599782
H	-9.050343	5.374182	0.064070
H	-9.935606	6.532460	-0.959744
H	-10.824385	5.325676	0.003790
C	-9.343661	-4.964004	1.257533
H	-10.206467	-5.513164	0.856555
H	-8.458587	-5.459451	0.836529
C	-9.317929	-5.087927	2.782038
H	-10.204801	-4.620104	3.234387
H	-9.296597	-6.145701	3.086114
H	-8.429226	-4.593877	3.202990
C	-4.667007	0.059281	-0.115285
C	-3.927726	0.282188	-1.284806
C	-3.978245	-0.074187	1.097406
C	-2.538384	0.353560	-1.244091
H	-4.451512	0.390155	-2.237166
C	-2.589182	0.009573	1.139945
H	-4.542190	-0.239014	2.018430
C	-1.851075	0.219517	-0.030851
H	-1.973702	0.516978	-2.165173
H	-2.065465	-0.092856	2.093450
C	-0.368226	0.293436	0.015353
C	0.261860	1.434833	0.557938
C	0.403357	-0.782836	-0.477010
C	1.695463	1.478844	0.624983
C	-0.464975	2.567387	1.040682
C	1.837118	-0.696207	-0.436857
C	-0.181877	-1.974642	-1.005144

C	2.326000	2.621546	1.209580
C	2.445915	0.421101	0.121413
C	0.183141	3.650225	1.574487
H	-1.553931	2.560824	0.975839
C	2.611162	-1.772244	-0.968069
C	0.598884	-2.993517	-1.484025
H	-1.268754	-2.065849	-1.020771
C	1.601524	3.679186	1.673066
H	3.532352	0.460446	0.161276
H	-0.392085	4.505429	1.934595
C	2.016019	-2.890570	-1.477420
H	0.133053	-3.897474	-1.881209
H	2.110890	4.536034	2.116668
H	2.631119	-3.697808	-1.878947
C	4.740683	-2.028106	0.169734
C	4.605845	-1.034592	-2.113800
C	6.220084	-1.928059	0.108168
C	6.085664	-0.949758	-2.148861
C	6.844847	-1.428802	-1.057833
C	6.987292	-2.368413	1.172500
C	6.721148	-0.445525	-3.270536
C	8.260072	-1.431374	-1.144890
C	8.391466	-2.376669	1.083469
H	6.482763	-2.735907	2.067637
C	8.124761	-0.447401	-3.354656
H	6.111870	-0.072128	-4.095393
C	9.021912	-1.937355	-0.067558
C	8.887049	-0.952578	-2.316387
H	9.002349	-2.749806	1.907337
H	8.632993	-0.073808	-4.245219
C	10.497649	-2.040283	-0.192059
C	10.362672	-1.031434	-2.449339
N	11.067535	-1.564503	-1.369416
O	11.182417	-2.528527	0.685103
O	10.939388	-0.678921	-3.456643
C	12.514573	-1.711840	-1.531932
H	12.860407	-0.840561	-2.101820
H	12.951277	-1.679157	-0.527564
C	12.886913	-3.005676	-2.233357
H	12.450565	-3.049795	-3.241287
H	13.980072	-3.073585	-2.333060
H	12.543910	-3.877758	-1.657837
N	4.041832	-1.640808	-0.981123
O	4.152774	-2.440104	1.144898
O	3.906231	-0.631801	-3.015596
C	4.475551	2.877888	0.141773
C	4.272868	1.930443	2.442692
C	5.902702	2.475320	0.119649
C	5.707619	1.562438	2.401230

C	6.472718	1.837647	1.245496
C	6.667703	2.710344	-1.009637
C	6.287491	0.931187	3.487992
C	7.842655	1.475264	1.218667
C	8.026093	2.348738	-1.035723
H	6.199019	3.189642	-1.870734
C	7.648264	0.580495	3.463234
H	5.669995	0.719793	4.362551
C	8.612435	1.754295	0.067955
C	8.420677	0.855455	2.348442
H	8.641037	2.543914	-1.915601
H	8.117467	0.096921	4.321666
C	10.060217	1.436199	0.054921
C	9.866579	0.528949	2.350512
N	3.755950	2.564945	1.303097
N	10.591790	0.854857	1.204024
O	3.563104	1.683336	3.391322
O	3.934849	3.419404	-0.796195
O	10.760458	1.673850	-0.909618
O	10.411703	0.014643	3.305252
C	12.038945	0.637770	1.251838
H	12.371041	0.521387	0.215142
H	12.205304	-0.304222	1.787417
C	12.766591	1.791044	1.918724
H	13.847661	1.589972	1.931278
H	12.602386	2.730918	1.371537
H	12.434258	1.921853	2.958352

Optimized double NDI acceptor (DA_2) structure of the triplet charge separated excited state.

C	6.313449	-2.478316	-0.864007
C	7.344476	-3.274068	-1.269658
C	8.544006	-2.482295	-1.174917
N	8.235876	-1.229578	-0.727113
C	6.885701	-1.197109	-0.544398
C	6.780965	3.291268	1.002398
C	5.898727	2.303354	0.676907
C	6.685160	1.152556	0.318284
N	8.012357	1.447561	0.409099
C	8.101763	2.744650	0.829084
C	6.138054	-0.085975	-0.091581
C	12.846173	2.849886	0.789119
C	11.810965	3.653121	1.166952
C	10.598445	2.943126	0.854691
N	10.903210	1.731198	0.307111
C	12.264515	1.649637	0.247324
C	9.297985	3.456068	1.072176
C	12.344758	-2.715330	-1.616186

C	13.229925	-1.736294	-1.273372
C	12.456003	-0.639251	-0.754392
N	11.129064	-0.957576	-0.785990
C	11.031303	-2.216060	-1.305106
C	9.837684	-2.952228	-1.492976
C	13.011725	0.568093	-0.272243
Zn	9.566973	0.250300	-0.205666
H	5.263493	-2.744504	-0.776984
H	7.276729	-4.312936	-1.581280
H	6.532838	4.300849	1.318043
H	4.813953	2.362134	0.663217
H	13.905592	3.072193	0.883414
H	11.887241	4.637235	1.621047
H	12.585196	-3.685960	-2.041013
H	14.311068	-1.778331	-1.372251
C	14.512843	0.679599	-0.242409
H	14.808910	1.727644	-0.374051
H	14.939543	0.145461	-1.100746
C	15.114140	0.132549	1.054489
H	16.209258	0.232250	1.037456
H	14.734731	0.677775	1.931229
H	14.869655	-0.931221	1.190195
C	9.962803	-4.367202	-1.990665
H	9.067530	-4.637642	-2.564083
H	10.797580	-4.436941	-2.699743
C	10.170261	-5.370089	-0.853071
H	9.327707	-5.351263	-0.146321
H	10.255146	-6.389642	-1.256280
H	11.087113	-5.147806	-0.287578
C	9.180378	4.831827	1.670783
H	10.026449	5.451794	1.349700
H	8.285645	5.330442	1.277267
C	9.115620	4.795436	3.199743
H	10.019525	4.336394	3.626685
H	9.028094	5.815660	3.600664
H	8.248147	4.215833	3.547921
C	4.665496	-0.219417	-0.053295
C	3.944645	-0.472292	-1.229643
C	3.964502	-0.070183	1.152453
C	2.556105	-0.543689	-1.203043
H	4.476939	-0.583228	-2.177156
C	2.577891	-0.166623	1.177442
H	4.513753	0.110974	2.079181
C	1.852854	-0.388945	-0.001085
H	2.001828	-0.718653	-2.127766
H	2.040603	-0.055233	2.121805
C	0.369791	-0.437756	0.025520
C	-0.286833	-1.528770	0.636258
C	-0.369346	0.620699	-0.549297

C	-1.721458	-1.537778	0.689106
C	0.407481	-2.644423	1.199063
C	-1.804870	0.565747	-0.518505
C	0.242151	1.765968	-1.146476
C	-2.396393	-2.623632	1.333296
C	-2.441238	-0.498401	0.108302
C	-0.277605	-3.672794	1.791392
H	1.496769	-2.675175	1.148726
C	-2.556108	1.619469	-1.124626
C	-0.515959	2.764662	-1.699427
H	1.330018	1.844460	-1.156087
C	-1.697168	-3.663630	1.871132
H	-3.527584	-0.518198	0.141964
H	0.271443	-4.517081	2.214172
C	-1.934439	2.690659	-1.699933
H	-0.028983	3.632261	-2.149597
H	-2.231927	-4.477921	2.361656
H	-2.530400	3.481678	-2.158039
C	-4.671082	1.874767	0.032351
C	-4.569499	0.988588	-2.302995
C	-6.145436	1.772657	-0.011576
C	-6.047678	0.942527	-2.331960
C	-6.786876	1.362562	-1.204716
C	-6.897773	2.135063	1.092998
C	-6.703139	0.532013	-3.483141
C	-8.202476	1.398162	-1.278256
C	-8.300901	2.176109	1.017280
H	-6.381350	2.415743	2.012264
C	-8.103748	0.562378	-3.551426
H	-6.107659	0.200675	-4.335332
C	-8.945917	1.849266	-0.163903
C	-8.848413	1.006577	-2.470437
H	-8.898392	2.494409	1.873133
H	-8.628691	0.253959	-4.456873
C	-10.412006	2.027875	-0.282395
C	-10.322818	1.111265	-2.578684
N	-11.001976	1.628767	-1.477496
O	-11.075086	2.525500	0.608269
O	-10.919916	0.812376	-3.594480
C	-12.446689	1.798044	-1.610347
H	-12.813127	0.947678	-2.198653
H	-12.866034	1.739483	-0.599721
C	-12.817775	3.116946	-2.264924
H	-12.397298	3.188116	-3.278284
H	-13.911847	3.201040	-2.343806
H	-12.453772	3.966641	-1.668816
N	-3.986621	1.516330	-1.139819
O	-4.059379	2.266341	1.003412
O	-3.877776	0.628681	-3.231485

C	-4.527066	-2.797260	0.225537
C	-4.336146	-1.931308	2.578145
C	-5.915311	-2.364126	0.199949
C	-5.742891	-1.560466	2.532511
C	-6.490675	-1.772729	1.350629
C	-6.678479	-2.524137	-0.971977
C	-6.348089	-0.967737	3.656798
C	-7.867015	-1.388560	1.320060
C	-8.007961	-2.143756	-1.001914
H	-6.195563	-2.962945	-1.846136
C	-7.683094	-0.606770	3.629274
H	-5.737286	-0.808814	4.546549
C	-8.618540	-1.596338	0.141156
C	-8.454737	-0.816385	2.471266
H	-8.615067	-2.270747	-1.898841
H	-8.167571	-0.160316	4.498783
C	-10.035620	-1.262877	0.115410
C	-9.875508	-0.485012	2.471248
N	-3.818777	-2.530081	1.412295
N	-10.582243	-0.746442	1.293999
O	-3.602779	-1.737823	3.538944
O	-3.950571	-3.330088	-0.714477
O	-10.741076	-1.422438	-0.879474
O	-10.456837	-0.013241	3.444512
C	-12.021748	-0.516401	1.328095
H	-12.337285	-0.348716	0.293078
H	-12.192414	0.397165	1.909789
C	-12.774232	-1.693446	1.924563
H	-13.855398	-1.488415	1.927479
H	-12.602029	-2.607098	1.336376
H	-12.458778	-1.875745	2.961913

Optimized double NDI acceptor (DA_2) structure of the singlet local excited state.

C	6.026225	-2.480868	-0.311599
C	6.949428	-3.478982	-0.428380
C	8.248588	-2.854376	-0.444570
N	8.100023	-1.490436	-0.348753
C	6.757717	-1.236202	-0.277873
C	7.232798	3.479783	0.061484
C	6.225101	2.556536	-0.041575
C	6.850778	1.261323	-0.051595
N	8.207087	1.402269	0.033613
C	8.468018	2.747850	0.106217
C	6.153841	0.031976	-0.164005
C	13.179697	2.217685	0.390076
C	12.257235	3.220649	0.449444
C	10.963557	2.618096	0.246476
N	11.114869	1.263070	0.073844

C	12.456407	0.990677	0.146277
C	9.751759	3.335909	0.224663
C	11.987198	-3.693514	-0.477446
C	12.993299	-2.776748	-0.322884
C	12.366993	-1.487610	-0.183779
N	11.008143	-1.632090	-0.247389
C	10.749357	-2.967097	-0.428816
C	9.465200	-3.558610	-0.526991
C	13.067344	-0.269641	0.000165
Zn	9.607764	-0.112556	-0.131249
H	4.946426	-2.583081	-0.239274
H	6.746947	-4.546222	-0.472855
H	7.120678	4.560469	0.096279
H	5.157915	2.746691	-0.121665
H	14.255261	2.319168	0.510968
H	12.457322	4.274345	0.626998
H	12.102402	-4.766830	-0.605409
H	14.060569	-2.981934	-0.304880
C	14.568355	-0.346544	0.116859
H	15.020191	0.582012	-0.257633
H	14.948667	-1.137987	-0.544652
C	15.046300	-0.605627	1.546577
H	16.145100	-0.666526	1.588801
H	14.722241	0.200127	2.222667
H	14.636521	-1.549881	1.936006
C	9.403965	-5.060394	-0.643257
H	8.502273	-5.353517	-1.197410
H	10.246562	-5.414939	-1.253457
C	9.423445	-5.768244	0.712757
H	8.560666	-5.468971	1.326749
H	9.388635	-6.861100	0.583452
H	10.334629	-5.519558	1.277179
C	9.809928	4.830418	0.411838
H	10.751740	5.221465	0.004855
H	9.018135	5.304960	-0.184796
C	9.668628	5.255794	1.874373
H	10.479038	4.834378	2.488139
H	9.703541	6.352338	1.967628
H	8.714869	4.906992	2.297975
C	4.673476	0.091036	-0.169528
C	3.938535	-0.356085	-1.278103
C	3.968909	0.599471	0.932547
C	2.547792	-0.297071	-1.284770
H	4.470431	-0.740902	-2.151260
C	2.578191	0.651729	0.929445
H	4.523818	0.943962	1.808254
C	1.850231	0.205777	-0.180451
H	1.990801	-0.640426	-2.159890
H	2.044257	1.040310	1.800019

C	0.364861	0.267476	-0.188938
C	-0.384647	-0.797230	0.354991
C	-0.285546	1.389449	-0.743950
C	-1.819874	-0.736158	0.321799
C	0.228495	-1.950778	0.933090
C	-1.720381	1.443844	-0.735787
C	0.426220	2.492752	-1.308708
C	-2.569110	-1.836823	0.838328
C	-2.451075	0.381406	-0.211972
C	-0.529464	-2.972912	1.440489
H	1.317773	-2.006108	0.965151
C	-2.368745	2.601921	-1.268085
C	-0.238903	3.573367	-1.825491
H	1.516889	2.462024	-1.321939
C	-1.948754	-2.922386	1.387381
H	-3.538750	0.417717	-0.216342
H	-0.044562	-3.845928	1.881638
C	-1.659441	3.637056	-1.801561
H	0.323096	4.405514	-2.253988
H	-2.545731	-3.751364	1.771494
H	-2.183148	4.509278	-2.195846
C	-4.325393	3.129804	0.029671
C	-4.509964	1.893360	-2.131004
C	-5.759369	2.861059	0.288362
C	-5.936538	1.619363	-1.833571
C	-6.515153	2.112134	-0.641507
C	-6.346659	3.324750	1.452688
C	-6.692944	0.868401	-2.716675
C	-7.883566	1.855873	-0.376308
C	-7.705616	3.075811	1.710943
H	-5.736052	3.889916	2.158774
C	-8.050557	0.615578	-2.452929
H	-6.217876	0.487446	-3.622221
C	-8.468829	2.358377	0.806691
C	-8.644406	1.114196	-1.306591
H	-8.180526	3.449521	2.619594
H	-8.658834	0.037849	-3.150543
C	-9.912391	2.141782	1.064047
C	-10.090726	0.894155	-1.067036
N	-10.628983	1.432630	0.099648
O	-10.462545	2.568673	2.058156
O	-10.783698	0.275308	-1.850643
C	-12.074603	1.316986	0.300587
H	-12.395039	0.426074	-0.249018
H	-12.238250	1.152467	1.372066
C	-12.819706	2.543858	-0.193204
H	-12.657147	2.697532	-1.270087
H	-13.899100	2.413357	-0.028226
H	-12.501290	3.446658	0.347110

N	-3.799131	2.620969	-1.167244
O	-3.624053	3.733918	0.809315
O	-3.962592	1.490449	-3.132785
C	-4.552060	-2.328273	-0.448036
C	-4.713731	-1.131217	1.734242
C	-6.030971	-2.311956	-0.550466
C	-6.192514	-1.132200	1.606189
C	-6.803285	-1.749360	0.490305
C	-6.652619	-2.889706	-1.644071
C	-6.972802	-0.569265	2.601114
C	-8.217530	-1.828181	0.425609
C	-8.055311	-2.963082	-1.708785
H	-6.033315	-3.307911	-2.439426
C	-8.375937	-0.655622	2.541074
H	-6.479319	-0.085176	3.445491
C	-8.830279	-2.459643	-0.679092
C	-8.992700	-1.296763	1.480929
H	-8.552869	-3.437318	-2.556441
H	-8.996756	-0.241623	3.337561
C	-10.304721	-2.621056	-0.713179
C	-10.466996	-1.471610	1.473843
N	-4.000959	-1.795492	0.727555
N	-11.022561	-2.109430	0.368379
O	-4.137805	-0.606525	2.661218
O	-3.842576	-2.792235	-1.311866
O	-10.869503	-3.196392	-1.619633
O	-11.162128	-1.089672	2.394539
C	-12.467530	-2.341750	0.371850
H	-12.807513	-2.244937	-0.666750
H	-12.915423	-1.541647	0.971472
C	-12.831192	-3.701213	0.941320
H	-13.923197	-3.830991	0.925759
H	-12.384449	-4.511933	0.348565
H	-12.493366	-3.793769	1.983797

Optimized double NDI acceptor (DA_2) structure of the singlet charge separated excited state

C	-6.239403	1.133037	-2.327225
C	-7.249388	1.544105	-3.145310
C	-8.479231	1.084295	-2.552007
N	-8.209477	0.394415	-1.407277
C	-6.854863	0.397609	-1.253189
C	-6.885959	-2.126056	2.768886
C	-5.975920	-1.593127	1.904995
C	-6.728133	-0.886765	0.901129
N	-8.060966	-1.002615	1.149022

C	-8.189681	-1.746419	2.287707
C	-6.142384	-0.205508	-0.193118
C	-12.923964	-1.455652	2.410343
C	-11.913175	-1.962484	3.171258
C	-10.687545	-1.697393	2.463678
N	-10.960414	-1.040762	1.301695
C	-12.315288	-0.887335	1.235433
C	-9.404061	-2.077697	2.925820
C	-12.283052	1.350912	-2.951766
C	-13.193316	0.907665	-2.039357
C	-12.446544	0.303255	-0.966819
N	-11.111949	0.391420	-1.230435
C	-10.980689	1.023519	-2.432878
C	-9.765215	1.347773	-3.077522
C	-13.033222	-0.282794	0.180095
Zn	-9.584494	-0.321074	-0.051355
H	-5.175703	1.324478	-2.438637
H	-7.148713	2.129244	-4.055286
H	-6.670248	-2.726645	3.648208
H	-4.894105	-1.688816	1.937733
H	-13.984496	-1.475778	2.645527
H	-12.012223	-2.463907	4.130045
H	-12.498369	1.858352	-3.888047
H	-14.274087	0.993680	-2.108978
C	-14.530148	-0.196888	0.314642
H	-14.902814	-1.066235	0.870481
H	-14.994647	-0.263353	-0.677411
C	-14.977436	1.091302	1.008676
H	-16.073754	1.121272	1.087004
H	-14.558922	1.161492	2.023556
H	-14.649088	1.979222	0.448457
C	-9.844845	2.106154	-4.375540
H	-8.979914	1.853828	-5.002132
H	-10.723881	1.772213	-4.942071
C	-9.909636	3.621011	-4.168298
H	-9.020235	3.988878	-3.635882
H	-9.964634	4.135291	-5.138476
H	-10.793710	3.904815	-3.578551
C	-9.325993	-2.820476	4.232456
H	-10.214230	-3.453874	4.351275
H	-8.473418	-3.511296	4.212849
C	-9.196431	-1.878423	5.431407
H	-10.057500	-1.197054	5.497766
H	-9.143628	-2.456231	6.365299
H	-8.287418	-1.263705	5.356728
C	-4.665538	-0.115575	-0.219830
C	-3.927467	-0.677204	-1.271257
C	-3.980876	0.537398	0.815400
C	-2.539240	-0.595218	-1.279466

H	-4.446546	-1.200027	-2.077781
C	-2.594970	0.636370	0.790590
H	-4.543856	0.986979	1.636467
C	-1.853136	0.067000	-0.252971
H	-1.971872	-1.046957	-2.096135
H	-2.071276	1.158847	1.594085
C	-0.372066	0.165937	-0.262030
C	0.241315	1.414826	-0.505951
C	0.407196	-0.985297	-0.009873
C	1.673542	1.505733	-0.474032
C	-0.494662	2.605452	-0.795453
C	1.839848	-0.873026	-0.016522
C	-0.161478	-2.264222	0.276388
C	2.307557	2.771674	-0.691474
C	2.432021	0.364276	-0.235861
C	0.149797	3.795388	-1.007678
H	-1.583294	2.558773	-0.850418
C	2.634724	-2.037486	0.221437
C	0.635342	-3.352985	0.512789
H	-1.247040	-2.367801	0.311419
C	1.566726	3.888387	-0.947363
H	3.516075	0.440407	-0.218216
H	-0.430756	4.694402	-1.226822
C	2.050790	-3.245305	0.478840
H	0.182336	-4.322448	0.731279
H	2.068327	4.844762	-1.099818
H	2.676377	-4.122059	0.654191
C	4.712900	-1.354670	1.264653
C	4.674794	-2.331361	-1.042316
C	6.184545	-1.261142	1.179403
C	6.151309	-2.258790	-1.074755
C	6.858879	-1.759415	0.039352
C	6.905628	-0.739380	2.242059
C	6.838433	-2.730855	-2.185221
C	8.276493	-1.778573	0.025837
C	8.309404	-0.766994	2.232058
H	6.358542	-0.334833	3.095222
C	8.238959	-2.742864	-2.198971
H	6.261685	-3.101880	-3.034119
C	8.989385	-1.310949	1.152949
C	8.954957	-2.286828	-1.101611
H	8.887847	-0.392151	3.078070
H	8.793450	-3.122438	-3.058821
C	10.460750	-1.462758	1.208776
C	10.432764	-2.377223	-1.094254
N	11.080037	-1.981208	0.075860
O	11.103153	-1.172950	2.200352
O	11.060979	-2.825941	-2.031567
C	12.531598	-2.128320	0.103690

H	12.893742	-1.881712	-0.902185
H	12.909434	-1.384487	0.814099
C	12.966607	-3.524540	0.509823
H	12.590539	-4.274470	-0.201050
H	14.064978	-3.588149	0.522808
H	12.599600	-3.771859	1.517042
N	4.061353	-1.919388	0.153895
O	4.075640	-0.993945	2.229631
O	4.011047	-2.747507	-1.965662
C	4.451129	2.214594	-1.632954
C	4.244162	3.191742	0.680248
C	5.850650	1.916674	-1.357902
C	5.663882	2.930763	0.888468
C	6.422533	2.291630	-0.118919
C	6.624498	1.247263	-2.322342
C	6.266551	3.292930	2.106271
C	7.805392	2.026357	0.115400
C	7.963193	0.982766	-2.089487
H	6.140839	0.956072	-3.255993
C	7.609761	3.044665	2.328281
H	5.643719	3.776763	2.860089
C	8.568063	1.384072	-0.885990
C	8.388861	2.415114	1.341737
H	8.583099	0.475524	-2.829767
H	8.097583	3.331067	3.261119
C	9.995510	1.162872	-0.686328
C	9.818870	2.211072	1.564238
N	3.728463	2.799553	-0.573489
N	10.536545	1.622559	0.518744
O	3.506871	3.690801	1.513957
O	3.880688	1.950411	-2.679203
O	10.706465	0.609672	-1.520381
O	10.393423	2.545649	2.592497
C	11.978327	1.512041	0.701147
H	12.315789	0.721302	0.022730
H	12.152275	1.196504	1.737173
C	12.697921	2.813900	0.397430
H	13.782868	2.686906	0.531752
H	12.517391	3.128290	-0.641622
H	12.361079	3.612296	1.074071

1.8 Acknowledgments

We thank Dr. Brian T. Phelan for the preliminary kinetic studies and helpful broader discussions of these molecules.

Chapter 2: Effect of Time Delay between Spin State Preparation and Measurement on Electron Spin Teleportation in a Covalent Donor-Acceptor-Radical System

This chapter is from the published work titled as above with the authors listed below.[88]

Laura Bancroft, Yunfan Qiu, Matthew D. Krzyaniak* and Michael R. Wasielewski*

Department of Chemistry, Center for Molecular Quantum Transduction, and Institute for Sustainability and Energy at Northwestern, Northwestern University, Evanston, IL 60208-3113

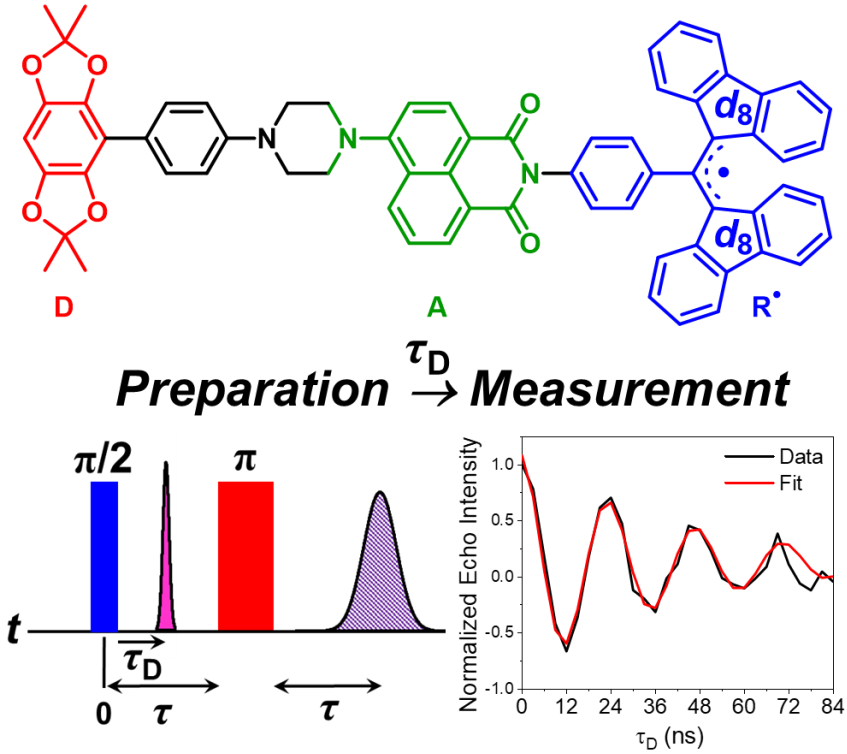

2.1 Abstract

We recently demonstrated photodriven quantum teleportation of an electron spin state in a covalent donor-acceptor-radical (D-A-R$^{\bullet}$). Following specific spin state preparation on R$^{\bullet}$ with a microwave pulse, photoexcitation of A results in two-step electron transfer producing D$^{\bullet+}$-A-R^{-}, where the spin state on R$^{\bullet}$ is teleported to D$^{\bullet+}$. This study examines the effects of varying the time (τ_D) between spin state preparation and photoinitiated teleportation. Using pulse-EPR spectroscopy, the spin echo of D$^{\bullet+}$ resulting from teleportation shows a complex damped oscillation as a function of τ_D that is simulated using a density matrix model, which provides a fundamental understanding of the echo behavior. Teleportation fidelity calculations also show oscillatory behavior as a function of τ_D due to the accumulation of a phase factor between $\langle S_x \rangle$ and $\langle S_y \rangle$. Understanding experimental parameters intrinsic to quantum teleportation in molecular systems is crucial to leveraging this phenomenon for quantum information applications.

2.2 Introduction

Transferring a quantum state over an arbitrary distance from one location to another without destroying the information it contains is possible through the agency of quantum entanglement.[89] The process is known as quantum teleportation[90] and has been demonstrated using both light and matter.[91-99] Recently, we achieved electron spin state teleportation in an ensemble of covalent organic donor-acceptor-stable radical molecules comprising a 2,2,6,6-tetramethylbenzo[1,2-d:4,5-d′]bis([1,3]dioxole) donor (D), a 4-aminonaphthalene-1,8-imide acceptor/chromophore (A), and a partly deuterated α,γ-bisdiphenylene-β-phenylallyl radical ($R^{\bullet}$) (D-A-$R^{\bullet}$, Figure 2.1).[23] Following preparation of a specific electron spin state on $R^{\bullet}$ in a magnetic field using a microwave pulse, photoexcitation of A results in the formation of an entangled electron spin pair $^{1}(D^{\bullet+}\text{-}A^{\bullet-})$. The spontaneous ultrafast electron transfer reaction $D^{\bullet+}\text{-}A^{\bullet-}\text{-}R^{\bullet} \rightarrow D^{\bullet+}\text{-}A\text{-}R^{-}$ constitutes the Bell state[100] measurement step necessary to carry out spin state teleportation. Quantum state tomography of the $R^{\bullet}$ and $D^{\bullet+}$ spin states using pulse-EPR spectroscopy showed that the spin state of $R^{\bullet}$ is teleported to $D^{\bullet+}$ with about 90% fidelity.

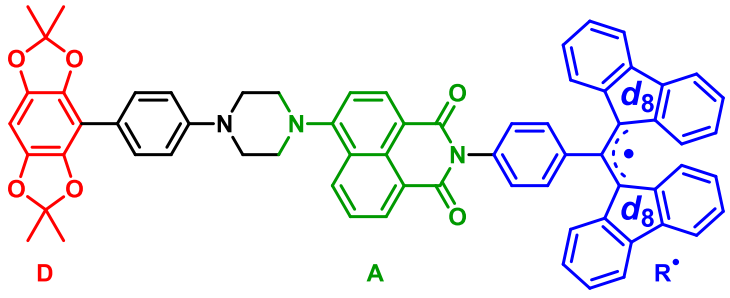

Figure 2.1. Structure of D-A-$R^{\bullet}$.

In our previous work, we noted that phase coherent rotation of the electron spin state teleported to $D^{\bullet+}$ occurs when the time interval between the initial π/2 microwave pulse that places

$R^{\bullet}$ into a superposition state and laser pulse that initiates teleportation is varied. A better understanding of this observation and how it relates to the teleportation fidelity will inform both future experimental and molecular design. Utilizing the D-A-$R^{\bullet}$ molecule shown in Figure 2.1, we observe a damped oscillation of the teleported state when the time between the initial $\pi/2$ microwave pulse and laser pulse is incremented. By simulating this behavior using density matrix methods, we show that it is a consequence of the differing resonant frequencies and magnetic environments of $R^{\bullet}$ and $D^{\bullet+}$.

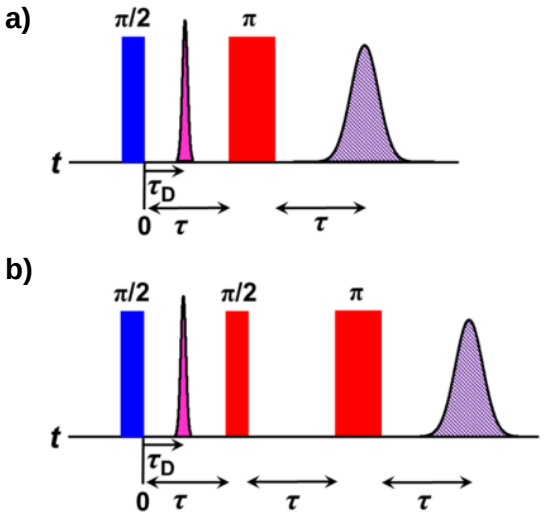

Figure 2.2. Microwave and laser pulse sequences for (a) 2-pulse and (b) 3-pulse teleportation experiments wherein the laser pulse is delayed by τ_D relative to the initial $\pi/2$ microwave pulse. Blue rectangles signify microwave pulses resonant with $R^{\bullet}$ and red rectangles signify microwave pulses resonant with $D^{\bullet+}$. Purple spikes signify the 416 nm laser pulse. Pulse turning angles are given above each pulse. The inter-pulse spacing of the microwave pulses is 200 ns.

The synthesis, structural characterization, photoinduced charge separation dynamics, and full quantum state tomography (QST) of teleportation in D-A-$R^{\bullet}$ have been described elsewhere.[23] Briefly, following photoexcitation of A, the triradical $D^{\bullet+}$-$A^{\bullet-}$-$R^{\bullet}$ is formed in 10 ps. Given that the

spins of $A^{\bullet-}$ and $R^{\bullet}$ are uncorrelated, $D^{\bullet+}$-$^1(A^{\bullet-}$-$R^{\bullet}) \rightarrow D^{\bullet+}$-A-$R^-$ in 108 ps with a 25% yield, while $D^{\bullet+}$-$^3(A^{\bullet-}$-$R^{\bullet}) \rightarrow$ D-A-$R^{\bullet}$ in 5 ns with a 75% yield.

2.3 Results, Analysis, and Discussion

2.3.1 Pulse-EPR Spectroscopy. Partial QST was performed for teleportation of the +x prepared state using the 2- and 3-pulse, 2-frequency experiments as a function of the time between the initial $\pi/2$ microwave pulse and laser pulse, τ_D (Figure 2.2). The data was collected in triplicate on three separate days with three separate samples. Additional experimental parameters for the triplicate data sets are included in Table S2.4. The phase cycles used in all experiments are provided in Table S2.5.

Figure 2.3 shows the QST of a state prepared along the +x direction of the Bloch sphere as a function of τ_D for data set 1. The 2-pulse teleportation experiment, Figures 2.3a,b, provides $\langle S_x \rangle$ and $\langle S_y \rangle$ from the in-phase and quadrature channels of the EPR spectrometer. A damped complex oscillation of the spin echo intensity is observed as τ_D is incremented to longer values, where the amplitude oscillates between $\langle S_x \rangle$ and $\langle S_y \rangle$. In addition, the spin echo moves closer in time to the

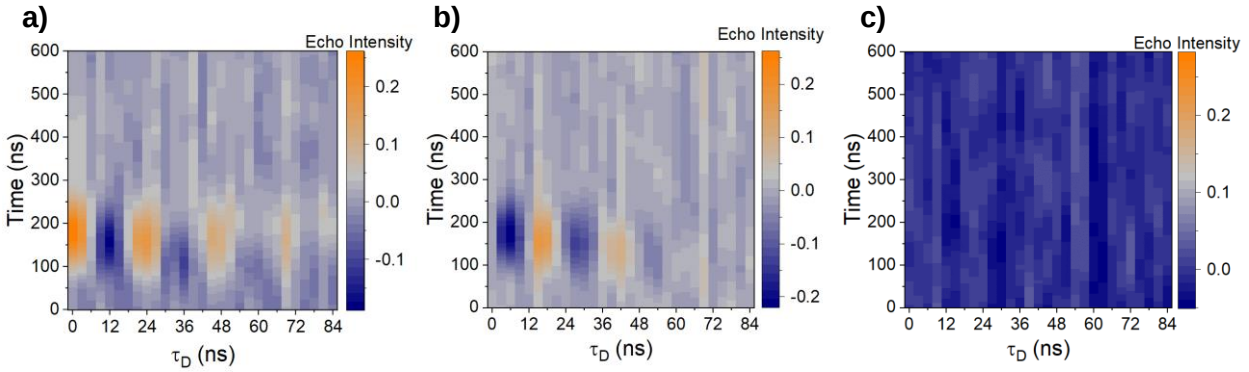

Figure 2.3. The spin echoes as a function of τ_D, which represent the measurement of a) $\langle S_x \rangle$, b) $\langle S_y \rangle$ and c) $\langle S_z \rangle$ of a state prepared along the +x. a) and b) were collected using 2-pulse teleportation scheme, c) was collected with the 3-pulse scheme. All three panels are from data set 1.

π microwave pulse with increasing τ_D values. As expected, the 3-pulse teleportation experiment, which provides $\langle S_z \rangle$, shows no spin echo (Figure 2.3c).

Fitting a line across the echo maxima and minima in the $\langle S_x \rangle$ data, Figure 2.4a, gives a data slice, Figure 2.4b, that emphasizes the oscillatory and damping behavior of the echo. A fit to the data slice using an exponentially damped sine wave yields a frequency and a decay lifetime, which averaged over the three data sets gives values of 42.2 ± 0.7 MHz and 38 ± 3 ns, respectively. The oscillation frequencies and decay lifetimes from fitting the individual data sets are provided in Table S2.1. Additional fitting details are also provided in section 2.5.3.

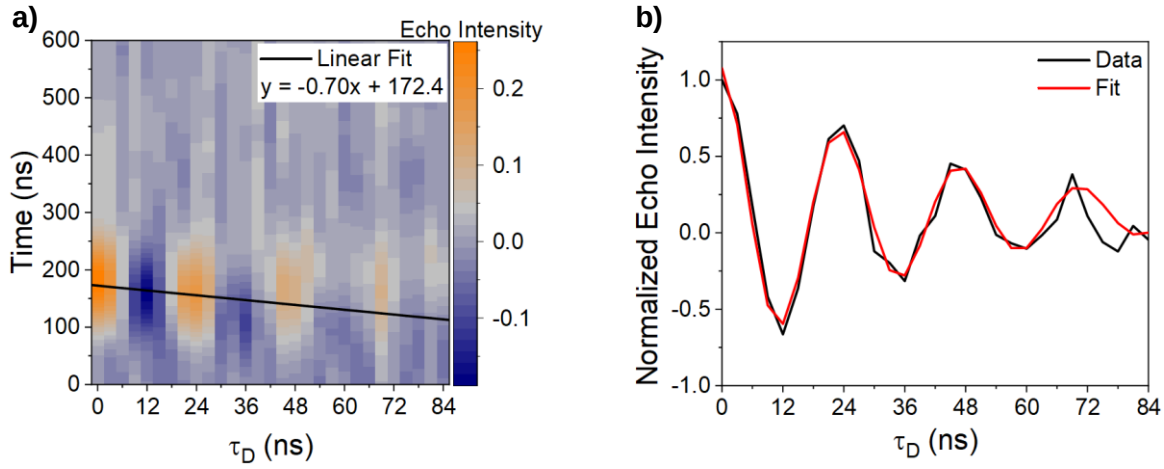

Figure 2.4. a) Data for $\langle S_x \rangle$ with linear fit across echo maxima and minima. b) Data slice with corresponding sinusoidal and exponential fit. Both figures are for data set 1.

2.3.2 Density Matrix Simulations. Simulation of the 2-pulse echo vs τ_D spectra was performed by evolution of the density matrix. Due to fast charge separation sequence $D\text{-}^{1*}A\text{-}R^{\bullet} \rightarrow D^{\bullet+}\text{-}^{1}(A^{\bullet-}\text{-}R^{\bullet}) \rightarrow D^{\bullet+}\text{-}A\text{-}R^{-}$, the evolution of the density matrix can be divided into two discrete $S = ½$ evolution periods, one before the laser pulse and one after it, greatly simplifying the analysis compared to previous treatments.[101-103] Based on the fact that the spins on $A^{\bullet-}$ and $R^{\bullet}$ are uncorrelated,[104] the corresponding

triplet intermediate $D^{\bullet+}$-^{3}($A^{\bullet-}$-$R^{\bullet}$), which constitutes 75% of the total triradical intermediate population, decays to D-A-$R^{\bullet}$ in 5 ns and thus can be safely neglected.

Initially, the thermal density matrix for each $R^{\bullet}$ spin packet is rotated by the initial $\pi/2$ microwave pulse generating the +x state. This density matrix then evolves for time τ_D, acquiring a phase of $(\omega_R + \Delta\omega_R)\tau_{D,}$ where $\Delta\omega_R$ represents the resonance offset of the individual spin packets of $R^{\bullet}$. Following the teleportation event, the density matrix begins evolving under the $D^{\bullet+}$ spin Hamiltonian adding an addition phase of $(\omega_D + \Delta\omega_D)(\tau - \tau_D)$, where $\Delta\omega_D$ represents the resonance offset of the individual spin packets of $D^{\bullet+}$, which are uncorrelated with those of $R^{\bullet}$. The density matrix is then refocused with a π microwave pulse resonant with $D^{\bullet+}$, subtracting a phase of $(\omega_D + \Delta\omega_D)\tau$ and forming a spin echo. The spin echo carries the residual phase of $(\omega_R + \Delta\omega_R)\tau_D - (\omega_D + \Delta\omega_D)\tau_D$.

The density matrix simulation was coded in Matlab,[105] and the spin echo was generated using the Easyspin[106] function *evolve*. The simulations used the experimentally determined *g*-values and line widths for both $R^{\bullet}$ and $D^{\bullet+}$.[23] Integration over the spin packet distributions utilized 30 evenly-spaced frequency points in the $R^{\bullet}$ spectrum over 45 MHz and 1024 evenly-spaced frequency points over 100 MHz in the $D^{\bullet+}$ spectrum. Specific frequency ranges were chosen to symmetrically capture the entirety of each spectrum. Experimental microwave pulse lengths, rectangular pulse shapes, and phase cycles were also incorporated into the numerical simulations for each experimental data set.

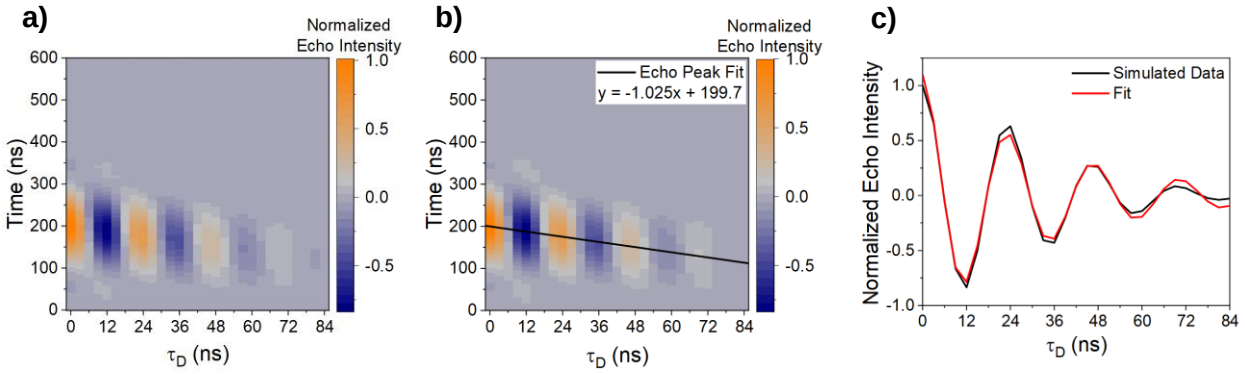

Figure 2.5. a) Simulated spin echoes as a function of τ_D, which represent the $\langle S_x \rangle$ measurement of a state prepared along +x. b) Simulated spin echoes with linear fit across the echo maxima and minima. c) Data slice along linear fit with corresponding fit. Simulations were generated using the experimental parameters from data set 1.

The simulation of the 2-pulse teleportation experiment as a function of τ_D is shown in Figure 2.5a. Qualitatively, the simulation agrees well with the experimental results, showing a damped complex oscillation. A linear fit, Figure 2.5b, and data slice, Figure 2.5c, were obtained in the same manner as the experimental data. The fit of all simulated data sets, as shown for data set 1 in Figure 2.5c, with the same model as the experimental data yields an average frequency of 42.2 ± 0.4 MHz and an average decay lifetime of 35.6 ± 0.2 ns. The oscillation frequencies and decay lifetimes from fitting the simulations of the individual data sets are provided in Table S2.2.

2.3.3 Teleportation Fidelity. The teleportation fidelity $F(\rho, \sigma)$, where $0 \leq F \leq 1$, was calculated as a function of τ_D using the well-known density matrix expression shown here.[23, 98, 107]

Equation 2.1

$$F(\rho, \sigma) \equiv \left(tr\sqrt{\rho^{1/2}\sigma\rho^{1/2}} \right)^2$$

where ρ and σ are density matrices for the starting and final spin states. The previously reported[23] entanglement fidelity of 0.91 was used and the values for the input density matrix were replaced

with an idealized input density matrix for which F =1. Our previously reported experimental input fidelity of 0.99 suggests that this change should not influence the fidelity calculation and the idealized input density matrix will allow an accurate comparison of teleportation fidelities as a function of τ_D.

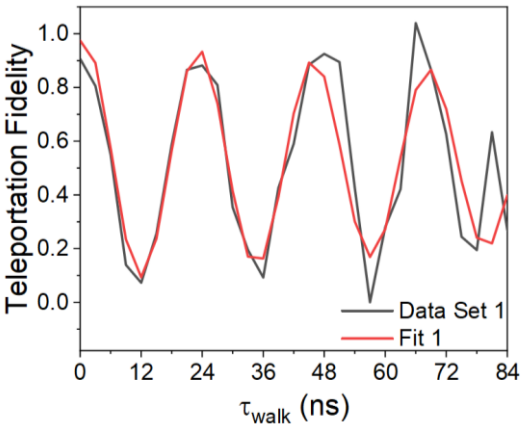

Figure 2.6. Teleportation fidelity calculated as a function of τ_D for data set 1 with corresponding fit.

The teleportation fidelity data as a function of τ_D were fit to extract an oscillation frequency from each data set. The fit protocol involved a sine wave to capture the oscillations and an exponential component to capture the shallower troughs particularly for data sets 2 and 3 (see section 2.5). The teleportation fidelity was calculated as a function of τ_D, and these data are presented in Figure 2.6 for data set 1. The fidelity oscillates with an average frequency for the triplicate data sets of 41 ± 2 MHz. Each peak returns to roughly the same maximum fidelity well above the 2/3 needed to confirm quantum entanglement.[108] Data sets 2 and 3 show similar oscillatory behavior, only with shallower troughs after the trough at around τ_D = 12 ns (see section 2.5).

2.3.4 Analysis of the Time Delay Effects. The QST as a function of τ_D has three main features: 1) oscillatory behavior of the echo intensity, 2) damping of the signal intensity as τ_D is increased, and 3) the movement of the echo closer in time to the π microwave pulse at longer τ_D values.

The oscillation of the spin echo can be understood in the context of the evolution of the density matrix. The spin state evolves under two different spin Hamiltonians resulting in the accumulation of a phase equal to their frequency difference. The experimentally obtained frequency of 42.2 ± 0.7 MHz agrees well with the frequency difference of the microwave pulses (40 MHz) used to target $R^{\bullet}$ and $D^{\bullet+}$ and is in good agreement with average oscillation frequency of the simulated data, 42.2 ± 0.4 MHz.

The damping of the echo, quantitatively illustrated with the 38 ± 3 ns damping lifetime, is much shorter than the previously reported phase memory time of $D^{\bullet+}$, T_m = 890 ns.[23] However, the damping is reproduced quite well in the density matrix simulation and can be interpreted as resulting from spectral diffusion. Initially, the spins dephase due to the magnetic environment of $R^{\bullet}$, following teleportation of the spin states to $D^{\bullet+}$, they continue to dephase, but now the spins are in a different magnetic environment and do so in an uncorrelated fashion. The π microwave pulse is unable to completely refocusing the coherence and the spin echo is damped due to destructive interference from the dephasing caused by two different magnetic environments.

This mechanism is fully supported by the density matrix simulation, with an average damping lifetime of 35.6 ± 0.2 ns. The simulation does not consider any T_m relaxation, and the damping is due solely to the two uncorrelated dephasing processes. If the dephasing occurs in a correlated fashion, i.e. dephasing of $R^{\bullet}$ occurs with a given frequency offset and continues with

the same offset after teleportation to $D^{\bullet+}$, the echo amplitude does not damp out as a function of τ_D. This understanding provides clues to how this teleportation experiment could be made more robust to avoid this particular mechanism of dephasing; for example, rather than initiate teleportation immediately following the generation of the quantum state, a Carr-Purcell-Meiboom-Gill[109, 110] pulse train could first be applied with the laser pulse after the echo is refocused.

The observation that the spin echo moves closer in time to the π pulse with increasing τ_D can be explained by considering the time period just before and after the laser pulse that initiates teleportation. The prepared spin state of $R^{\bullet}$ evolves initially under its spin Hamiltonian, then dephases under the spin Hamiltonian of $D^{\bullet+}$ after the laser pulse occurs at τ_D. As a result, the spin ensemble of $R^{\bullet}$ prior to the laser pulse cannot be refocused completely following teleportation. This process is somewhat analogous to shortening the time between the microwave pulses in a Hahn echo sequence, only here it is the time between the laser pulse and the π pulse, which determines when the echo will appear. Since the time between the microwave pulses is fixed in the experiment, the time at which the spin echo of $D^{\bullet+}$ appears also changes as τ_D changes. This is somewhat analogous to varying the time between the $\pi/2$ and π pulses in a standard Hahn echo experiment, so that the echo should appear at $(\tau - \tau_D)$ after the π microwave pulse. By fitting the maxima and minima in the echo intensity, the average slope of the linear fit is -0.70 ± 0.10 with an average intercept of 165 ± 5 ns. These values are close to the ideal situation for these experimental conditions, where the slope should be -1 and the y-intercept should be 150 ns. Analyzing the corresponding fit lines to each 2-dimensional simulated data set, the average slope is -1.019 ± 0.014 and the average intercept is 201 ± 1 ns. The difference between the intercepts of

the experimental and simulated data is due to microwave resonator deadtime. Since the simulations are not subject to resonator deadtime, the simulated echo data begins directly after the π microwave pulse and is not delayed. The simulated fits show good agreement with the idealized situation, giving credence to the argument that the echo moves closer to the π microwave pulse with increasing τ_D analogous to adjusting the time delay between Hahn echo microwave pulses. Overall, the high level of agreement between the experimental data and simulations suggests that our approach to the density matrix evolution can serve as a predictive model to explore other pulse sequences and protocols for spin teleportation experiments.

In the 3-pulse teleportation experiment, only a very weak signal is present. This is the desired outcome as this experiment measures $\langle S_z \rangle$ and with properly calibrated turning angles, all of the spins should be in the xy-plane. While no interesting dynamics occur in this experiment, it is nevertheless necessary to collect this data in order to calculate the fidelity.

As seen in Figure 2.6 (and Figure S2.6), the teleportation fidelity oscillates as a function of τ_D. The fidelity plots might, at first glance, appear to suggest that the system is not teleporting when τ_D is in a trough as $F_{teleport} < 2/3$ required to confirm quantum teleportation. And in a manner of speaking that is true, the initially prepared state is not perfectly teleported, it is however teleported with an additional phase factor related to the difference between the spin Hamiltonians and τ_D, i.e. the oscillation frequency of the spin echo. Fitting the fidelity oscillation gives an average frequency of 41 ± 2 MHz, which not surprisingly, agrees very well with the oscillation frequency of the observed spin echo.

2.4 Conclusions

This study examined the effects of changing the interval between producing particular spin state on a stable radical and initiating the quantum measurement event, in this case the laser-driven electron transfer, on electron spin state teleportation in a D-A-R$^{\bullet}$ molecule. The 2-pulse teleportation experiment as a function of τ_D showed a damped oscillation of the teleported spin echo. A density matrix model was used to simulate these results and provide the insight necessary to understand the spin echo behavior. The teleportation fidelity calculations show oscillations as a function of τ_D due to the accumulation of a phase factor between $\langle S_x \rangle$, and $\langle S_y \rangle$. Overall, these investigations elucidate how spin state evolution and the ability to control it by varying both optical and microwave pulse input to the system can enhance the observation and leveraging of teleportation in molecular systems for QIS applications.

2.5 Supporting Information

2.5.1 Sample Preparation

Samples of the D-A-RH precursor were oxidized to form D-A-R• before performing EPR experiments. First, ~7.5 mg MnO2 was sonicated in 0.25 mL anhydrous tetrahydrofuran (THF) using a 20 mL scintillation vial for 10 minutes. Then 0.5 mL ~0.1 mM solution of D-A-RH in THF, 0.5 µL of 1,5-diazabicyclo[4.3.0]non-5-ene, and a magnetic stir bar were added to the scintillation vial and the contents were stirred vigorously for 20 minutes. The resulting mixture was filtered through a pipet column containing silica gel and eluted with more THF. The THF was then evaporated by a stream of N_2 gas and the resulting dry sample was reconstituted in ~3 drops of filtered PrCN that had been dried and stored over molecular sieves.

Solutions of D-A-R$^{\bullet}$ were placed in a 10 cm-long quartz tube (Vitrocom 1.50 mm ID x 1.80 mm OD). Sample solution was added to a height of ~1 cm in the tube, which was quickly equipped with an optical fiber (core diameter of 1 mm and a numerical aperture of 0.39 (Thorlabs)) was threaded into a Bruker sample holder rod. The protective layers of the fiber were removed from one end to expose the core and prevent chemical interactions with the sample. This ~2 cm exposed tip was positioned ≤1 mm above the surface of the sample for optimal photoexcitation. The fiber was held in position relative to the sample surface by ~4 cm of heat-shrink tubing positioned far enough from the sample, so that it was protected from heat degradation while securing the fiber. The sample was secured in the sample holder rod so the bottom of the fiber was 22 mm below the bottom of the sample holder rod. The sample was slowly submerged into liquid N_2 to ensure proper glassing of PrCN to aid photoexcitation before quickly inserting the sample into the pre-cooled resonator at 85 K.

The short length of fiber from the sample holder rod was coupled to a longer fiber coming from a pulsed laser set-up for photoexcitation. Laser pulses were produced by a frequency-tripled 10 Hz Nd:YAG laser (Spectra-Physics Quanta-Ray Lab 150 or Continuum Precision II 8000) directed into an optical parametric oscillator (Spectra-Physics Basi-scan or Continuum Panther, respectively). Pulses were 7 ns at full-width half-max, 416 nm, and 0.3 mJ as measured coming out of the fiber before being directed into the sample holder rod fiber. Once the longer fiber was connected to the sample holder rod fiber and secured, the resonant frequency was adjusted by moving the sample vertically and rotating it within the resonator so the resonant frequency was between 33.62-33.63 GHz.

2.5.2 Pulse-EPR Experiments

All electron paramagnetic resonance (EPR) experiments were conducted at 85 K using instrumentation described previously[111] with one exception, support for the Keysight M8190A arbitrary waveform generator has been integrated into the control software SpecMan[112], so all aspects of the pulse programming were handled by the software.

Three-pulse transient nutation experiments[113] were conducted at the resonator frequency ±20 MHz on R$^{\bullet}$ at a constant *g*-value to calibrate the pulse lengths.

All data was processed in the same fashion, first the dark spectrum, collected 50 ms following photoexcitation, was subtracted from the corresponding photoexcited light spectra. The spectra were then Fourier filtered to remove excess noise and a minor off-resonance feature at ~40 MHz due to R$^{\bullet}$ by applying a low-pass 60 MHz Gaussian frequency filter centered around 0 MHz. The spectrum at τ_D = 0 ns (defined as when the laser pulse occurs immediately after the first $\pi/2$ microwave pulse) was then phased to maximize the real part of the signal, and that phase was applied to all subsequent laser delays.

2.5.3 Additional Teleportation Laser Delay Experiments

Real components of the 2-pulse teleportation laser delay experiments from data sets 2 and 3 are in Figure S2.1. The plots include the 2-dimensional processed data with linear fits across the echo maxima and minima and data slices with corresponding fits of summed echo intensity across the linear fit. The data are very similar to data set 1, with only small differences in signal intensity and some noise at longer τ_D values.

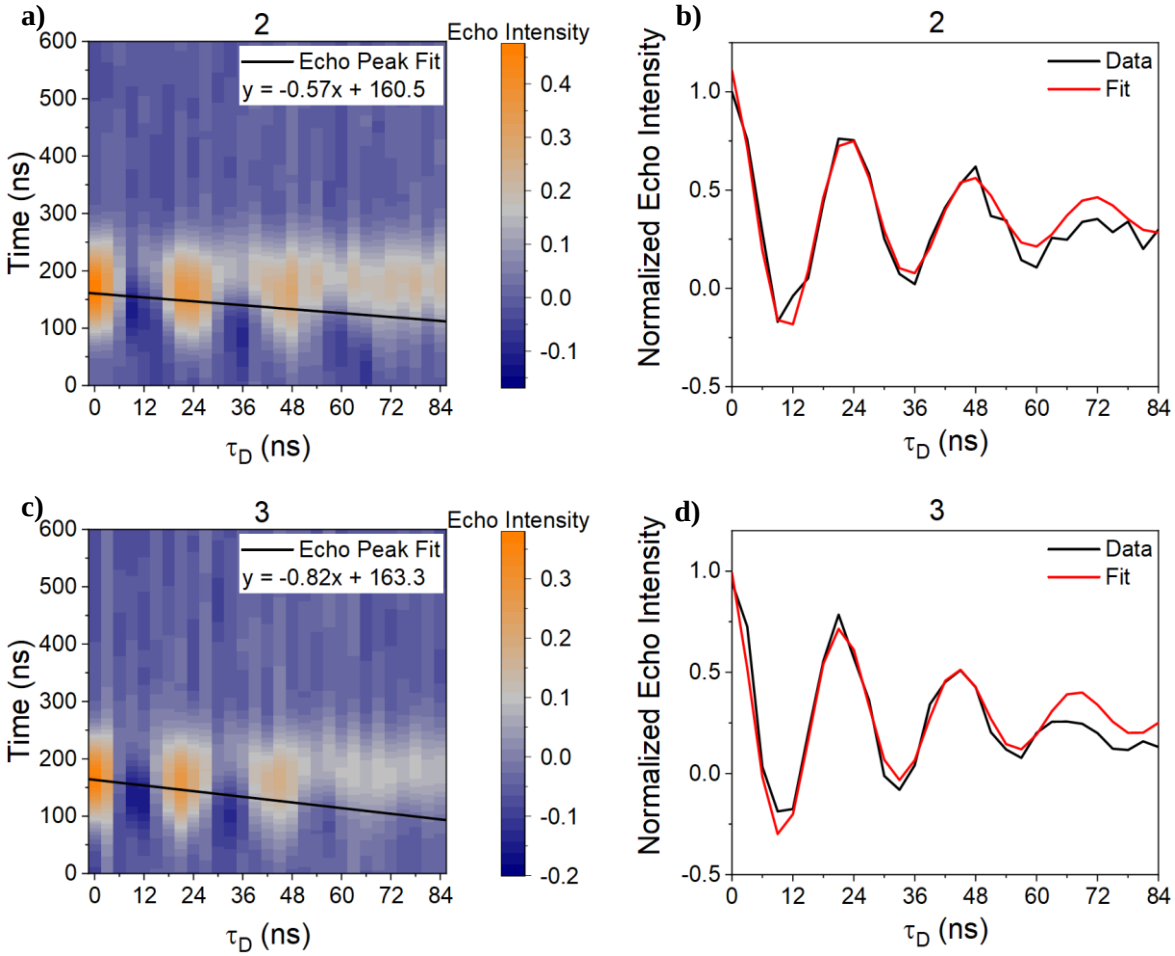

Figure S2.1. Additional 2-pulse teleportation laser delay experiments for data sets 2 and 3, as indicated by the number above the plots. Panels (a) and (c) are the 2-dimensional processed data sets with linear fits across the echo peak maxima and trough minima and (b) and (d) are normalized slices taken from integrating around the fitted lines with corresponding fits.

The equation used to fit the summed slice data is

Equation S2.1

$$fit_D = A_1 + A_2 * \ sin(A_3 * 2\pi * \tau_D \ + \ A_4) * e^{-\tau_D/A_5}$$

where A_1 is the y-axis offset of the signal, A_2 is the amplitude of the oscillation, A_3 is the frequency of the sine modulation, A_4 is the phase offset of the sine wave, and A_5 is the decay or damping

lifetime of the oscillations. Values denoted by A_n were given initial guesses and then fit to the data using the *fminsearch* function in MATLAB. Note that only the real parts of the data were used in these fits for simplicity.

The fit values for the summed slices of the 2-dimensional data are included in Table S2.1. The oscillation frequencies average at 42.2 MHz with a standard deviation of 0.7 MHz. The decay lifetime of the signals average to 38 ns with a standard deviation of 3 ns. Discussion of these values is included in the main text.

Data Set	Oscillation Frequency (MHz)	Decay Lifetime (ns)
1	42.4	42.4
2	41.3	36.0
3	43.0	36.9
Average	42.2	38
Standard Deviation	0.7	3

Table S2.1. Individual oscillation frequency and damping lifetime fit parameters for the 2-pulse teleportation $\langle S_x \rangle$ data slice. Average and standard deviation values also included.

Real components of the 3-pulse teleportation laser delay data from data sets 2 and 3 are shown in Figure S2.2. The data look similar to data set 1 with slight differences in the signal intensity and the presence of some noise at longer τ_D values, particularly in data set 3.

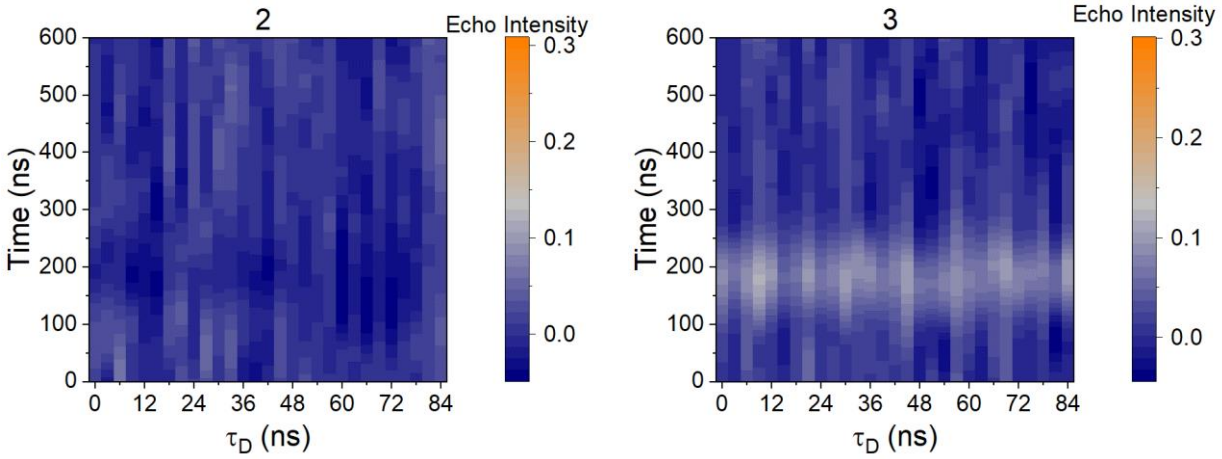

Figure S2.2. Additional 2-dimensional processed data sets for 3-pulse teleportation laser delay experiments from data sets 2 and 3, as indicated by the number above the plots.

Figure S2.3 compares the real and imaginary components of the 2-pulse teleportation laser delay experiments. Although the 2-pulse teleportation laser data were phased to minimize the imaginary component for the $\tau_D = 0$ ns slice, there is still signal in the imaginary channel. This imaginary signal is out-of-phase with the real channel signal by $\pi/2$. This phase offset is also present in the laser delay simulations, Figure S2.5, and comes from the teleportation event not being observed by the detector designated as the real channel. The teleported echo appears instead in the detector designated as the imaginary channel. Other than the phase offset, the signals have similar amplitudes and noise associated with the real and imaginary components of the same data set.

2.5.4 Additional 2-Pulse Teleportation Laser Delay Simulation Details

In Figure S2.4 are the 2-dimensional real-component simulations of the 2-pulse teleportation laser delay experiments using experimental parameters from data sets 2 and 3 along with linear fit through the peak maxima and trough minima. Linear fit equation is included in the

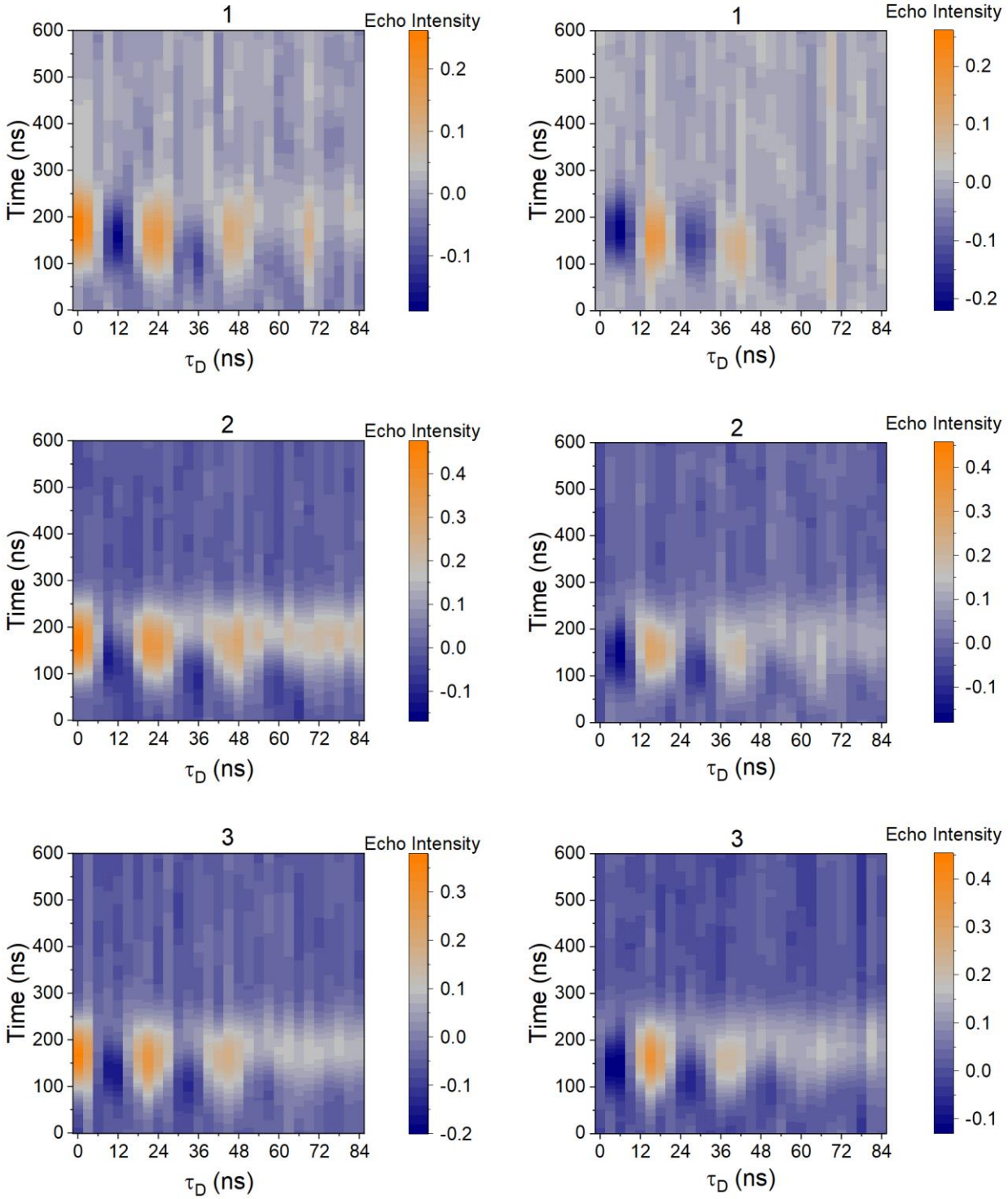

Figure S2.3. Comparison of real and imaginary components for 2-pulse teleportation τ_D experiments. Left-side data are the real components and right-side data are the imaginary components. Numbers above the plots refer to the data set number.

upper right corner of each plot. The simulated data look similar to the experimental data with quantitative values provided below in Table S2.2 for the data slice along the linear fit. Figure S2.4 also contains the simulation slices taken along the linear fit with corresponding fit using the same fit routine as described above for the experimental data. As with the 2-dimensional simulations, the slice along the linear fit of the simulation looks similar to the experimental data. Table S2.2

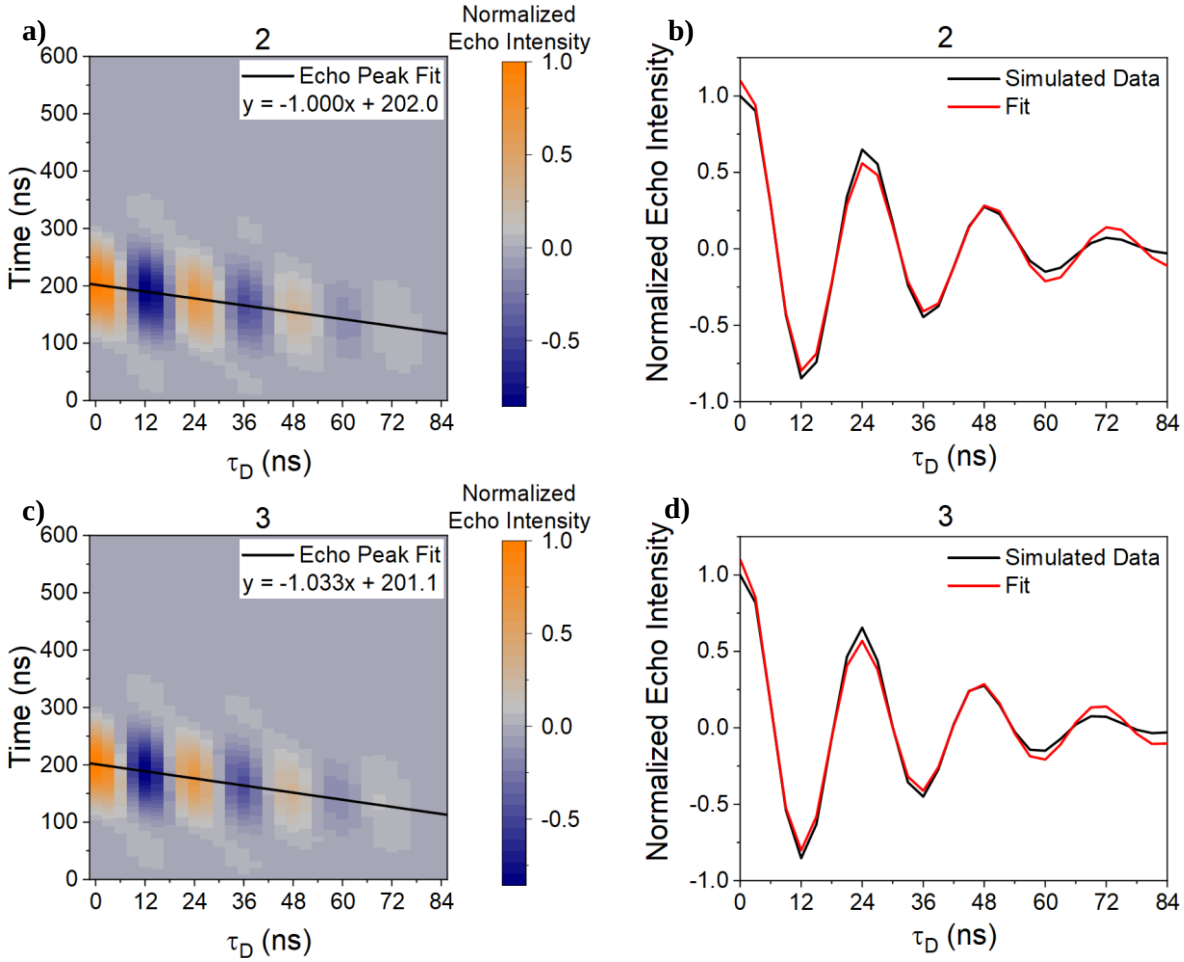

Figure S2.4. Additional real-component simulations of the 2-pulse teleportation τ_D experiments with experimental parameters from data sets 2 and 3, as indicated by the number above the plots. Panels (a) and (c) are the normalized 2-dimensional processed data sets with linear fits across the echo peak maxima and trough minima and (b) and (d) are normalized slices taken from integrating around the fitted lines with corresponding fits.

gives oscillation frequency and damping lifetime of each simulation set along with the average and standard deviation values. These values are similar to the fit parameters from the experimental data given in Table S2.1 shown earlier.

Figure S2.5 contains the side-by-side comparisons of the real and imaginary components of the 2-pulse teleportation laser delay simulations. As with the experimental data, the real and imaginary components of the simulations look similar except the phase offset for a given τ_D value. The origin of the phase offset is also the same as with the experimental data – that the teleportation event is occurring, but it cannot be detected in-phase with the same detector as the nutation frequencies of $R^{\bullet}$ and $D^{\bullet+}$ beat against each other to constructively and destructively interfere as a function of τ_D.

Data Set Parameters Used	Oscillation Frequency (MHz)	Decay Lifetime (ns)
1	42.5	35.4
2	41.6	35.9
3	42.4	35.4
Average	42.2	35.6
Standard Deviation	0.4	0.2

Table S2.2. Individual Oscillation frequency and damping lifetime fit parameters for the simulated 2-pulse teleportation $\langle S_x \rangle$ data slice. Average and standard deviation values also included.

The magnetic field values in the simulations were varied slightly from experimental values for the resulting linear slice oscillation frequencies to be within 1-2 MHz to experimental values. The magnetic field value was kept at 11.989 kG for each set of simulations. All other values, such

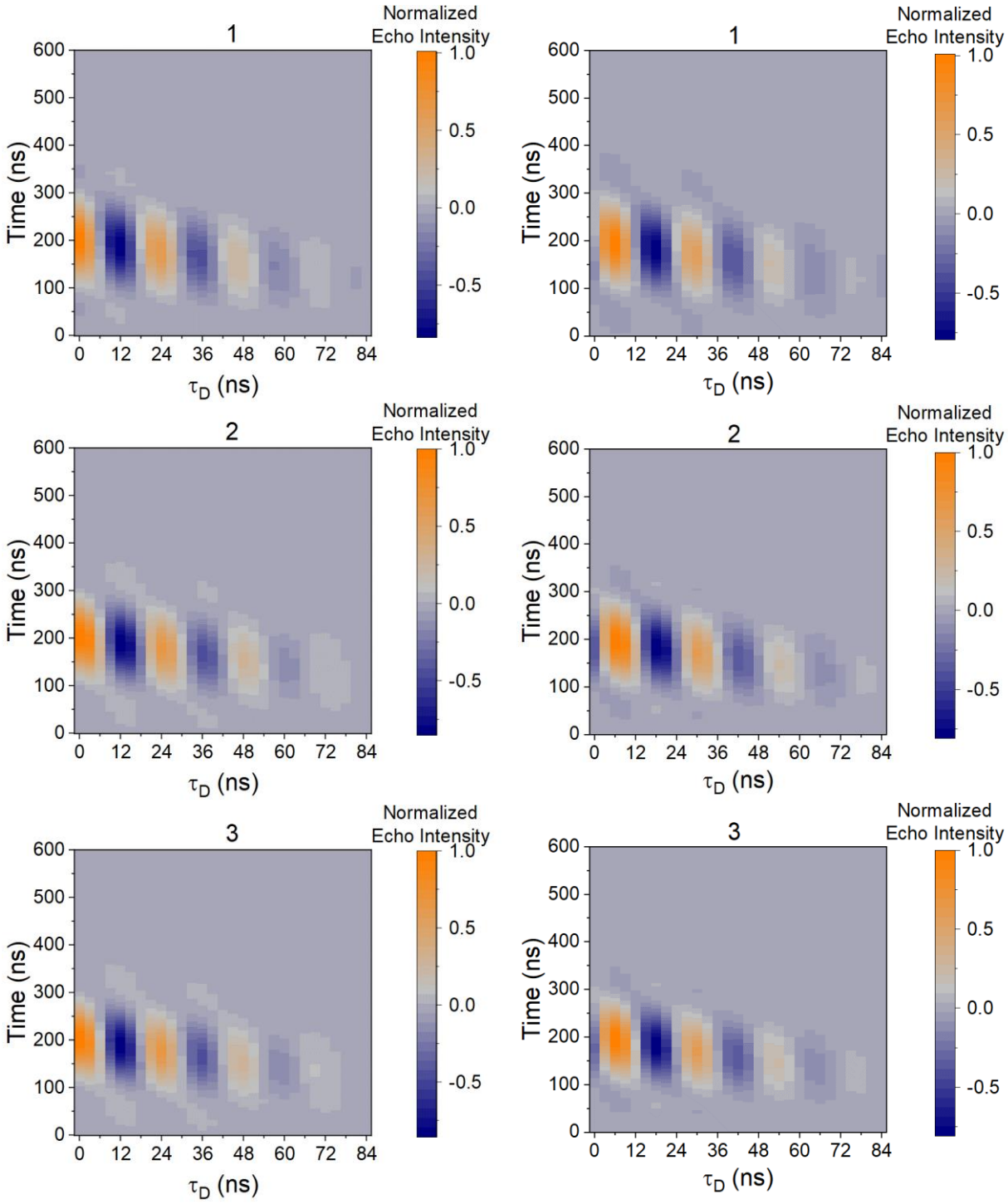

Figure S2.5. Comparison of real and imaginary components for 2-pulse teleportation τ_D simulations. Left-side plots are the real components and right-side plots are the imaginary components. Numbers above the plots refer to the data set number corresponding to the experimental parameters that were input into the simulations.

as center frequency and pulse length, were kept consistent with experimental conditions. This deviation is attributed to magnetic field instability and non-linear calibration inconsistencies and is within a few Gauss of experimental values.

2.5.5 Additional Fidelity Data and Calculation Details

The data below in Figure S2.6 show the additional teleportation fidelity values versus τ_D for data sets 2 and 3. The data appear similar to that presented in data set 1 in the main text, only with decreasing troughs in the oscillations at longer τ_D values. Peak teleportation fidelities stay above 2/3 and are therefore evidence of entanglement and quantum teleportation.

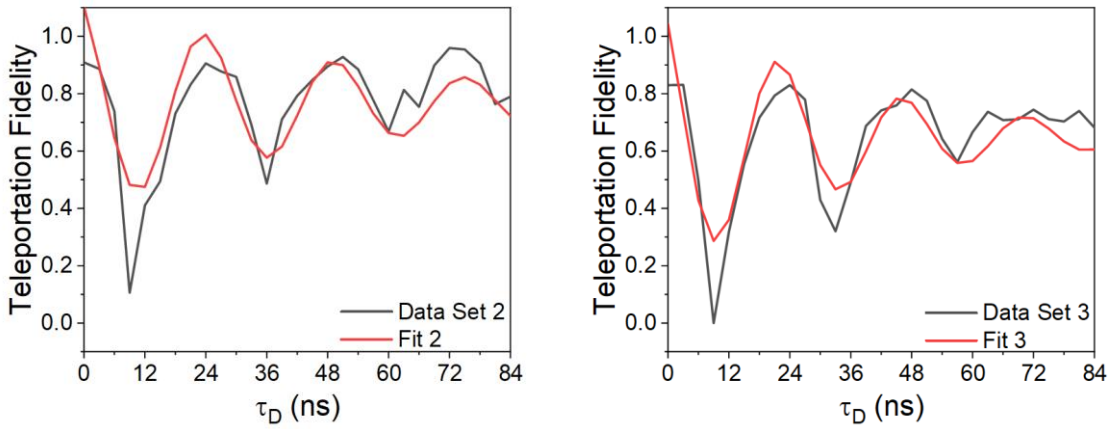

Figure S2.6. Teleportation fidelity as a function of τ_D and corresponding fits for data sets 2 and 3.

Teleportation density matrices were normalized starting with the following equation for the data at each τ_D value

Equation S2.2

$$d = abs(X + iY + Z)$$

where *d* is some divisor that, when applied to each input of the density matrix, will normalize the density matrix to $\sqrt{\langle S_x\rangle^2 + \langle S_y\rangle^2 + \langle S_z\rangle^2} = 1$. *X*, *Y*, and *Z* are the non-normalized expectation values of a particular τ_D value for the real 2-pulse, imaginary 2-pulse, and real 3-pulse data, respectively. These values were obtained from summing across the full-width at half-max of each echo along the fit line determined from the real 2-pulse teleportation laser delay data as described in the main text. The final normalization step divides *X*, *Y*, and *Z* by *d* to result in $\langle S_x \rangle$, $\langle S_y \rangle$, and $\langle S_z \rangle$.

The teleportation density matrix, $\rho_{teleport}$, for each value of τ_D is then constructed with the following format

Equation S2.3

$$\rho_{teleport} = \frac{1}{2}\begin{bmatrix} 1 + \langle S_z\rangle & \langle S_x\rangle - i\langle S_y\rangle \\ \langle S_x\rangle + i\langle S_y\rangle & 1 - \langle S_z\rangle \end{bmatrix}$$

Then, using the idealized input density matrix, ρ_{ideal},

Equation S2.4

$$\rho_{ideal} = \begin{bmatrix} 0.5 & 0.5 \\ 0.5 & 0.5 \end{bmatrix}$$

and the entanglement fidelity, F_{ent}, reported previously as 0.91, the teleportation fidelity, $F_{teleport}$, was calculated for each τ_D value using

Equation S2.5

$$F_{teleport} = F_{ent} * real\left(tr\left(\sqrt{\sqrt{\rho_{ideal}} * \rho_{teleport} * \sqrt{\rho_{ideal}}}\right)\right)^2$$

The teleportation fidelity data as a function of τ_D were fit using the following function, fit_{fid}, for each data set

Equation S2.6

$$fit_{fid} = B_1 + B_2 * \sin(B_3 * 2\pi * \tau_D + B_4) * e^{-\tau_D/B_5}$$

where B_1 is the vertical offset of the sine wave, B_2 is an amplitude modifier for the signal, B_3 is the frequency of sinusoidal oscillations, B_4 is the phase offset of the sine wave, and B_5 captures the amplitude evolution time of the shallower troughs at later τ_D values, particularly in data sets 2 and 3. All B_n values were given initial guesses and then fit to the data using the *fminsearch* function in MATLAB.

The fit value of primary importance to this study is the oscillation frequency, B_3. The individual frequency values, as well as average and standard deviation of these values, is provided in Table S2.3 below.

Data Set	Fidelity Oscillation Frequency (MHz)
1	44.2
2	39.0
3	41.1
Average	41
Standard Deviation	2

Table S2.3. Oscillation frequencies with standard deviation from fits of teleportation fidelity versus τ_D data.

2.5.6 Experimental Instrument Parameters

In Table S2.4 are the experimental parameters for all data sets. In Table S2.5, the phase cycles used in the 2- and 3-pulse teleportation laser delay experiments are included.

Data Set	Center Microwave Frequency (GHz)	R• Resonant Magnetic Field at Center Microwave Frequency (kG)	Microwave Frequency R• (GHz)	Microwave Frequency $D^{\bullet+}$ (GHz)	Laser Delay Experimental Magnetic Field (kG)
1	33.6274	11.992	33.6074	33.6474	11.985
2	33.6254	11.997	33.6054	33.6454	11.990
3	33.6265	11.998	33.6065	33.6465	11.991

Data Set	R• $\pi/2$ Microwave Pulse Length (ns)	$D^{\bullet+}$ $\pi/2$ Microwave Pulse Length (ns)	$D^{\bullet+}$ π Microwave Pulse Length (ns)
1	35	38.5	73
2	33	36	68
3	33	34	65

Table S2.4. Microwave frequency, magnetic field, and microwave pulse length parameters for triplicate 2- and 3-pulse τ_D teleportation experiments.

2-Pulse Laser Delay Experiments				
Step	**P_1 (π/2)**	**P_2 (π)**	**Det 1**	**Det 2**
1	+x	+x	+a	+b
2	+x	-x	+a	+b
3	+x	+y	-a	-b
4	+x	-y	-a	-b

3-Pulse Laser Delay Experiments					
Step	**P_1 (π/2)**	**P_2 (π/2)**	**P_3 (π)**	**Det 1**	**Det 2**
1	+x	+x	+x	+a	+b
2	+x	+x	-x	+a	+b
3	+x	+x	+y	-a	-b
4	+x	+x	-y	-a	-b
5	+x	+y	+x	+b	-a
6	+x	+y	-x	+b	-a
7	+x	+y	+y	-b	+a
8	+x	+y	-y	-b	+a
9	+x	-x	+x	-a	-b
10	+x	-x	-x	-a	-b
11	+x	-x	+y	+a	+b
12	+x	-x	-y	+a	+b
13	+x	-y	+x	-b	+a
14	+x	-y	-x	-b	+a
15	+x	-y	+y	+b	-a
16	+x	-y	-y	+b	-a

Table S2.5. Phase cycles used for (top) 2-pulse and (bottom) 3-pulse τ_D EPR experiments. P_n refers to the phase of the n^{th} pulse in the indicated pulse sequence and Det n refers to the phase of each of the quadrature detectors.

2.6 Acknowledgements

I thank Dr. Brandon K. Rugg for his phenomenal preliminary work on this project, the remaining sample used for the majority of these data, and his incredible mentorship. We also thank Jonathan D. Shultz for his help with MATLAB coding.

References

1. Bancroft, L.; Zhang, J.; Harvey, S. M.; Krzyaniak, M. D.; Zhang, P.; Schaller, R. D.; Beratan, D. N.; Young, R. M.; Wasielewski, M. R., Charge Transfer and Spin Dynamics in a Zinc Porphyrin Donor Covalently Linked to One or Two Naphthalenediimide Acceptors. *The Journal of Physical Chemistry A* **2021,** *125* (3), 825-834.

2. Krüger, H. W.; Michel-Beyerle, M. E.; Seidlitz, H., The influence of electron hopping on the recombination dynamics of radical ion pairs in liquid solution. *Chem. Phys. Lett.* **1982,** *87* (1), 79-82.

3. Michel-Beyerle, M. E.; Krüger, H. W.; Haberkorn, R.; Seidlitz, H., Nanosecond time-resolved magnetic field effect on radical recombination in solution. *Chem. Phys.* **1979,** *42* (3), 441-447.

4. Haberkorn, R.; Michel-Beyerle, M. E.; Marcus, R. A., On spin-exchange and electron-transfer rates in bacterial photosynthesis. *Proc. Natl. Acad. Sci. USA* **1979,** *76* (9), 4185-4188.

5. Liu, Y.; Flood, A. H.; Moskowitz, R. M.; Stoddart, J. F., Versatile Self-Complexing Compounds Based on Covalently Linked Donor–Acceptor Cyclophanes. *Chem. - Eur. J.* **2005,** *11* (1), 369-385.

6. Phelan, B. T.; Zhang, J.; Huang, G.-J.; Wu, Y.-L.; Zarea, M.; Young, R. M.; Wasielewski, M. R., Quantum coherence enhances electron transfer rates to two equivalent electron acceptors. *J. Am. Chem. Soc.* **2019,** *141* (31), 12236-12239.

7. Werner, U.; Sakaguchi, Y.; Hayashi, H.; Nohya, G.; Yoneshima, R.; Nakajima, S.; Osuka, A., Magnetic field effects in the radical ion pair recombination of fixed-distance triads consisting of porphyrins and an electron acceptor. *J. Phys. Chem.* **1995,** *99* (38), 13930-13937.

8. Wu, Y.; Zhou, J.; Nelson, J. N.; Young, R. M.; Krzyaniak, M. D.; Wasielewski, M. R., Covalent Radical Pairs as Spin Qubits: Influence of Rapid Electron Motion between Two Equivalent Sites on Spin Coherence. *J. Am. Chem. Soc.* **2018,** *140* (40), 13011-13021.

9. McConnell, H. M., Electron densities in semiquinones by paramagnetic resonance. *J. Chem. Phys.* **1956,** *24* (3), 632-632.

10. McConnell, H. M., Indirect Hyperfine Interactions in the Paramagnetic Resonance Spectra of Aromatic Free Radicals. *J. Chem. Phys.* **1956,** *24* (4), 764-766.

11. Phelan, B. T.; Zhang, J.; Huang, G.-J.; Wu, Y.-L.; Zarea, M.; Young, R. M.; Wasielewski, M. R., Quantum Coherence Enhances Electron Transfer Rates to Two Equivalent Electron Acceptors. *J. Am. Chem. Soc.* **2019,** *141* (31), 12236-12239.

12. Phelan, B. T.; Schultz, J. D.; Zhang, J.; Huang, G.-J.; Young, Ryan M.; Wasielewski, M. R., Quantum coherence in ultrafast photo-driven charge separation. *Faraday Discuss.* **2019,** *216*, 319-338.

13. Daviso, E.; Alia, A.; Prakash, S.; Diller, A.; Gast, P.; Lugtenburg, J.; Matysik, J.; Jeschke, G., Electron−Nuclear Spin Dynamics in a Bacterial Photosynthetic Reaction Center. *J. Phys. Chem. C* **2009,** *113* (23), 10269-10278.

14. Hoff, A. J.; Rademaker, H.; Van Grondelle, R.; Duysens, L. N. M., On the magnetic field dependence of the yield of the triplet state in reaction centers of photosynthetic bacteria. *Biochim. Biophys. Acta, Bioenerg.* **1977,** *460* (3), 547-554.

15. Wasielewski, M. R., Self-Assembly Strategies for Integrating Light Harvesting and Charge Separation in Artificial Photosynthetic Systems. *Acc. Chem. Res.* **2009,** *42* (12), 1910-1921.

16. Rudolf, M.; Kirner, S. V.; Guldi, D. M., A multicomponent molecular approach to artificial photosynthesis – the role of fullerenes and endohedral metallofullerenes. *Chem. Soc. Rev.* **2016,** *45* (3), 612-630.

17. Biskup, T.; Schleicher, E.; Okafuji, A.; Link, G.; Hitomi, K.; Getzoff, E. D.; Weber, S., Direct observation of a photoinduced radical pair in a cryptochrome blue-light photoreceptor. *Angew. Chem., Int. Ed. Engl.* **2009,** *48* (2), 404-407.

18. Hiscock, H. G.; Worster, S.; Kattnig, D. R.; Steers, C.; Jin, Y.; Manolopoulos, D. E.; Mouritsen, H.; Hore, P. J., The quantum needle of the avian magnetic compass. *Proc. Natl. Acad. Sci. USA* **2016,** *113* (17), 4634-4639.

19. Kelber, J. B.; Panjwani, N. A.; Wu, D.; Gómez-Bombarelli, R.; Lovett, B. W.; Morton, J. J. L.; Anderson, H. L., Synthesis and investigation of donor–porphyrin–acceptor triads with long-lived photo-induced charge-separate states. *Chem. Sci.* **2015,** *6* (11), 6468-6481.

20. Krzyaniak, M. D.; Kobr, L.; Rugg, B. K.; Phelan, B. T.; Margulies, E. A.; Nelson, J. N.; Young, R. M.; Wasielewski, M. R., Fast photo-driven electron spin coherence transfer: the effect of electron-nuclear hyperfine coupling on coherence dephasing. *J. Mater. Chem. C* **2015,** *3* (30), 7962-7967.

21. Nelson, J. N.; Krzyaniak, M. D.; Horwitz, N. E.; Rugg, B. K.; Phelan, B. T.; Wasielewski, M. R., Zero Quantum Coherence in a Series of Covalent Spin-Correlated Radical Pairs. *J. Phys. Chem. A* **2017,** *121* (11), 2241-2252.

22. Nelson, J. N.; Zhang, J.; Zhou, J.; Rugg, B. K.; Krzyaniak, M. D.; Wasielewski, M. R., CNOT gate operation on a photogenerated molecular electron spin-qubit pair. *J. Chem. Phys.* **2020,** *152* (1), 014503/1-014503/7.

23. Rugg, B. K.; Krzyaniak, M. D.; Phelan, B. T.; Ratner, M. A.; Young, R. M.; Wasielewski, M. R., Photodriven quantum teleportation of an electron spin state in a covalent donor-acceptor-radical system. *Nat. Chem.* **2019,** *11* (11), 981-986.

24. Norris, J. R.; Uphaus, R. A.; Crespi, H. L.; Katz, J. J., Electron Spin Resonance of Chlorophyll and the Origin of Signal I in Photosynthesis. *Proceedings of the National Academy of Sciences* **1971,** *68* (3), 625.

25. Polizzi, N. F.; Jiang, T.; Beratan, D. N.; Therien, M. J., Engineering opposite electronic polarization of singlet and triplet states increases the yield of high-energy photoproducts. *Proc. Natl. Acad. Sci. U. S. A.* **2019,** *116* (29), 14465-14470.

26. DiVincenzo, D. P., The Physical Implementation of Quantum Computation. *Prog. Phys.* **2000,** *48* (9-11), 771-783.

27. Schulten, K.; Wolynes, P. G., Semi-classical description of electron-spin motion in radicals including effect of electron hopping. *J. Chem. Phys.* **1978,** *68* (7), 3292–3297.

28. Knapp, E. W.; Schulten, K., Magnetic field effect on the hyperfine-induced electron spin motion in radicals undergoing diamagnetic–paramagnetic exchange. *J. Chem. Phys.* **1979,** *71* (4), 1878-1883.

29. Schulten, K., The effect of intramolecular paramagnetic-diamagnetic exchange on the magnetic field effect of radical pair recombination. *J. Chem. Phys.* **1985,** *82* (3), 1312-16.

30. Michel-Beyerle, M. E.; Krueger, H. W.; Haberkorn, R.; Seidlitz, H., Nanosecond time-resolved magnetic field effect on radical recombination in solution. *Chem. Phys.* **1979,** *42* (3), 441-7.

31. Haberkorn, R.; Michel-Beyerle, M. E.; Marcus, R., On spin-exchange and electron-transfer rates in bacterial photosynthesis. *Proc. Natl. Acad. Sci. USA* **1979,** *76*, 4185-4188.

32. Krueger, H. W.; Michel-Beyerle, M. E.; Seidlitz, H., The influence of electron hopping on the recombination dynamics of radical ion pairs in liquid solution. *Chem. Phys. Lett.* **1982,** *87* (1), 79-82.

33. Krueger, H. W.; Michel-Beyerle, M. E.; Knapp, E. W., Electron hopping and magnetic field dependent spin dynamics of radical ions in solution. *Chem. Phys.* **1983,** *74* (2), 205-16.

34. Werner, U.; Sakaguchi, Y.; Hayashi, H.; Nohya, G.; Yoneshima, R.; Nakajima, S.; Osuka, A., Magnetic field effects in the radical ion pair recombination of fixed-distance triads consisting of porphyrins and an electron acceptor. *J. Phys. Chem.* **1995,** *99* (38), 13930-13937.

35. Petrov, N. K.; Alfimov, M. V.; Budyka, M. F.; Gavrishova, T. N.; Staerk, H., Intramolecular electron hopping in double carbazole molecules studied by the fluorescence-detected magnetic field effect. *J. Phys. Chem. A* **1999,** *103*, 9601-9604.

36. Closs, G. L.; Forbes, M. D. E.; Norris, J. R., Spin-Polarized Electron-Paramagnetic Resonance-Spectra of Radical Pairs in Micelles - Observation of Electron Spin-Spin Interactions. *J. Phys. Chem.* **1987,** *91* (13), 3592-3599.

37. Steiner, U. E.; Ulrich, T., Magnetic field effects in chemical kinetics and related phenomena. *Chem. Rev.* **1989,** *89* (1), 51-147.

38. Norris, J. R.; Morris, A. L.; Thurnauer, M. C.; Tang, J., A general model of electron spin polarization arising from the interactions within radical pairs. *J. Chem. Phys.* **1990,** *92,* 4239-4249.

39. Till, U.; Hore, P. J., Radical pair kinetics in a magnetic field. *Mol. Phys.* **1997,** *90* (2), 289-296.

40. Tang, J.; Norris, J. R., Multiple-quantum EPR coherence in a spin-correlated radical pair system. *Chem. Phys. Lett.* **1995,** *233* (1), 192-200.

41. Phelan, B. T.; Schultz, J. D.; Zhang, J.; Huang, G.-J.; Young, R. M.; Wasielewski, M. R., Quantum coherence in ultrafast photo-driven charge separation. *Faraday Discuss.* **2019,** *216* (Ultrafast Photoinduced Energy and Charge Transfer), 319-338.

42. Wu, Y.; Nalluri, S. K. M.; Young, R. M.; Krzyaniak, M. D.; Margulies, E. A.; Stoddart, J. F.; Wasielewski, M. R., Charge and Spin Transport in an Organic Molecular Square. *Angew. Chem., Int. Ed.* **2015,** *54* (41), 11971-11977.

43. Weiss, E. A.; Tauber, M. J.; Ratner, M. A.; Wasielewski, M. R., Electron Spin Dynamics as a Probe of Molecular Dynamics: Temperature-Dependent Magnetic Field Effects on Charge Recombination within a Covalent Radical Ion Pair. *J. Am. Chem. Soc.* **2005,** *127* (16), 6052-6061.

44. Cao, H.; Fujiwara, Y.; Haino, T.; Fukazawa, Y.; Tung, C.-H.; Tanimoto, Y., Magnetic Field Effects on Intramolecular Exciplex Fluorescence of Chain-Linked Phenanthrene and N,N-Dimethylaniline: Influence of Chain Length, Solvent, and Temperature. *Bull. Chem. Soc. Jpn.* **1996,** *69* (10), 2801-2813.

45. Walters, V. A.; de Paula, J. C.; Jackson, B.; Nutaitis, C.; Hall, K.; Lind, J.; Cardozo, K.; Chandran, K.; Raible, D.; Phillips, C. M., Electronic Structure of Triplet States of Zinc(II) Tetraphenylporphyrins. *The Journal of Physical Chemistry* **1995,** *99* (4), 1166-1171.

46. Young, R. M.; Dyar, S. M.; Barnes, J. C.; Juríček, M.; Stoddart, J. F.; Co, D. T.; Wasielewski, M. R., Ultrafast Conformational Dynamics of Electron Transfer in ExBox4+⊂Perylene. *J. Phys. Chem. A* **2013,** *117* (47), 12438-12448.

47. Mauck, C. M.; Young, Ryan M.; Wasielewski, M. R., Characterization of Excimer Relaxation via Femtosecond Shortwave- and Mid-Infrared Spectroscopy. *J. Phys. Chem. A* **2017,** *121* (4), 784-792.

48. Chen, M.; Krzyaniak, M. D.; Nelson, J. N.; Bae, Y. J.; Harvey, S. M.; Schaller, R. D.; Young, R. M.; Wasielewski, M. R., Quintet-triplet mixing determines the fate of the multiexciton state produced by singlet fission in a terrylenediimide dimer at room temperature. *Proc. Natl. Acad. Sci. USA* **2019,** *116* (17), 8178-8183.

49. Weigend, F.; Ahlrichs, R., Balanced basis sets of split valence, triple zeta valence and quadruple zeta valence quality for H to Rn: Design and assessment of accuracy. *Phys. Chem. Chem. Phys.* **2005,** *7* (18), 3297-3305.

50. Zheng, J. J.; Xu, X. F.; Truhlar, D. G., Minimally augmented Karlsruhe basis sets. *Theor. Chem. Acc.* **2011,** *128* (3), 295-305.

51. Grimme, S.; Ehrlich, S.; Goerigk, L., Effect of the Damping Function in Dispersion Corrected Density Functional Theory. *J. Comput. Chem.* **2011,** *32* (7), 1456-1465.

52. Frisch, M. J.; Trucks, G. W.; Schlegel, H. B.; Scuseria, G. E.; Robb, M. A.; Cheeseman, J. R.; Scalmani, G.; Barone, V.; Petersson, G. A.; Nakatsuji, H.; Li, X.; Caricato, M.; Marenich, A. V.; Bloino, J.; Janesko, B. G.; Gomperts, R.; Mennucci, B.; Hratchian, H. P.; Ortiz, J. V.; Izmaylov, A. F.; Sonnenberg, J. L.; Williams; Ding, F.; Lipparini, F.; Egidi, F.; Goings, J.; Peng, B.; Petrone, A.; Henderson, T.; Ranasinghe, D.; Zakrzewski, V. G.; Gao, J.; Rega, N.; Zheng, G.; Liang, W.; Hada, M.; Ehara, M.; Toyota, K.; Fukuda, R.; Hasegawa, J.; Ishida, M.; Nakajima, T.; Honda, Y.; Kitao, O.; Nakai, H.; Vreven, T.; Throssell, K.; Montgomery Jr., J. A.; Peralta, J. E.; Ogliaro, F.; Bearpark, M. J.; Heyd, J. J.; Brothers, E. N.; Kudin, K. N.; Staroverov, V. N.; Keith, T. A.; Kobayashi, R.; Normand, J.; Raghavachari, K.; Rendell, A. P.; Burant, J. C.; Iyengar, S. S.; Tomasi, J.; Cossi, M.; Millam, J. M.; Klene, M.; Adamo, C.; Cammi, R.; Ochterski, J. W.; Martin, R. L.; Morokuma, K.; Farkas, O.; Foresman, J. B.; Fox, D. J. *Gaussian 16 Rev. A.03*, Wallingford, CT, 2016.

53. Cave, R. J.; Newton, M. D., Generalization of the Mulliken-Hush treatment for the calculation of electron transfer matrix elements. *Chem. Phys. Lett.* **1996,** *249* (1-2), 15-19.

54. Aidas, K.; Angeli, C.; Bak, K. L.; Bakken, V.; Bast, R.; Boman, L.; Christiansen, O.; Cimiraglia, R.; Coriani, S.; Dahle, P.; Dalskov, E. K.; Ekstrom, U.; Enevoldsen, T.; Eriksen, J. J.; Ettenhuber, P.; Fernandez, B.; Ferrighi, L.; Fliegl, H.; Frediani, L.; Hald, K.; Halkier, A.;

Hattig, C.; Heiberg, H.; Helgaker, T.; Hennum, A. C.; Hettema, H.; Hjertenaes, E.; Host, S.; Hoyvik, I. M.; Iozzi, M. F.; Jansik, B.; Jensen, H. J. A.; Jonsson, D.; Jorgensen, P.; Kauczor, J.; Kirpekar, S.; Kjrgaard, T.; Klopper, W.; Knecht, S.; Kobayashi, R.; Koch, H.; Kongsted, J.; Krapp, A.; Kristensen, K.; Ligabue, A.; Lutnaes, O. B.; Melo, J. I.; Mikkelsen, K. V.; Myhre, R. H.; Neiss, C.; Nielsen, C. B.; Norman, P.; Olsen, J.; Olsen, J. M. H.; Osted, A.; Packer, M. J.; Pawlowski, F.; Pedersen, T. B.; Provasi, P. F.; Reine, S.; Rinkevicius, Z.; Ruden, T. A.; Ruud, K.; Rybkin, V. V.; Salek, P.; Samson, C. C. M.; de Meras, A. S.; Saue, T.; Sauer, S. P. A.; Schimmelpfennig, B.; Sneskov, K.; Steindal, A. H.; Sylvester-Hvid, K. O.; Taylor, P. R.; Teale, A. M.; Tellgren, E. I.; Tew, D. P.; Thorvaldsen, A. J.; Thogersen, L.; Vahtras, O.; Watson, M. A.; Wilson, D. J. D.; Ziolkowski, M.; Agren, H., The Dalton quantum chemistry program system. *Wiley Interdiscip. Rev. Comput. Mol. Sci.* **2014,** *4* (3), 269-284.

55. Basel, B. S.; Zirzlmeier, J.; Hetzer, C.; Reddy, S. R.; Phelan, B. T.; Krzyaniak, M. D.; Volland, M. K.; Coto, P. B.; Young, R. M.; Clark, T.; Thoss, M.; Tykwinski, R. R.; Wasielewski, M. R.; Guldi, D. M., Evidence for Charge-Transfer Mediation in the Primary Events of Singlet Fission in a Weakly Coupled Pentacene Dimer. *Chem* **2018,** *4* (5), 1092-1111.

56. Michl, J., Photophysics of organic molecules in solution. In *Handbook of Photochemistry*, 3rd ed.; Montalti, M.; Credi, A.; Prodi, L.; Gandolfi, M. T., Eds. CRC Press, Taylor & Francis: 2006; pp 1-48.

57. Jones, R. N., The Ultraviolet Absorption Spectra of Anthracene Derivatives. *Chem. Rev.* **1947,** *41* (2), 353-371.

58. Miura, T.; Scott, A. M.; Wasielewski, M. R., Electron Spin Dynamics as a Controlling Factor for Spin-Selective Charge Recombination in Donor-Bridge-Acceptor Molecules. *J. Phys. Chem. C* **2010,** *114* (48), 20370-20379.

59. Scott, A. M.; Miura, T.; Ricks, A. B.; Dance, Z. E. X.; Giacobbe, E. M.; Colvin, M. T.; Wasielewski, M. R., Spin-Selective Charge Transport Pathways through p-Oligophenylene-Linked Donor-Bridge-Acceptor Molecules. *J. Am. Chem. Soc.* **2009,** *131* (48), 17655-17666.

60. Anderson, P. W., Theory of Magnetic Exchange Interactions:Exchange in Insulators and Semiconductors. In *Solid State Physics*, Seitz, F.; Turnbull, D., Eds. Academic Press: 1963; Vol. 14, pp 99-214.

61. Thamyongkit, P.; Speckbacher, M.; Diers, J. R.; Kee, H. L.; Kirmaier, C.; Holten, D.; Bocian, D. F.; Lindsey, J. S., Swallowtail Porphyrins: Synthesis, Characterization and Incorporation into Porphyrin Dyads. *J. Org. Chem.* **2004,** *69* (11), 3700-3710.

62. Marcus, R. A., On the Theory of Oxidation-Reduction Reactions Involving Electron Transfer. I. *J. Chem. Phys.* **1956,** *24* (5), 966-978.

63. Marcus, R. A., Theory of electron-transfer reactions. VI. Unified treatment for homogeneous and electrode reactions. *J. Chem. Phys.* **1965,** *43* (2), 679-701.

64. Closs, G. L.; Miller, J. R., Intramolecular long-distance electron transfer in organic molecules. *Science* **1988,** *240* (4851), 440-447.

65. Marcus, R. A., Chemical and electrochemical electron-transfer theory. *Annu. Rev. Phys. Chem.* **1964,** *15* (1), 155-196.

66. Marcus, R. A.; Sutin, N., Electron transfers in chemistry and biology. *Biochim. Biophys. Acta* **1985,** *811* (3), 265-322.

67. Denden, Z.; Ezzayani, K.; Saint-Aman, E.; Loiseau, F.; Najmudin, S.; Bonifácio, C.; Daran, J.-C.; Nasri, H., Insights on the UV/Vis, Fluorescence, and Cyclic Voltammetry Properties and the Molecular Structures of ZnII Tetraphenylporphyrin Complexes with Pseudohalide Axial Azido, Cyanato-N, Thiocyanato-N, and Cyanido Ligands. *Eur. J. Inorg. Chem.* **2015,** *2015* (15), 2596-2610.

68. Hartnett, P. E.; Mauck, C. M.; Harris, M. A.; Young, R. M.; Wu, Y.-L.; Marks, T. J.; Wasielewski, M. R., Influence of Anion Delocalization on Electron Transfer in a Covalent Porphyrin Donor-Perylenediimide Dimer Acceptor System. *J. Am. Chem. Soc.* **2017,** *139* (2), 749-756.

69. Mauck, C. M.; Young, R. M.; Wasielewski, M. R., Characterization of Excimer Relaxation via Femtosecond Shortwave- and Mid-Infrared Spectroscopy. *J. Phys. Chem. A* **2017,** *121* (4), 784-792.

70. Alzola, J. M.; Powers-Riggs, N. E.; La Porte, N. T.; Young, R. M.; Marks, T. J.; Wasielewski, M. R., Photoinduced electron transfer from zinc meso-tetraphenylporphyrin to a one-dimensional perylenediimide aggregate: Probing anion delocalization effects. *J. Porphyrins Phthalocyanines* **2020,** *24* (1/3), 143-152.

71. Kikuchi, K.; Kurabayashi, Y.; Kokubun, H.; Kaizu, Y.; Kobayashi, H., Triplet yields of some tetraphenylporphyrins and octaethylporphyrins. *J. Photochem. Photobiol., A* **1988,** *45* (2), 261-63.

72. Hurley, J. K.; Sinai, N.; Linschitz, H., Actinometry in monochromatic flash photolysis: the extinction coefficient of triplet benzophenone and quantum yield of triplet zinc tetraphenyl porphyrin. *Photochem. Photobiol.* **1983,** *38* (1), 9-14.

73. Anderson, P. W., New Approach to the Theory of Superexchange Interactions. *Phys. Rev.* **1959,** *115* (1), 2-13.

74. Kobori, Y.; Sekiguchi, S.; Akiyama, K.; Tero-Kubota, S., Chemically Induced Dynamic Electron Polarization Study on the Mechanism of Exchange Interaction in Radical Ion Pairs Generated by Photoinduced Electron Transfer Reactions. *J. Phys. Chem. A* **1999,** *103* (28), 5416-5424.

75. Kramers, H. A., The interaction of magnetogenic atoms in paramagnetic crystals. *Physica* **1934,** *1*, 182-192.

76. Weiss, E. A.; Ratner, M. A.; Wasielewski, M. R., Direct Measurement of Singlet-Triplet Splitting within Rodlike Photogenerated Radical Ion Pairs Using Magnetic Field Effects: Estimation of the Electronic Coupling for Charge Recombination. *J. Phys. Chem. A* **2003,** *107* (19), 3639-3647.

77. Leggett, A. J.; Chakravarty, S.; Dorsey, A. T.; Fisher, M. P. A.; Garg, A.; Zwerger, W., Dynamics of the dissipative two-state system. *Reviews of Modern Physics* **1987,** *59* (1), 1.

78. Nitzan, A., *Chemical Dynamics in Condensed Phases: Relaxation, Transfer, and Reactions in Condensed Molecular Systems*. Oxford University Press: New York, USA, 2006.

79. Zarea, M.; Ratner, M. A.; Wasielewski, M. R., Electron transfer in a two-level system within a Cole-Davidson vitreous bath. *J. Chem. Phys.* **2014,** *140* (2), 024110/1-024110/6.

80. Steiner, U. E.; Schäfer, J.; Lukzen, N. N.; Lambert, C., J-resonance line shape of magnetic field-affected reaction yield spectrum from charge recombination in a linked donor–acceptor dyad. *J. Phys. Chem. C* **2018,** *122* (22), 11701-11708.

81. Klein, J. H.; Schmidt, D.; Steiner, U. E.; Lambert, C., Complete monitoring of coherent and incoherent spin flip domains in the recombination of charge-separated states of donor-iridium complex-acceptor triads. *J. Am. Chem. Soc.* **2015,** *137* (34), 11011-11021.

82. Fajer, J.; Borg, D.; Forman, A.; Adker, A.; Varadi, V., Cation radicals of tetraalkylprophyrins. *J. Am. Chem. Soc.* **1974,** *96* (4), 1238-1239.

83. Batchelor, S.; Kay, C.; McLauchlan, K.; Shkrob, I., Time-resolved and modulation methods in the study of the effects of magnetic fields on the yields of free-radical reactions. *J. Phys. Chem.* **1993,** *97* (50), 13250-13258.

84. Kelley, R. F.; Shin, W. S.; Rybtchinski, B.; Sinks, L. E.; Wasielewski, M. R., Photoinitiated Charge Transport in Supramolecular Assemblies of a 1,7,N,N‘-Tetrakis(zinc porphyrin)-perylene-3,4:9,10-bis(dicarboximide). *J. Am. Chem. Soc.* **2007,** *129* (11), 3173-3181.

85. Weller, A., Photoinduced Electron Transfer in Solution: Exciplex and Radical Ion Pair Formation Free Enthalpies and their Solvent Dependence. *Z. Phys. Chem.* **1982,** *133* (1), 93-98.

86. Kelley, R. F.; Tauber, M. J.; Wasielewski, M. R., Intramolecular Electron Transfer through the 20-Position of a Chlorophyll a Derivative: An Unexpectedly Efficient Conduit for Charge Transport. *J. Am. Chem. Soc.* **2006,** *128* (14), 4779-4791.

87. Fajer, J.; Borg, D. C.; Forman, A.; Dolphin, D.; Felton, R. H., Pi-cation radicals and dications of metalloporphyrins. *J. Am. Chem. Soc.* **1970,** *92*, 3451-3459.

88. Bancroft, L.; Qiu, Y.; Krzyaniak, M. D.; Wasielewski, M. R., Effect of the Time Delay between Spin State Preparation and Measurement on Electron Spin Teleportation in a Covalent Donor–Acceptor–Radical System. *The Journal of Physical Chemistry Letters* **2022,** *13* (1), 156-160.

89. Pirandola, S.; Eisert, J.; Weedbrook, C.; Furusawa, A.; Braunstein, S. L., Advances in quantum teleportation. *Nature Photon.* **2015,** *9*, 641-652.

90. Bennett, C. H.; Brassard, G.; Crépeau, C.; Jozsa, R.; Peres, A.; Wootters, W. K., Teleporting an unknown quantum state via dual classical and Einstein-Podolsky-Rosen channels. *Phys. Rev. Lett.* **1993,** *70* (13), 1895-1899.

91. Bouwmeester, D.; Pan, J.-W.; Mattle, K.; Eibl, M.; Weinfurter, H.; Zeilinger, A., Experimental quantum teleportation. *Nature* **1997,** *390* (11), 575-579.

92. Boschi, D.; Branca, S.; De Martini, F.; Hardy, L.; Popescu, S., Experimental Realization of Teleporting an Unknown Pure Quantum State via Dual Classical and Einstein-Podolsky-Rosen Channels. *Phys. Rev. Lett.* **1998,** *80* (6), 1121-1125.

93. Barrett, M. D.; Chiaverini, J.; Schaetz, T.; Britton, J.; Itano, W. M.; Jost, J. D.; Knill, E.; Langer, C.; Leibfried, D.; Ozeri, R.; Wineland, D. J., Deterministic quantum teleportation of atomic qubits. *Nature* **2004,** *429* (6993), 737-739.

94. Riebe, M.; Häffner, H.; Roos, C. F.; Hänsel, W.; Benhelm, J.; Lancaster, G. P. T.; Körber, T. W.; Becher, C.; Schmidt-Kaler, F.; James, D. F. V.; Blatt, R., Deterministic quantum teleportation with atoms. *Nature* **2004,** *429* (6993), 734-737.

95. Sherson, J. F.; Krauter, H.; Olsson, R. K.; Julsgaard, B.; Hammerer, K.; Cirac, I.; Polzik, E. S., Quantum teleportation between light and matter. *Nature* **2006,** *443*, 557-560.

96. Steffen, L.; Salathe, Y.; Oppliger, M.; Kurpiers, P.; Baur, M.; Lang, C.; Eichler, C.; Puebla-Hellmann, G.; Fedorov, A.; Wallraff, A., Deterministic quantum teleportation with feed-forward in a solid state system. *Nature* **2013,** *500*, 319-324.

97. Nielsen, M. A.; Knill, E.; Laflamme, R., Complete quantum teleportation using nuclear magnetic resonance. *Nature* **1998,** *396* (6706), 52-55.

98. Gao, W. B.; Fallahi, P.; Togan, E.; Delteil, A.; Chin, Y. S.; Miguel-Sanchez, J.; Imamoglu, A., Quantum teleportation from a propagating photon to a solid-state spin qubit. *Nat Commun* **2013,** *4*, 2744.

99. Pfaff, W.; Hensen, B. J.; Bernien, H.; van Dam, S. B.; Blok, M. S.; Taminiau, T. H.; Tiggelman, M. J.; Schouten, R. N.; Markham, M.; Twitchen, D. J.; Hanson, R., Unconditional quantum teleportation between distant solid-state quantum bits. *Science (Washington, DC, U. S.)* **2014,** *345* (6196), 532-535.

100. Nielsen, M. A.; Chuang, I. L., *Quantum Computation and Quantum Information*. Cambridge University Press: Cambridge, UK, 2000; p 702 pp.

101. Kandrashkin, Y. E.; Salikhov, K. M., Numerical Simulation of Quantum Teleportation Across Biological Membrane in Photosynthetic Reaction Centers. *Appl. Magn. Res.* **2010,** *37*, 549-566.

102. Salikhov, K. M.; Golbeck, J. H.; Stehlik, D., Quantum teleportation across a biological membrane by means of correlated spin pair dynamics in photosynthetic reaction centers. *Appl. Magn. Res.* **2007,** *31*, 237-252.

103. Kandrashkin, Y. E., Influence of Spin Decoherence on the Yield of Photodriven Quantum Teleportation in Molecular Triads. *J. Phys. Chem. Lett.* **2021,** *12* (27), 6405-6410.

104. Rugg, B. K.; Phelan, B. T.; Horwitz, N. E.; Young, R. M.; Krzyaniak, M. D.; Ratner, M. A.; Wasielewski, M. R., Spin-Selective Photoreduction of a Stable Radical within a Covalent Donor–Acceptor–Radical Triad. *Journal of the American Chemical Society* **2017,** *139* (44), 15660-15663.

105. Brenner, M. H.; Cai, D.; Swanson, J. A.; Ogilvie, J. P., Two-photon imaging of multiple fluorescent proteins by phase-shaping and linear unmixing with a single broadband laser. *Opt. Express* **2013,** *21* (14), 017256, 9 pp.

106. Stoll, S.; Schweiger, A., EasySpin, a comprehensive software package for spectral simulation and analysis in EPR. *J. Magn. Reson.* **2006,** *178* (1), 42-55.

107. Gilchrist, A.; Langford, N. K.; Nielsen, M. A., Distance measures to compare real and ideal quantum processes. *Phys. Rev. A* **2005,** *71* (6), 062310.

108. Grosshans, F.; Grangier, P., Quantum cloning and teleportation criteria for continuous quantum variables. *Physical Review A* **2001,** *64* (1), 010301.

109. Carr, H. Y.; Purcell, E. M., Effects of Diffusion on Free Precession in Nuclear Magnetic Resonance Experiments. *Physical Review* **1954,** *94* (3), 630-638.

110. Meiboom, S.; Gill, D., Modified Spin-Echo Method for Measuring Nuclear Relaxation Times. *Rev. Sci. Instrum.* **1958,** *29* (8), 688-691.

111. Rugg, B. K.; Krzyaniak, M. D.; Phelan, B. T.; Ratner, M. A.; Young, R. M.; Wasielewski, M. R., Photodriven quantum teleportation of an electron spin state in a covalent donor–acceptor–radical system. *Nature Chemistry* **2019,** *11* (11), 981-986.

112. Epel, B.; Gromov, I.; Stoll, S.; Schweiger, A.; Goldfarb, D., Spectrometer manager: A versatile control software for pulse EPR spectrometers. *Concepts in Magnetic Resonance Part B: Magnetic Resonance Engineering* **2005,** *26B* (1), 36-45.

113. Astashkin, A. V.; Schweiger, A., Electron-spin transient nutation: a new approach to simplify the interpretation of ESR spectra. *Chem. Phys. Lett.* **1990,** *174*, 595-602.